Stellingen

behorende bij het proefschrift

Oscillations in Rail Vehicle Traction Drives

Analysis of Electromechanics

Max Winterling

22 september 1997

I

De door leverancier en gebruiker opgestelde specificatie van aandrijfcomponenten van tractieaandrijvingen dient rekening te houden met de trillingen en de dynamische belastingen die kunnen optreden tijdens een cyclus van aanzetten en remmen van het voertuig.

II

De in dit proefschrift gepropageerde filosofie van de beschouwing van de aandrijving als systeem kan alleen succesvol worden toegepast als elke leverancier van aandrijfcomponenten deze hanteert.

III

Het falen van elektrische aandrijfconcepten ligt in de aanpak om het luchtspleetkoppel van de motor te beheersen en niet het aan te drijven werktuig of voertuig.

IV

Met het oog op gebruikersvriendelijkheid en geluidsemissie zouden technische apparaten niet door technici moeten worden ontworpen.

V

De toenemende complexiteit van computer software aan de ene kant en de presenteerbaarheid van de resultaten aan de andere kant verleidt zelfs wetenschappers deze te gebruiken zonder methoden en achtergronden te kennen.

VI

Het samengaan van wetenschap en techniek bestaat uit het inzicht van technici wetenschap als instrument te gebruiken en het inzicht van wetenschappers de techniek als voedingsbodem van de wetenschap te gebruiken.

VII

Hoe minder de materie begrepen wordt hoe ingewikkelder de theorieën om deze te beschrijven.

VIII

Zou in het treinverkeer hetzelfde aantal verkeersdoden en gewonden vallen als in het autoverkeer, dan was elk verkeer via spoor wettelijk verboden.

IX

Ondanks het feit dat meer dan de helft van de Nederlanders niet bij een godsdienst is aangesloten drukt het calvinisme een stempel op de Nederlandse cultuur.

X

De invoering van de Euro zal de verschillen in de culturen die de staatshuishoudingen bepalen niet kunnen vereffenen.

XI

Het systematisch uit de slaap houden is een beproefde martelmethode. In dit licht bezien draagt het ouderschap een portie masochisme in zich.

OSCILLATIONS IN RAIL VEHICLE TRACTION DRIVES

ANALYSIS OF ELECTROMECHANICS

OSCILLATIONS IN RAIL VEHICLE TRACTION DRIVES

ANALYSIS OF ELECTROMECHANICS

PROEFSCHRIFT

ter verkrijging van de graad van doctor
aan de Technische Universiteit Delft,
op gezag van de Rector Magnificus Prof.dr.ir. J. Blaauwendraad,
in het openbaar ter verdedigen ten overstaan van een commissie,
door het College van Dekanen aangewezen,
op maandag 22 september 1997 te 10 uur 30

door

Max Wolfgang WINTERLING

elektrotechnisch ingenieur

geboren te Wiesbaden, Duitsland

Dit proefschrift is goedgekeurd door de promotor:
Prof.Dr.-Ing. W. Deleroi

Samenstelling promotiecommissie:

Rector Magnificus,	voorzitter
Prof.Dr.-Ing. W. Deleroi,	Technische Universiteit Delft, promotor
Prof.ir. J.A. Schot,	Technische Universiteit Delft
Prof.dr.ir. P. Meijers,	Technische Universiteit Delft
Prof.ir. O.H. Bosgra,	Technische Universiteit Delft
Prof.dr.ir. R. Belmans,	Katholieke Universiteit Leuven, België
Prof.Dr.-Ing. H.P. Beck,	Technische Universität Clausthal, Duitsland
Ir. E. Tuinman	Holec Ridderkerk

This study was carried out at Delft University of Technology, Power Electronics and Electrical Machines Group, in collaboration with Holec Ridderkerk, Department of Machines, and was financed by Holec Ridderkerk.

Published and distributed by:

Delft University Press
Mekelweg 4
2628 CD Delft
The Netherlands
Telephone: +31 15 2783254
Fax: +31 15 2781661
E-mail: DUP@DUP.TUDelft.NL

CIP-DATA KONINKLIJKE BIBLIOTHEEK, DEN HAAG

Winterling, M.W.

Oscillations in Rail Vehicle Traction Drives : Analysis of Electromechanics / M.W. Winterling - Delft : Delft University Press. - Illustrations.
Thesis Delft University of Technology. - With ref. - With summary in Dutch. - With summary in German.
ISBN 90-407-1514-9
NUGI 841
Subject headings: Oscillations, light-rail vehicles, mechanical drive design.

Abstract

The need for transport has become ever more essential in today's society. Travel from home to work and travel abroad have increased traffic by car, aeroplane and train. In the past years there has been much investment in railway transport. On the one hand, high-speed trains have become an alternative to the aeroplane, on the other hand, light-rail vehicles in urban and suburban transport have become an alternative to cars. Since the growing traffic on highways often means traffic jams, railway transport is a serious alternative. However, railway transport has to be attractive. This means comfortable trains, metros or trams which travel fast and with a high frequency of service. These demands require new developments. An example is the low-floor tram with a floor height of 30 centimetres from the platform.

The development of electric light-rail vehicles such as electrical multiple-units, metro and tram cars with induction motor drives and new bogie and car-body constructions yielded lightweight vehicles and at the same time higher performance in order to save energy and to increase velocity and frequency of passenger transport.

Lifetime requirements are today part of customer specifications for rail vehicles. Specifications of components of rail vehicle drives such as gearboxes, couplings and suspensions have to guarantee lifetime of 30 years or more. The dynamic load conditions of these components influence their lifetime. Peaks and oscillations of mechanical torques and forces have to be known in order to specify and develop rail vehicle drives. Therefore the vehicle drive including electrical drive, mechanical drive and wheel-rail contact has to be examined. In view of the variety of mechanical and electrical drive concepts of light-rail vehicles flexibility of the method to determine drive dynamics is recommended.

Mechanical oscillations may be free, damped oscillations or forced oscillations. The sources of oscillations are the electrical drive by the ripple torque generated by the inverter fed induction motor, by the control system and by fault situations such as stator short circuit of the motor. The wheel-rail contact may cause oscillations by shock loads and slip-stick phenomena which influence the entire drive.

This thesis proposes a procedure to measure and to calculate mechanical oscillations in traction drives in order to obtain an overview of oscillation phenomena in a short time.

Measurements have to be done by using sensors in the electrical and mechanical drive during a standard cycle of acceleration and braking. By simultaneous sampling of signals, an overview will be obtained in the desired frequency band. Time and frequency analysis by cascade plots evince speed dependent oscillations and resonance phenomena. Measurements were performed on three light-rail vehicles on track and on a locomotive on a roller bench.
Measurements showed that main causes of oscillations are the traction inverter, the mechanical drive and the wheel-rail contact. The highest oscillation amplitudes occur with excitation of weakly damped natural frequencies such as with slip-stick oscillations and cardan shaft resonances.

Flexible modelling has been obtained by applying multi-body system modelling of the mechanical structure which enables the derivation of equations of motion from the mechanical structure of rigid bodies in three dimensions. Models of the electrical drive and the wheel-rail contact coupled to the models of mechanical structures enable the investigation of mechanical oscillations of drive lines, bogies and entire vehicles. Software has been developed for flexible modelling and simulation of traction drive dynamics.

Taking two examples of light-rail vehicle drives, dynamics during a traction cycle were simulated including ripple torques, wheel slip and short-circuit of the traction motor. The damping of mechanical components plays an important role for the amplitude and propagation of mechanical oscillations. A well-damped drive line is always recommended to limit amplitudes of ripple torques and the possible resonances and to limit amplitudes of transients. Optimization of inverter switching patterns has to obviate mechanical resonances and torque transients due to changes in switching patterns.
The possibility of wheel slip limits torque peaks at motor short-circuits. Accelerating or braking near the maximum of transmittable force from wheel to rail, slip-stick oscillations may occur, which are partly damped by the drive line. However, to minimize these oscillations, active damping by the control system is necessary.

The results of the research show that analysis of oscillations in traction drives requires analysis of the entire system. To minimize oscillations, not only the control system but also the drive components have to be optimized. Specification of components have to include dynamic load conditions, which can be calculated and measured by the procedures presented in this thesis. The interaction between the variables used for optimization makes minimization of oscillations a difficult task.

Acknowledgements

During the past four years the research was supported by both organizations and people. First I wish to thank my promotor, Prof. W. Deleroi, for the "coaching" of my activities by discussing ideas and results and by providing contacts. Further I owe thanks to Erik Tuinman for continuous input and fruitful discussions, Prof. J.A. Schot for his encouragement, suggestions and corrections, Prof. P. Meijers for his interest and the discussions on mechanics and wheel-rail contact. I thank Prof. O.H. Bosgra for his interest and suggestions on the subject, Prof. H.P. Beck for the collaboration during the past year and our discussions and Prof. R. Belmans for his suggestions.

A part of the experimental research was performed within the European Union project "Human Capital and Mobility - Access to Large Installations". I thank the European commission for the financial support and "Consorzio Ricerche Innovative per il Sud" and Ansaldo Trasporti for the technical and organisational support.

I wish to thank the staff of "Nederlandse Spoorwegen, Materieel Engineering" and the staff of "Technisch Onderzoek". In particular I am indebted to Ir. A. van Himbergen, for his collaboration.

I thank staff and students of the Power Electronics and Electrical Machines group of the Technical University of Delft for their hospitality throughout the four years and their support of my research activities.

My thanks go to Henk Huisman, former Measurements and Control Group of Technical University of Delft, for his collaboration, suggestions and initiatives. Two students I would like to thank in particular are P.J. van Overloop for his contribution and enthusiasm as thesis student and during his stay at Naples Facilities and C. Söffker of the Technical University of Clausthal for his work on system identification in Naples.

I thank my colleagues of the Holec Traction Department, Machines Department and Services Department for their support and helpful attitude and Holec Ridderkerk for financing this research.

Thanks go to Mrs. Zaat-Jones for the careful correction of the language.

Last but far from least I thank my wife Tina for her support and understanding and my children Federico and Floriana who gave me a lot of joy during the years of research.

Contents

1 Introduction 1

1.1 Light-rail vehicle traction drives 1
1.2 State of research 4
1.3 Problem statement 5
1.4 Outline of the thesis 6

2 Electromechanical Traction Drives 9

2.1 Introduction 9
2.2 System description 9
2.3 Drive components 11
2.4 Drive operation 18
2.5 Oscillation sources 20

3 Measurement of oscillations 23

3.1 Introduction 23
3.2 Experiment design 24
3.2.1 Sensors and transducers 24
3.2.2 Experiments 30
3.2.3 Data-acquisition 33
3.3 Oscillation analysis 34
3.3.1 Data processing 34
3.3.2 Oscillations during a traction cycle 38
3.3.3 Converter harmonics 54

3.3.4 Rail influences 63
3.4 Conclusions 67

4 Flexible Modelling 69

4.1 Introduction 69
4.2 Electrical drive 70
4.2.1 Traction motor 70
4.2.2 Inverter and control 83
4.3 Modelling of mechanics 86
4.3.1 Multi-body system modelling 86
4.3.2 Mechanical drive 89
4.3.3 Suspensions 94
4.4 Wheel-rail contact 98
4.4.1 Fundamentals 98
4.4.2 A practical model 100
4.5 System model 103
4.6 Software implementation 107
4.7 Conclusions 109

5 Simulation and Analysis 111

5.1 Introduction 111
5.2 Methodology 112
5.2.1 Simulation 112
5.2.2 Validation 114
5.2.3 Optimization 115
5.3 Drive dynamics 116
5.3.1 Traction motor 116
5.3.2 Mechanical drive 120
5.3.3 Electromechanical drive 128
5.4 Inverter harmonics 133
5.4.1 Oscillation amplitudes 133
5.4.2 Hollow shaft drive 137
5.4.3 Quill shaft drive 141

5.5 Influences of the wheel-rail contact 143
5.5.1 Slip-stick oscillations 143
5.5.2 Inverter short-circuit 144
5.6 Conclusions 147

6 Conclusions 149

6.1 Results 149
6.2 Recommendations for further research 151

References 153

List of Symbols 163

Appendix A 167

Appendix B 169

Appendix C 173

Appendix D 175

Appendix E 177

Appendix F 179

Samenvatting 185

Zusammenfassung 189

Curriculum Vitae 193

1 Introduction

1.1 Light-rail vehicle traction drives

Since Werner von Siemens presented his electrically driven vehicle at the World Fair of Berlin in 1879, electrical traction has made way in international, national, urban and suburban transport. In the research being presented in this thesis, light-rail vehicles for passenger service are considered.
Light-rail vehicles are electrical multiple units, vehicles for underground service, and tram cars. Light-rail vehicles are usually composed of coupled car bodies placed on bogies which can be driven by one or more motors. Figure 1.1.1 shows schematically three examples of the composition of some types of vehicles. The electrical multiple-unit has two cars. Each car is placed on two bogies, one motor bogie and one non-driven bogie. As a variation, there are multiple car units with driven and non-driven cars. Typical values for acceleration of electrical multiple units are 0.7-0.8 m/s^2 and for braking 0.7-1.0 m/s^2, while the maximum speed of the vehicle is 100 to 160 km/h. During emergency braking, values of 1.2 m/s^2 may be reached. The second example shows a tram with two cars and three bogies. All bogies are driven by one motor per axle. The acceleration and braking of a tram is higher than that of electrical multiple-units while its maximum speed is about 80 km/h. New tram-car developments are the design of low-floor vehicles with a minimum vehicle floor height of 180 mm. Some of the low-floor trams are equipped with bogies that include wheel axles, others have single-wheel drives. Their performance is comparable to that of conventional tram-cars, however, drive design has changed significantly. Figure 1.1.1 shows a low-floor tramway with single-wheel drives where all wheels are driven by hub motors.

Thirty years ago light rail vehicles were not as "light" as today. The traction motor was a DC motor with rheostatic torque control. The DC motor was a large and heavy motor with a maximum speed of about 2500 rpm. The commutator brushes

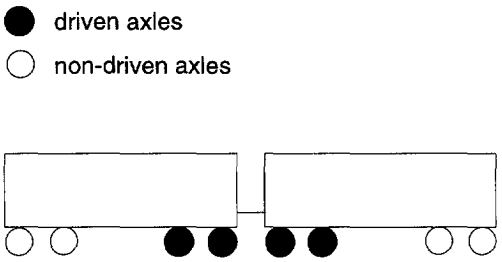

Electrical multiple-unit

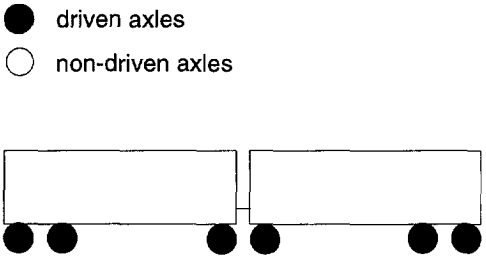

Tram-car configuration

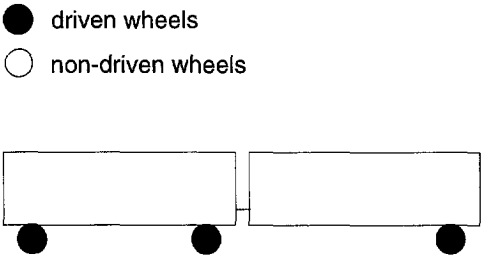

Configuration of low-floor tram-car

Figure 1.1.1 Schematic configuration of light-rail vehicles.

were one of the weak points of this motor, limiting the current and voltage and leading to the degradation of insulation by brush dust. The motor was controlled by resistances in series with the motor which were gradually short-circuited during acceleration.

By introducing power electronics in traction drives, the thyristor chopper, a DC-DC converter, made continuous torque control possible. However, the motor was still of the same type and voltage and current harmonics generated by the chopper caused additional losses.

Thyristor converters have also been developed to supply load-commutated synchronous motors for traction drives, as applied in the French "train a grande vitesse" (TGV), which, however, does not belong to the light-rail traffic.

With the introduction of power semiconductors as the Gate-Turn-Off thyristor (GTO) and microelectronics, which made control algorithms and optimized switching patterns feasible, the inverter-fed squirrel cage motor became the standard traction motor. This motor was free of rotor maintenance in term of brushes and was more compact than the DC motor in terms of power density and torque density. More recently, the application of Insulated-Gate-Bipolar-Transistors (IGBT) allowed higher switching frequencies of converters in order to further reduce the harmonic contents of converter waveforms and to allow faster control of the drive.

At the same time compact and light bogie constructions were introduced. The aims here were minimum weight for energy saving, minimum maintenance and maximum comfort. These aims were intended to be reached by the integration of motor and mechanical drive within the bogie with a minimum of unsprung mass [KRA93, ZIJ94].

As a result, the drive which is state of the art is lighter on the one hand and more powerful on the other hand. However, switching converters resulted in discontinuous power flow which caused harmonics in currents and thus additional losses in the traction motor, vibrations and audible noise in the drive, which could reduce the lifetime of components.

Finally, low-floor tramway concepts led to new bogie and motor concepts. The wheel axle has been omitted in many concepts, so that each wheel has a single drive which is integrated, as much as possible, into the wheel. Still, the problem of reduction of unsprung masses in a single-wheel drive remains [HON95].

Not only have bogies become lighter, car-body developments have also gone in the direction of light-weight constructions. As this thesis deals with electromechanical drives, the accent is more on drive concepts than on vehicle dynamics. Locomotives with pulled cars present other problems, such as the dynamics of a chain of cars,

while the torque is transmitted only by the locomotive. These dynamics were not investigated in the research reported here.

1.2 State of research

Research on vibrations in traction drives is not new because research on this field has existed since the construction of the first vehicle. However, developments in drive technology and demands on maintainability have demanded continuous efforts in research on drive dynamics.

A great amount of research has been done in the field of railway vehicles and drive dynamics. Here, we discuss only research on the integration of electrical and mechanical drive and the analysis of system dynamics.

Research in this field can be divided into three topics:

- detection of oscillations due to fault conditions in electrical machines
- influence of induction machine torque pulsations on electromechanical drives
- oscillations in vehicle drives and their suppression.

The first topic is not treated in this thesis. It covers, e.g., the detection of winding faults and broken rotor bars and requires detailed analysis and knowledge of traction motor design. However, it may be of future interest in the research on oscillations. A single reference is made, however, as it combines vibration analysis by measurements with accelerometers and broken rotor bar detection [MUE96].

The influence of torque pulsations has been investigated by several researchers. Pestle and Varley have given an overview on the design of mechanical drives driven by electrical machines and have emphasized the need to design a drive as a system. [PES89]. Andresen et al. and Grieve et al. have presented an analysis of the influence of converter harmonics on the torsional stress of mechanical drives [AND82, GRI89]. Calculation of torsional stress caused by a current source inverter drive has been performed by Meister, while voltage-source inverter drives have been investigated by Keve and by Blaajberg [BLA93, KEV91, MEI92]. The influence of drive parameters on resonance phenomena has been treated by these researches.

Oscillations in rail vehicle drives caused by the contact between wheel and rail have been the subject of a number of recent research programmes. Various concepts of wheel slip control for high performance locomotives to minimize the phenomena described by Doppler have been developed. The purpose of the control strategy is

both to keep the force between wheel and rail near the maximum of adhesion and to prevent the slip-stick oscillations at the other hand. Models of the electrical and mechanical drive have been developed; they have various degrees of complexity. [DOP74, DUS92, BUS95, JOE95, SCH95, ENG96].
Asano et al. proposed a control concept to suppress vibrations in an induction-motor-driven hybrid vehicle [ASA92].
Oscillations in traction drives due to converter harmonics have been investigated by Ghiara et al., who considered a chopper driven locomotive [GHI92]. Poeze modelled an electrical multiple-unit equipped with induction motor drives and investigated oscillations caused by converter harmonics [POE92]. Poeze's work was the point of departure of the research discussed in this thesis.
Finally, oscillations in industrial drives such as rolling mills have been treated by several authors. Naitoh et al. and Butler et al. discussed the problem of the damping of torsional vibrations [BUT92, NAI94].
The importance of knowledge about the oscillation characteristics of electromechanical drives in general has been underscored by a number of researchers, and specifically for traction drives. A generalized approach to the determination of all types of oscillations in traction drives is, however, still missing.

1.3 Problem statement

This thesis deals with low-frequency dynamics of traction drives which are part of light-rail vehicles. Low frequencies are frequencies that are experienced by passengers as vibrations or frequencies of vibrations that may damage components. Vibrations which make the passenger feel uncomfortable will make him abandon trains. Vibrations on components will cause wear and tear which will keep the vehicles out of service. Here, we discuss the latter aspect. The system behaviour of the combined electrical and mechanical drive is here emphasized in trying to integrate the aspects of electrical and mechanical engineering.

The aim of this research can be split into two topics: Design and Reliability. Reliability means to keep the drive in operational condition and to solve and foresee the problems of vehicles in active service. On the one hand there may be damage to components which has to be analyzed in order to find the cause. To find causes is not an easy task, if the cause is not an accident. Causes can be also wear, construc-

tion faults, design errors or even specification errors. Traction drives are complex electromechanical systems which are in service under the roughest conditions. In order to find the cause of damage, methods have to be developed. In practice, fatal damages should be prevented by condition monitoring. The method to be developed must be suitable to monitor the drive and be able to give diagnoses to facilitate maintenance.

In addition to keeping in motion the vehicles in service by maintenance and repair, which is the task of the service engineer, there is the task of the designer whose intention must be to develop economically competitive drives with low initial costs and minimum operational costs, and a guaranteed lifetime of about 30 years. The designer's task is quite complex because it has to cover all the disciplines involved. First, the system is built up of a variety of components such as the traction motor, static converters, gearboxes, couplings, the bogie and so on. Then each component has to be developed while taking into account a variety of aspects:

electrical:	insulation of motor windings
	semiconductors
mechanical:	audible noise
	vibrations
	ageing
thermal:	motor and semiconductors
	gearbox and bearings
environmental:	ambient conditions
	electromagnetic compatibility.

Taking into consideration these design aspects, finite-element methods are the analysis tool to design and evaluate local stresses in traction motors, mechanical components and cooling units. Components will be designed and tested properly but they have to work together in the final product, the vehicle.

Here, not the detailed design of components is discussed, but the general design of the entire drive as a system, in regard to the interaction of components, in order to analyze oscillations. This means that phenomena and models are related to structures, components and their mutual parameters.

In summarizing the defined problem, the following questions have to be answered:

Which oscillations occur ?

How are they generated ?

How can they be described ?

How can they be measured ?

How can they be avoided ?

The problem statement is therefore:

- Develop a test procedure including data processing which enables the detection of oscillations in traction drives.

- Develop a method to model in a flexible and universal way traction drives, including electrical and mechanical drives, in order to describe and predict oscillations.

- Apply the developed methods to traction drives in real service and test the validity.

- Apply the developed methods to minimize oscillations.

1.4 Outline of the thesis

There are two main parts to the research, the methodology and the subject itself. Knowledge of oscillations is the aim of the research, while methodology is the medium to obtain the knowledge. Knowledge of the subject will lead to insight into failure modes and stress analysis and to design rules for traction drives.
The methodology is the core of the thesis as it aims to be universal, while phenomena and vehicles are specific cases to which the methodology is applied. The methodology has to be a synthesis of the methods used to investigate a mechanical structure, a switching converter, an electrical machine and a control system.
The traction drive under consideration is described in Chapter 2. Drive components and operation of the drive are explained as well as oscillation sources and phenomena, introducing the terminology used in this thesis. Limits of the investigated system are given.
The methodology is divided into several steps. First, experimental research has to lead to an overview of oscillation phenomena which can be observed. Here phenomena are pointed out taking into account of a variety of vehicles and their structures. An attempt is made to indicate causalities. This is treated in Chapter 3. Then, modelling is used to gain insight into mechanisms and causalities on the one hand and the influence of structures and parameters on the other hand. Modelling has to be flexible so that models can be developed for different structures and

degrees of complexity. For every model, the structure and phenomena to be investigated have to be noted. Chapter 4 discusses modelling and models.
Mechanisms and causes have to be explained by using simulation. Simulation is performed in the time domain and in the frequency domain in order to capture the majority of oscillation phenomena. Simulations are compared with measurements for validation. Chapter 5 treats simulation and validation of the electromechanical drive in various conditions of operation and in various modes of oscillations, emphasizing the interaction between electrical and mechanical drive.
In chapter 6, the evaluation of the problem statement, including a view on future research is given.

2 Electromechanical Traction Drives

2.1 Introduction

Considering the variety of traction drives that have been developed, an overview is given of the general structure of the drive system under consideration. A system description is followed by a description of drive components and their function. The choice of components to be included in research on oscillation is discussed.
Operation of the traction drive is described, introducing the terminology to be used in the thesis. Finally oscillation sources and phenomena are explained.

2.2 System description

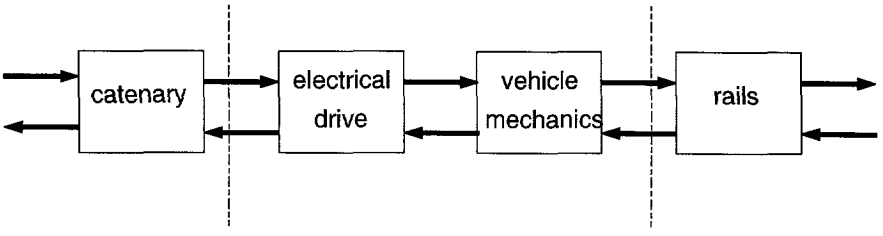

Figure 2.2.1 System description of a rail vehicle in its environment.

A system description of a railway vehicle system in its environment is given in Figure 2.2.1. The system consists of the electrical drive and the vehicle mechanics placed between the catenary and rails, including civil construction. This system is

investigated from the catenary to the rails while the dynamics of the line and substation and the civil construction and resulting dynamics are excluded.

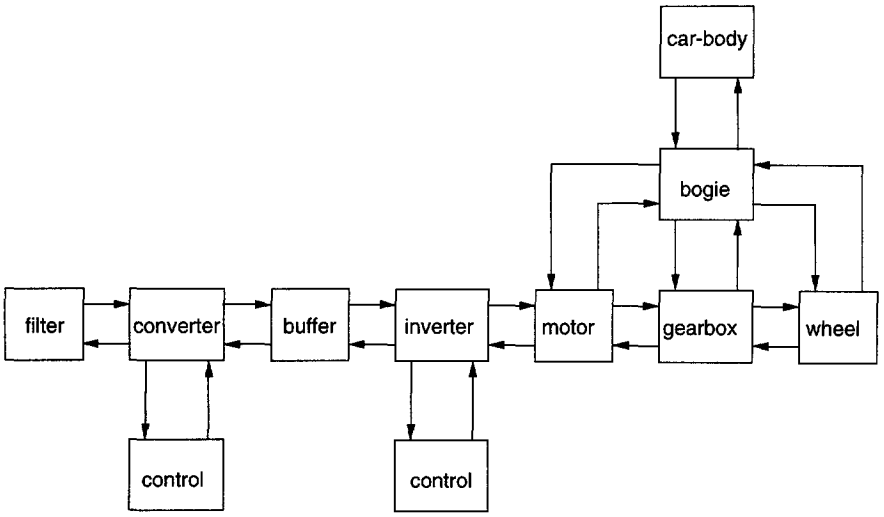

Figure 2.2.2. System description of a traction drive.

Figure 2.2.2 gives a closer look at the vehicle system under consideration. Light-rail vehicles have been developed for various supply voltages and supply systems, even as multiple supply systems. State railway catenary voltages are, e.g., 25 kV, 50 Hz AC (a part of France, Malaysia), 15 kV, 16⅔ Hz AC (Germany, Austria), 3 kV DC (Belgium, Italy) and 1.5 kV DC (The Netherlands). Tramway supply lines usually are DC lines with voltages from 600 V to 750 V, either via catenary or via third rail. A power converter has to convert the catenary voltage to the DC link inverter voltage, for tramway supplies a converter can be avoided in some cases. Modern electrical traction drives are bidirectional, which means that energy can be delivered to the catenary during braking. In cases when regenerative braking is not possible, energy is dissipated into resistors, since on-board storage devices do not provide economic solutions at the moment. The electrical drive is composed of a static converter and the traction motors, equipped with a control system which has to control motor torque and the power flow from catenary to the motor and vice versa. A single motor may be supplied by a single inverter, but in most cases two or more motors are supplied by one inverter while a vehicle is equipped with two or more inverters.

The car-body of the vehicle is placed on bogies. In the case of a motor driven bogie, the drive torque is transmitted by a gearbox to the wheel shaft. There are various concepts of bogies and drive lines for light-rail vehicles. Some of them are investigated in this thesis.
Since the main purpose of the research is the analysis of interaction between motor and mechanical drive, a variety of converter and control concepts have been excluded from investigation.

2.3 Drive components

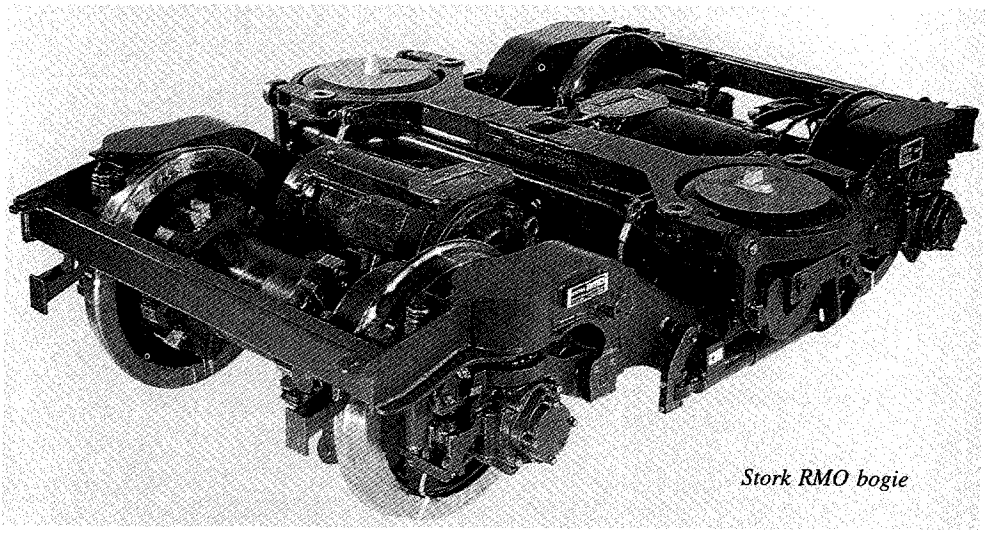

Figure 2.3.1 Electrical multiple-unit bogie (courtesy of Stork RMO).

Bogie
Figure 2.3.1 shows the example of a recently developed motor driven bogie. The main components of a bogie are the traction motor, the gearbox transmission and the wheel-sets which are connected by elastic or rigid couplings. Motor and gearbox are suspended from the bogie frame. The wheel-sets are suspended from the bogie frame by the primary suspension, while the car body is suspended from the bogie by the secondary suspension. In some cases a transverse beam between the bogie frame and the car body provides an additional suspension.

Traction motor

The traction motor under consideration is the induction squirrel-cage motor. Figure 2.3.2 shows a view of an electrical multiple-unit motor. For low power an alternative to the induction motor is the synchronous motor with permanent magnets which has a higher power density and is more efficient at low speeds [HEN94]. The induction motor, however, is the motor type most often used in recent light-rail vehicles with a superior power and torque density at high speeds [KEM94, DRE94, TUI96]. The induction motor is usually fed by voltage-source inverters in traction drives.

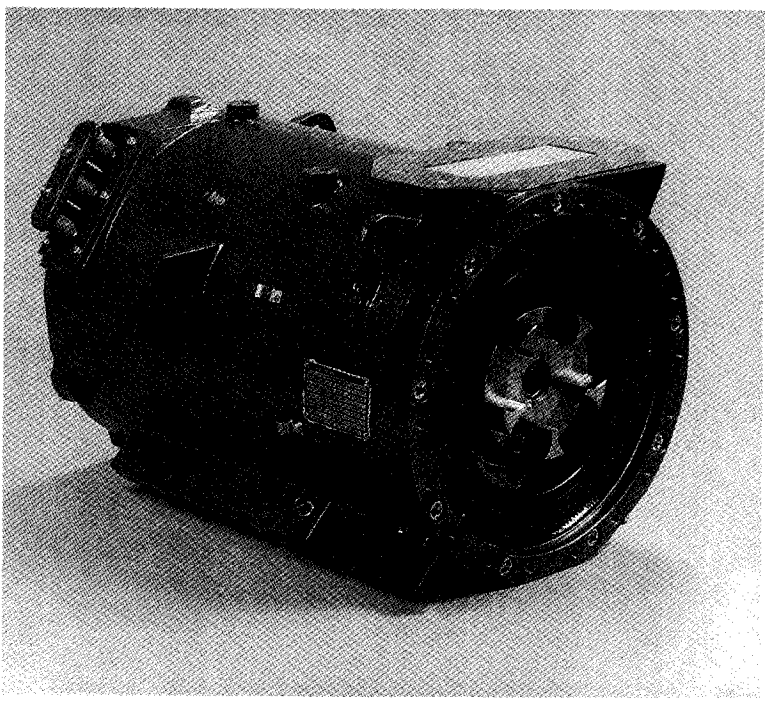

Figure 2.3.2 Induction motor for traction (courtesy of Holec Ridderkerk).

Line filter and converter

Figure 2.3.3 shows a block diagram of the power converter. The task of the line filter is to suppress converter harmonics which may interfere with signalling frequencies in the catenary and to suppress current and voltage transients near substations that may exceed peak values of the converter. The task of the line

converter is conversion of the catenary voltage into a constant DC voltage to supply the inverter. The line converter may be bidirectional for driving and regenenerative braking. Since regenerative braking is not always possible, a brake chopper is placed between the inverter and the line converter which allows the dissipation of energy into resistors. In some cases the line converter is omitted, e.g., with tram car drives the inverter of which is directly fed by the catenary voltage of 600 V or 750 V. The catenary filter and line converter dynamics have been excluded from investigation, since the drive under consideration mainly operates with a voltage DC link. Due to the capacitor in the DC link, the voltage ripple is small in comparison with that of the DC voltage.

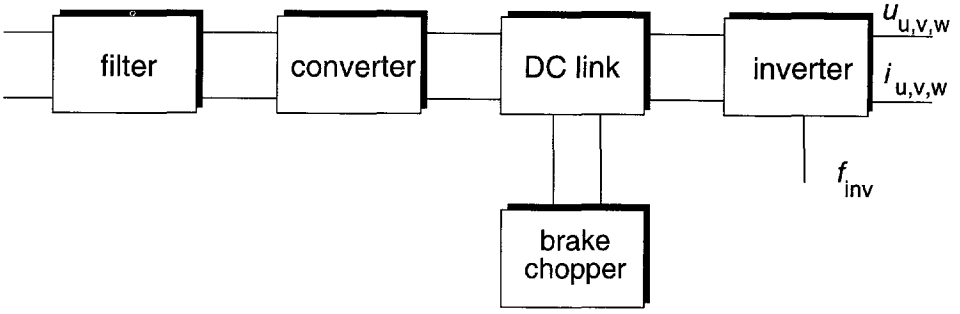

Figure 2.3.3 Block diagram of power converter.

Voltage-source inverter

The circuit diagram of the inverter is given in Figure 2.3.4. A symmetrical three-phase voltage is generated by the six switches connected to the DC voltage u_{cinv}. Figure 2.3.5 shows the generated waveforms. By applying pulse patterns, sinusoidal waveforms can be approximated, such as those illustrated in Figure 2.3.6. However, switching voltages will generate harmonics. Gate-Turn-Off Thyristors have been applied as switches in traction inverters for years, allowing the switching of high currents at high voltages at a switching frequency of hundreds of Hertz. More recently, the Insulated-Gate-Bipolar Transistor has been introduced into traction inverter technology. It allows a higher switching frequency with a DC voltage up to values higher than 750 V.

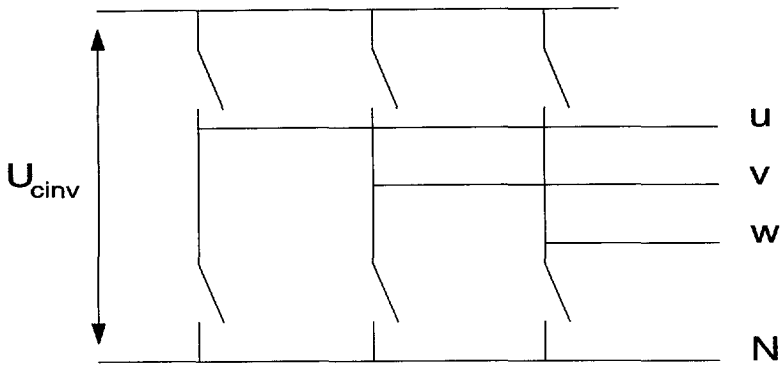

Figure 2.3.4 Schematic diagram of three-phase inverter.

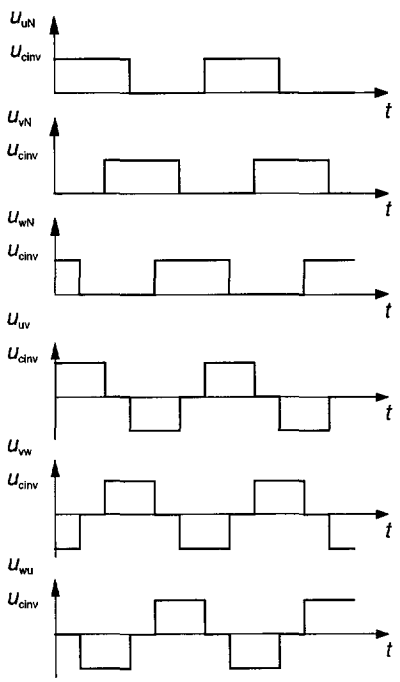

Figure 2.3.5 Inverter waveforms.

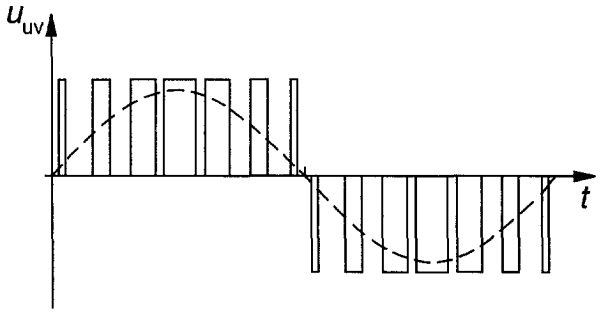

Figure 2.3.6 Pulse-width-modulated (PWM) inverter waveform.

There are numerous concepts of pulse-width modulation, following different criteria [DEP88, HOL93 ,VEL94 ,POL92]. Some of the criteria are:
- a minimum of the sum of converter and motor losses
- elimination of torque harmonics
- suppression of mechanical resonances
- suppression of converter harmonics which may interfere with signalling frequencies in the catenary.

The task of a pulse-width modulation technique is to optimize the pulse pattern following the above criteria. Pulse-width modulation patterns can be generated off-line or on-line, depending on the applied control system on the one hand and the processor speed on the other hand. In practice, a compromise has to be found.

Control

The design of control systems and algorithms has been excluded from the thesis because of the variety of algorithms which have been applied and developed over the past years. However, based on the open-loop model, a few remarks are made regarding the control tasks.

Traction control consists of:
- electrical motor control, i.e., control of the torque generated by the motor,
- drive control, i.e., control of the force transmitted from wheel to rail.

The ideal motor control is instantaneous torque control, which provides an instantaneous torque response to the torque reference by compensating the motor time constants.

A control system which provides fast torque response is based on flux vector orientation. [BLA73]. An example of a basic scheme is shown in Figure 2.3.7. A motor model calculates torque and flux in field coordinates from phase currents and shaft speed. The control system has a flux and torque setpoint. PI controllers provide current setpoints in field coordinates. Voltage setpoints are generated for the inverter by PI controllers and a decoupling algorithm or hysteresis controllers.

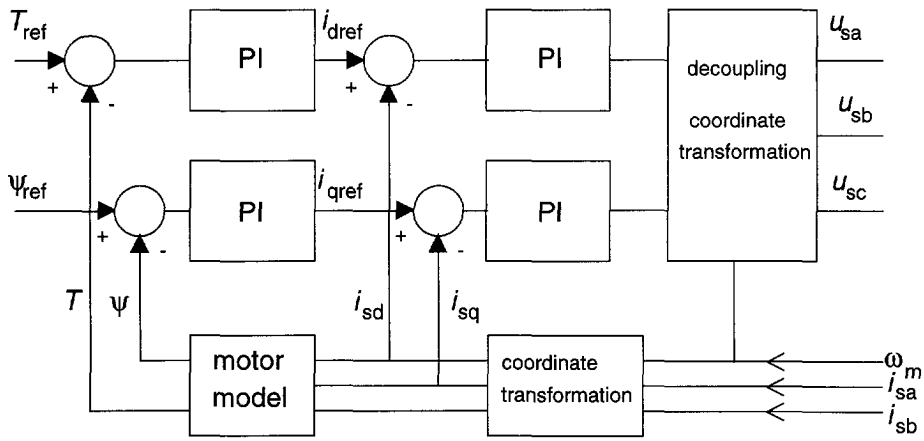

Figure 2.3.7 Principle of vector control.

Direct Self-Control

In order to improve torque response Direct Self-Control has been introduced by Depenbrock as shown schematically in Figure 2.3.8 [DEP85, JAE88]. Torque and stator flux are calculated by using a machine model, that measures stator currents, DC link voltage, the switching states of the inverter and the rotor speed of the motor. A hysteresis controller compares the calculated stator flux with the reference flux generating the torque-generating voltage reference vector $K_{1,2,3}$. The torque hysteresis controller compares the calculated torque with the reference torque and generates the voltage vector of the inverter, which may be the torque-generating voltage vector or the zero voltage vector. A fast torque response is obtained. The described scheme is valid at rated field of the induction motor down to the minimum speed of the motor. Below the minimum speed Indirect Self-Control (ISC) is

applied, using torque and flux regulators which generate sinusoidal voltage references that are transformed into inverter switching states by pulse-width modulation (PWM). In the field weakening range, the flux reference is omitted and the torque is controlled by a torque regulator acting on the flux hysteresis controller.

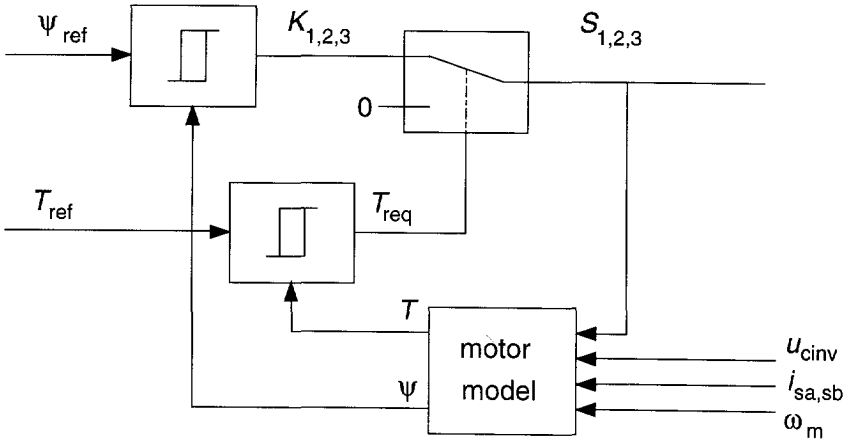

Figure 2.3.8 Principle of Direct Self-Control.

The above-mentioned two control systems are not investigated within the context of this thesis but have been mentioned because of their application as state of the art in traction drive control.

The ideal drive control maintains the force transmitted from wheel to rail without transients. The drive control includes the elasticity of the mechanical drive and the dynamics of the power converter. The main control task is to guarantee transmission of the required torque to the rails, maintaining the stability of the system. Considering the poorly damped wheel shaft, the control system has to provide active damping of oscillations by increasing the damping. Several concepts have been presented [ENG96, BUS95]. The difficulty lies in the absence of sensors which measure the wheel speed, so that traction control is based on motor control.

2.4 Drive operation

Oscillations in traction drives can occur under two kinds of circumstances:
1. normal operation of the drive,
2. faulty drive conditions.

Operation of the drive may coincide with various track conditions and various wheel conditions. Normal conditions of operation can be described by a standardized traction cycle. A cycle can be divided into acceleration from standstill, coasting, which means rolling at zero reference torque, or maintaining speed, braking to standstill and stop time. There are variations such as starting with or without motor flux at standstill, and various sequences of acceleration and braking from and to various vehicle speeds. The cycle can be divided into several steps:

- building up the flux of the induction motor (approximately one second)
- building up torque with a limited rise time in order to avoid jerk on the vehicle (approximately one second)
- acceleration with a defined torque
- coasting (rolling with zero reference torque) or maintaining speed at reduced torque
- braking with defined torque up to standstill
- standstill.

Figure 2.4.1 shows an example of the torque and speed of a traction cycle. A torque-speed characteristic is given in Figure 2.4.2.

Torque is limited by the maximum current of motor, inverter or catenary. Constant torque can be generated up to the maximum power of the drive which may be determined by motor, inverter or catenary. At higher speeds the torque is further limited by the reactive power of the drive. Up to a certain frequency, depending on motor design, the motor flux is kept constant by increasing the stator voltage with the stator frequency. At maximum stator voltage, given by the motor winding insulation, the voltage is kept constant with increasing frequency so that the flux decreases, the field-weakening region. Maximum speed of the drive may be limited by the mechanical transmission, by the motor circumference speed and the lubrication of motor bearings, but also by the inverter frequency.

During braking the energy may be delivered to the catenary or dissipated in braking resistors, depending on the catenary voltage and control parameters. At low speed

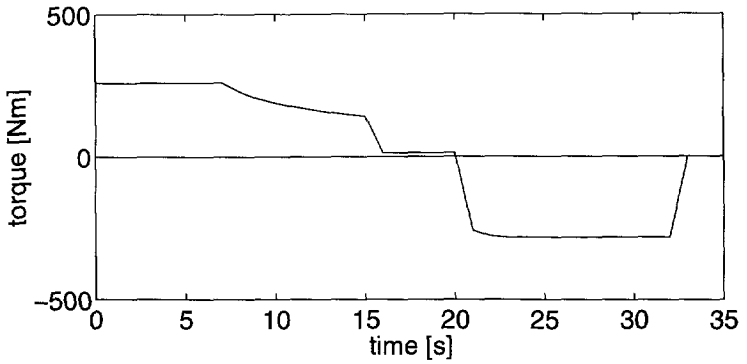

Torque during traction cycle.

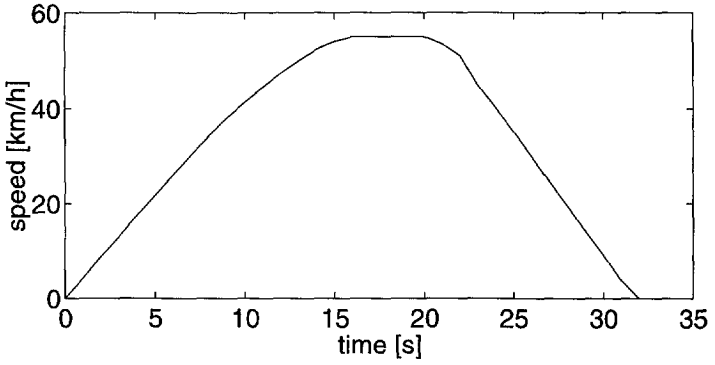

Speed during traction cycle.

Figure 2.4.1 Example of a traction cycle.

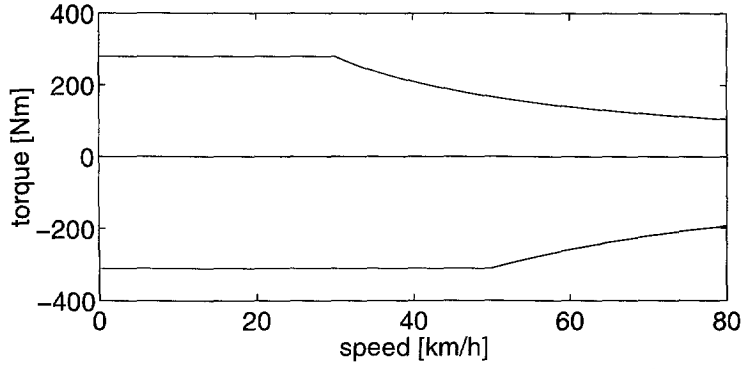

Figure 2.4.2 Torque-speed characteristic of a traction drive.

and during emergency braking, the mechanical brake, which is usually a disc brake on the wheel axle, will be operating. For trams, a magnetical rail brake and sand-distributing devices assist the braking effort during emergency braking.

2.5 Oscillation sources

Under normal operation at a single drive level there can be the following causes of oscillation:

Converter voltage harmonics
Normally, they are generated because converter voltages are switched voltages. Therefore there will be current harmonics in the converter currents. The current harmonics cause losses but may also cause resonances as they meet natural frequencies of the converter circuit. Further, voltage harmonics cause current harmonics and flux harmonics. These harmonics generate together with the fundamentals a series of torque harmonics. The torque harmonics stress the mechanical drive and may cause mechanical resonances.

Motor fields
As the motor field distribution is not sinusoidal due to windings, slotting, saturation or eccentricity, harmonic torques can be generated by harmonic fields under normal operation conditions. Transient fields normally decay, however, in certain circumstances, transients are undamped and cause torque oscillations.

Critical speed of mechanical drive
During acceleration or braking, the natural frequencies of the mechanical drive can be excited thus generating radial oscillations. The same applies to torsional and radial oscillations introduced by the motor and track-induced excitation.

Responses caused by the control system
Usually the control system is based on torque control. The operator has a limited number of setpoints. The torque response due to changing the setpoint will cause a transient in the drive. Further, there are control functions such as wheel slip control, which cause torque transients.

Responses caused by the rails
On the one hand, there are switches and crossings under various rail conditions which cause transients in the drive, on the other hand, there is the loss of adhesion which may cause oscillations of the mechanical drive.

If oscillations are caused by the converter, motor or control system, the design can be optimized to eliminate their causes, or reduce oscillations. If oscillations are caused by the rails, the design can only be optimized to minimize oscillations without the possibility of eliminating the causes. Oscillations caused by loss of adhesion can be minimized by appropriate control design.

Fault conditions can be classified as follows:

Asymmetries in the convertor
There can be differences between voltages in a three-phase system which cause additional fields and thus torques. There can also be converter faults which cause high transient torques such as short-circuits of the motor caused by the inverter.

Asymmetries in the motor and drive
Motor asymmetries can be winding faults in the stator or in the rotor, such as broken rotor bars. Eccentricity of the rotor can also occur; this causes additional fields and torques. If more motors are supplied in parallel by a single inverter they can interchange energy if wheel diameters or motor parameters are not equal.

Mechanical drive
Several of the causes of mechanical oscillations are imbalance, misalignment, resonances, rolling element bearing faults, gear faults and mechanical looseness. In combination with suspended mountings or flexible drive components they can excite the drive.

Loss of traction
Faults in the electrical drive or the mechanical drive, such as coupling failures, can cause the loss of traction of one or more motors in a vehicle. Transients will occur first, followed by asymmetries in the vehicle propulsion.

Oscillation phenomena which can occur in the drive system can be classified as being:

- harmonic sinusoidal
- general periodic
- damped natural oscillation
- pulse function
- step function.

Converter harmonics and motor field harmonics cause periodic oscillations generated by internal sources. Transients will appear as damped natural vibrations while wheel-rail influences will mostly usually as pulse functions or statistical random signals.

Above, the possible causes of oscillations which are known *a priori* have been listed. The research has to show if and how these phenomena occur, their mutual dependence and which other phenomena occur.

3 Measurement of Oscillations

3.1 Introduction

The first step in the research is to design experiments which facilitates the measurement of oscillations in the field. Measurements give the researcher an idea what oscillations are measurable and what oscillations occur under the various conditions. The main questions are: what should be measured, how to conduct the measurements and how to interpret the measured signals. A procedure must be followed which obviates errors that could generate an amount of measured data acquired under conditions that are not clearly defined.

When the aim of the measurement is defined, the following four steps have to be taken:

- choice of sensors
- choice of experiments
- data acquisition
- data processing.

Because this is the standard procedure when carrying out any measurement, we apply it here to measurements of oscillations.

The choices that are made are determined by the phenomena which are expected to be measured. The placement and choice of sensors includes sensors to be placed in the electrical drive, the mechanical drive and the control system through the selection of signals which are representative for the oscillations in the drive under consideration. The optimum between a minimum number of sensors and the maximum information about oscillation phenomena has to be found.
The choice of experiments includes traction cycle parameters such as acceleration,

coasting and braking time. Traction effort during acceleration and braking, rail and track conditions and ambient conditions have to be defined and to be documented. The definition of experiment conditions is essential for analysis. Data-acquisition parameters have to be chosen carefully in order to avoid the loss of valid signal information. These aspects of experiment design are discussed in section 3.2.

Data analysis is discussed in section 3.3. The first step in analysing data is plotting in the time domain. Acquired data have to be analyzed in order to evaluate the information that the signals contain. Frequency domain analysis is commonly used for vibration monitoring and analysis. Well-known methods are applied to detect and analyze phenomena. Various phenomena under normal operation conditions are analyzed.

Measurements on track and on a roller bench were performed in order to gather as much information as possible. Four different vehicle types were under investigation, an electrical multiple-unit, a metro vehicle, a tram-car equipped with a prototype low-floor bogie and a locomotive; the latter was tested on a test bench for railway vehicles [OVE95, WIN94, WIN94/2, WIN94/2, WIN94/3, WIN95, WIN95/2, WIN95/3].

3.2 Experiment design

3.2.1 Sensors and transducers

The choice of sensors depends on the phenomena to be measured on the one hand and on the structure of the drive on the other hand. The main limitation is the access to points of measurement. For example, rotating shafts of a gearbox transmission have to be equipped with sensors before mounting the gearbox. Further, signals of the control system which are not included in the monitoring system of the control are difficult to access.

Figures 3.2.1 to 3.2.4 show the drive types and corresponding sensor configurations investigated during the research. Figure 3.2.1 shows the electrical multiple-unit drive. A DC-DC converter (A) converts the catenary voltage into a constant DC voltage. The inverter controlled by the control system supplies a three-phase voltage

to the two motors of the bogie which are in parallel. The motor shaft is connected to the pinion wheel of the gearbox by an elastic coupling. The gearbox provides the transmission of the torque to the wheel axle thus reducing the angular speed. The gear wheel is mounted on a hollow shaft which is coupled to the wheel axle by an elastic coupling. Motor and gearbox housing are connected rigidly to each other and are suspended in the bogie frame by three rubber silent blocs (S1,S2,S3). The position of torque sensors has been indicated by the letter t, the position of accelerometers by the letter a and the position of displacement sensors by the letter d. The sensors, as indicated in Figure 3.2.1, were chosen to investigate the oscillations of the electrical and mechanical drive in the bogie frame. Using the existing sensors of the electrical drive, the inverter currents, instead of the motor currents, were measured so that distribution of currents between the motors is not taken into account. However, the angular acceleration of the second motor was derived from measurement of the angular velocity in order to obtain information from both motors. Reduction of mechanical sensors was obtained by assuming that axial displacement of the motor, the horizontal acceleration of the gearbox and the axial acceleration of the wheel axle are uniform.

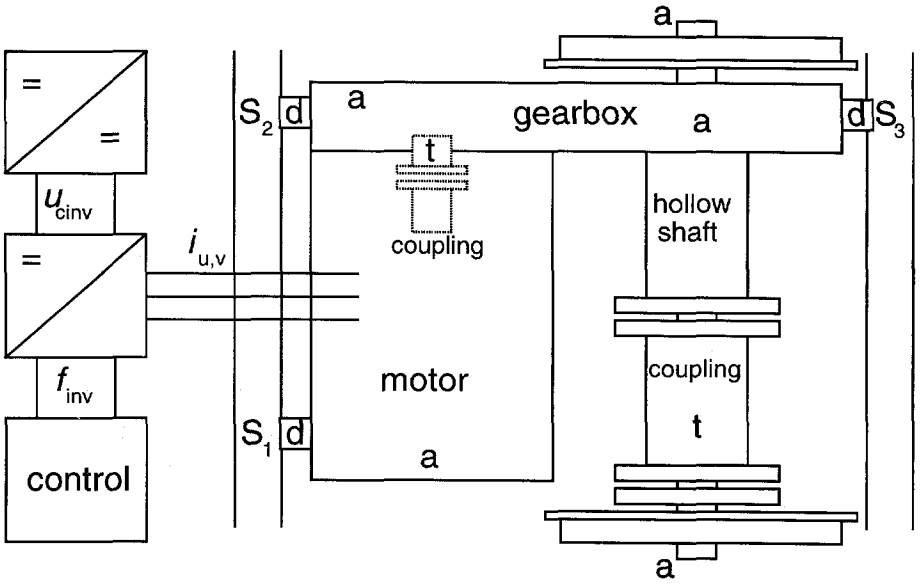

Figure 3.2.1 Sensor configuration in electrical multiple-unit drive.

Figure 3.2.2 shows the sensor configuration of the metro vehicle drive. The composition of the vehicle is the same as the tram-car shown in Figure 1.1.1 in

section 1.1. Each inverter supplies three motors in parallel. Inverter currents and the angular speed of all three single motors were measured. The drive is composed of a cardan shaft and a bevel gearbox. The cardan shaft is connected to motor and gearbox by elastic couplings. The cardan shaft torque was measured on the second of the three bogies, i.e. the one which supports both car bodies. Reference torque and feedback torque of the inverter control represent the sum of torques of all three motors.
With this configuration, mainly torque oscillations and peaks generated by the electrical drive were investigated.

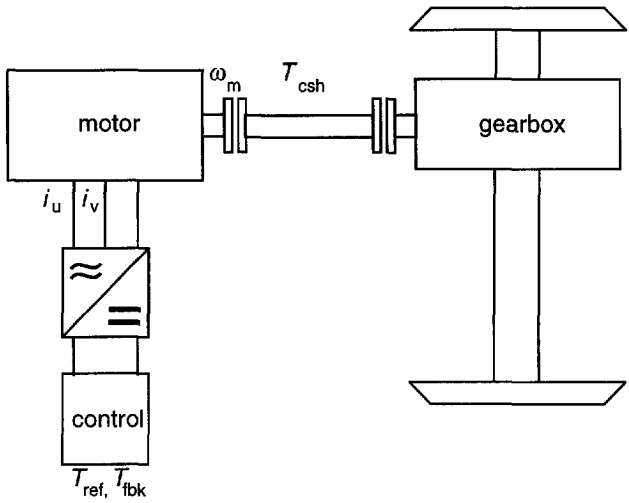

Figure 3.2.2 Sensor configuration in metro vehicle drive.

The low-floor bogie drive is depicted in Figure 3.2.3. Each wheel is driven by its own motor and a planetary gearbox. Each motor is supplied by one inverter. The control acts on both inverters of the bogie, so that an electrical axle instead of a rigid axle has been realized. Drive oscillations and shock loads excited by the rails were measured.

Last, Figure 3.2.4 shows the sensor configuration of the locomotive drive. The drive configuration is similar to the electrical multiple-unit drive, however, the motor shaft is connected rigidly to the pinion wheel of the gearbox. The sensor configuration is similar to the metro vehicle drive configuration. In addition, DC link voltage and current of the inverter and catenary voltage were measured. Due to the capacity

of the test bench facilities, more electrical drive signals could be acquired, while the monitoring interface of the previously described vehicles limited the number of electrical drive signals.

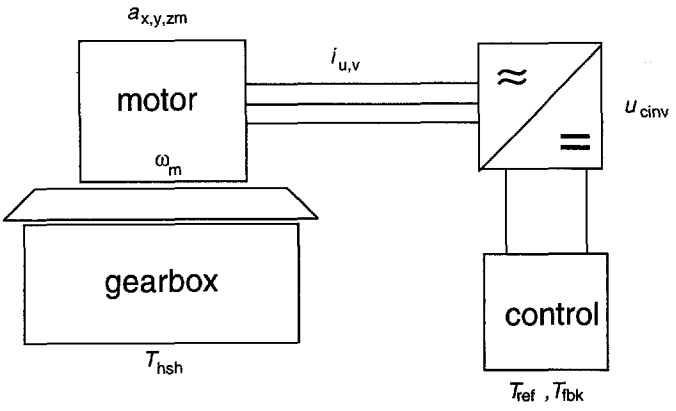

Figure 3.2.3 Sensor configuration in low-floor bogie drive.

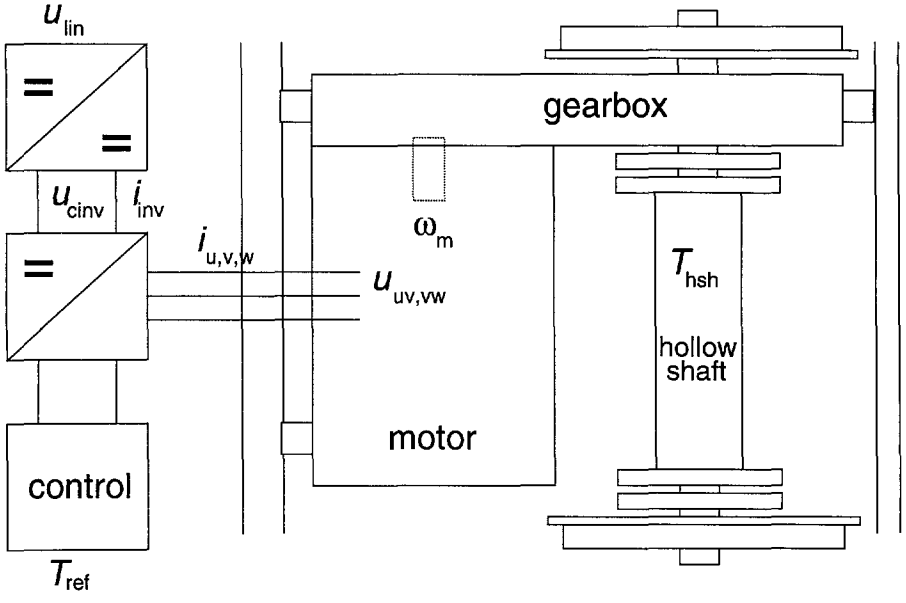

Figure 3.2.4 Sensor configuration of locomotive drive.

symbol	signal	function/place	part of the system
T_{ref}	torque	reference	control system
T_{fbk}	torque	feedback	control system
f_{inv}	frequency	inverter	control system
u_{lin}	voltage	catenary	power converter
u_{cinv}	voltage	inverter DC link	power converter
i_{cinv}	current	inverter DC link	power converter
$u_{uv,vw,wu}$	voltage	inverter line	power converter
$i_{u,v,w}$	current	inverter phase	power converter
ω_m	angular speed	motor shaft	traction motor
α_m	angular acceleration	motor shaft	traction motor
ax,y,z_m	acceleration	motor housing	traction motor
x,y,z_m	displacement	motor housing suspension with respect to the bogie frame	traction motor
T_{cpm}	torque	coupling motor side	mechanical drive
T_{hsh}	torque	hollow shaft wheel side	mechanical drive
T_{csh}	torque	cardan shaft	mechanical drive
ax,y,z_{gm}	acceleration	gearbox housing motor side	mechanical drive
ax,y,z_{gw}	acceleration	gearbox housing wheel side	mechanical drive
ax,y,z_{pg}	acceleration	wheel axle bearing housing gearbox side	mechanical drive
ax,y,z_{pc}	acceleration	wheel axle bearing housing coupling side	mechanical drive
x,y,z_{gm}	displacement	gearbox housing motor side suspension with respect to the bogie frame	mechanical drive
x,y,z_{gw}	displacement	gearbox housing wheel side suspension with respect to the bogie frame	mechanical drive

Table 3.1 Sensors and signals for measurements.

Table 3.1 shows the signals and sensors which have been used throughout the experiments. Voltage and current sensors and control system signals are usually present in the electrical drive system and can be used for measurement purposes. In such experiments the quality of the signals derived from the electrical drive in terms of precision, bandwidth and noise of the signals has to be specified.
Mechanical sensors which are commonly used are

- strain gages for torques on axles
- piezoelectric accelerometers for acceleration
- linear voltage differential transformers (LVDT) for position

[PRO94, BRA91].

One of the most valid but also most difficult measurements is the measurement by strain gages of torque on rotating axles of the drive. The major difficulty is the harsh environment of the measurement. A traction drive is exposed to humidity and dirt, to high shock loads excited by the rails and also to electromagnetic fields from traction motors and converter coils.

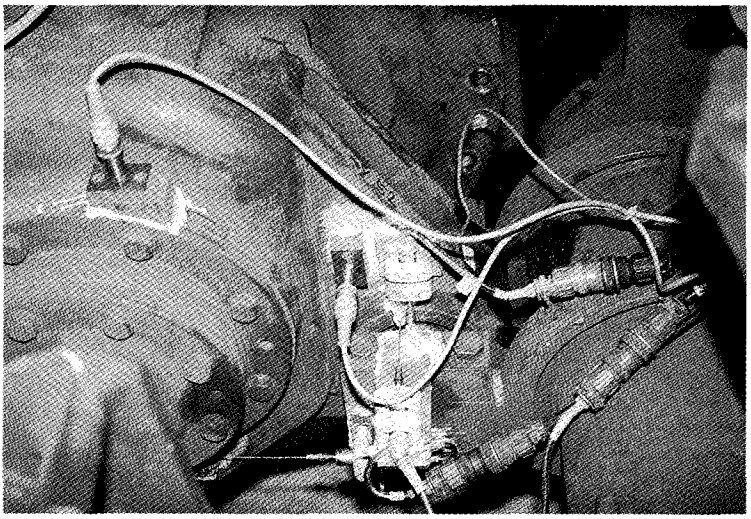

Figure 3.2.5 Acceleration and displacement sensors on a bogie (courtesy of Nederlandse Spoorwegen).

The choice and placing of acceleration and displacement sensors is less critical. It is important to choose the right sensors' positions and the appropriate ranges. Short wiring to the amplifier and galvanic separation from the drive is recommended. Figure 3.2.5. shows acceleration and displacement sensors on the gearbox suspen-

sion of a bogie. The ranges of the sensors depend on their position in the drive. The range of acceleration sensors depends on their position related to the rails, as forces generated by the wheel-rail contact are the highest within the drive and they increase with speed. Accelerations up to 70 g can be reached when passing a switch at 160 km/h. Displacement sensors with a range of 1 mm or 5 mm are usually chosen. Due to the high resolution of the sensors small displacements can be measured.

Accurate wiring is one of the essential prerequisites to achieving successful measurements. Short wires are required between sensor and signal conditioning unit because of the above mentioned environmental conditions. As distances within a vehicle between bogie, power converter and data acquisition system may be several meters the elimination of noise has to be considered. In some cases long cables are used for signal transport; these will be sensitive to electromagnetic fields and ground loops. The following rules have to be respected:

- Only strong signals should be transmitted by cables, which means that signal conditioning should be as close as possible to the sensor.
- The cables should be as short as possible and as far away as possible from power circuit cables. Depending on the type of signal source, single-ended ground referenced, single-ended non-referenced, or differential amplifier input configuration should be chosen as appropriate.
- The grounding of signals should be concentrated in one point and be kept separately from power circuit grounding.

3.2.2 Experiments

Experiments on track must be well planned as a vehicle has to be available and the track has to be free in order to obtain well-defined traction cycles. Therefore experiments have to be performed at night when there is no service, or in the daytime while taking account the scheduling of trains in regular service. As tests on track are expensive and often not repeatable because of the time limit, experiments on test rigs are an alternative. Distinctions can be made the three types of test rig. First, there is the classical motor test rig with a DC machine or/and an inertia as load. Second, there is a test rig for drives including gearbox transmission and (part of) the bogie as described, e.g., by Welsch [WEL95]. Last, there are vehicle test benches which enable the simulation by a roller rig of vehicle operation on rails.

Worldwide, there are several vehicle test benches as mentioned by Vinyolas et al. [VIN93]. We performed measurements with a locomotive on a vehicle test bench shown in Figure 3.2.6 and described by Vitrano et al. [VIT93].

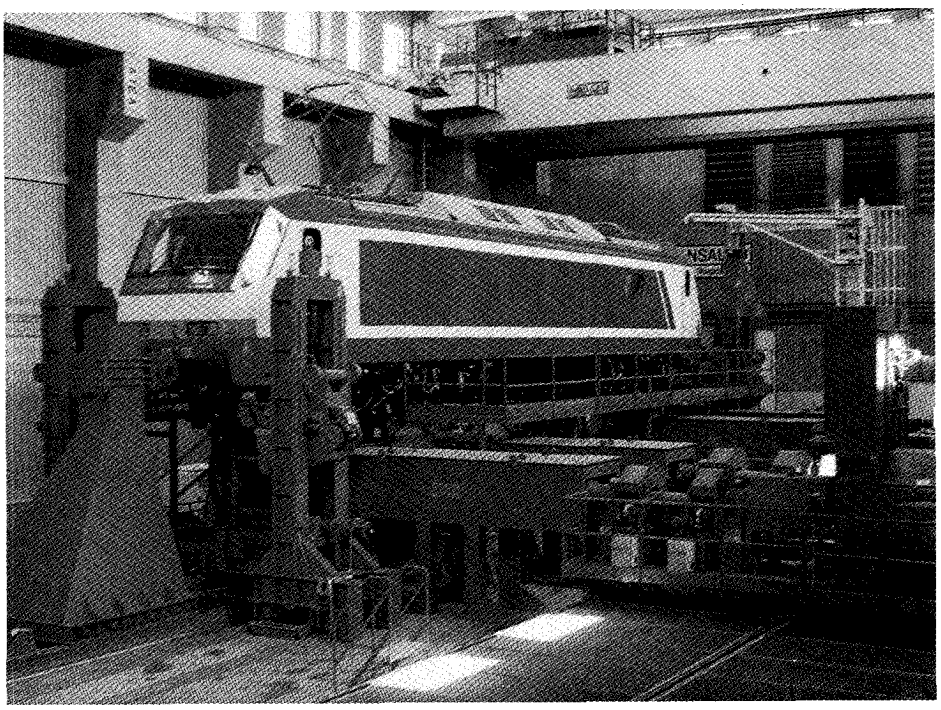

Figure 3.2.6 Locomotive on vehicle test bench (courtesy of Ansaldo Trasporti).

Defining experiments means defining test conditions as there are:

- control system parameters
- torque reference as function of time (traction cycle)
- track and rail conditions
- ambient conditions.

The control system parameters are not here discussed since they depend on the individual system under consideration.

The drive cycle parameters are:

- acceleration time
- coasting (zero reference torque) time

- braking time
- standstill time
- torque during acceleration
- torque during braking (electrical and mechanical braking).

Track and rail conditions are:

- ramps, tunnels, bridges
- curves, crossings, switches
- specific rail faults as described in a test rig specification [ALT78]
- humidity of rails, dirt and surface conditions.

Ambient conditions are:

- temperature
- humidity
- wind.

The following strategy to define experiments has to be followed in order to measure the oscillation characteristics of a drive in a defined frequency band under defined conditions.

A traction cycle with constant torque or constant power during acceleration and braking enables the covering of a certain frequency band within a limited time. The electrical multiple unit reaches 60 km/h after 25 seconds at maximum torque. At that speed the inverter frequency is approximately 56 Hz, the motor shaft frequency is little less than 28 Hz and the wheel shaft frequency is 6.5 Hz. The fifth harmonic of the motor current has a frequency of 280 Hz while the gear tooth frequency of the gear wheels is approximately 448 Hz. By varying the torque and the maximum speed test time, the acceleration and frequency band can be chosen. The choice depends on the phenomena to be investigated. In practice, it may not be easy to maintain constant reference torque during operation, as the operator on the one hand and the control system on the other may react to external influences such as signalling or wheel slip.

Experiments at constant or slowly varying speed may be useful to investigate phenomena which occur at a certain frequency of a drive. However, tests at constant speed are only possible if the drive is speed controlled. Experiments on specific tracks are useful to investigate dynamics in curves and oscillations excited by switches and crossings. Fault operation can be simulated or generated, but sometimes it is not controllable or not desirable as it may lead to damages in the case of inverter faults, which lead to motor short-circuit. In any case, the amount of data has to be limited to avoid an abundance of information.

3.2.3 Data-acquisition

After having specified signals and tests the digital data-acquisition system which stores the signals has to be defined. A data-acquisition channel includes a sensor, signal conditioning, amplifier, anti-aliasing filter and analog-to-digital converter. The parameters of data-acquisition have to be chosen properly as there are:

- amplification
- filter characteristics and cut-off frequency
- data-acquisition resolution
- sampling frequency.

The amplification factor has to be chosen such that the maximum range of the analog-to-digital converter is used for the maximum resolution of the signal. The amplifier inputs may be single-ended or differential, depending on signals sources and noise suppression requirements.

Analogue filtering is necessary in order to obviate the aliasing of signals. Shannon's sampling theorem states that "to recover a continuous-time signal exactly, the sampling frequency should be chosen such that the signal does not contain any frequencies above the Nyquist frequency" which is half of the sampling frequency [BOS94]. In practice, anti-alias filtering is done in two stages. First, the signals are filtered by an analogue filter and sampled at a high frequency. Then the sampled signals are filtered digitally thus obtaining the desired bandwidth [AUS96].

The sample frequency is determined by the bandwidth. It is recommended to choose the sample frequency to be more than ten times the bandwidth to obtain sufficient resolution while Shannon's theorem requires a minimum of two times the bandwidth. Usually, a sample frequency of 1 kHz is chosen, in some cases 2 kHz or 5 kHz. The storage capacity of the system is a limitation. In the case of recording by an analogue or digital data recorder the storage capacity is highest.

Sampling has to be simultaneous for all channels to apply correlation analysis correctly. This can be obtained by one analog-to-digital converter per channel, which is an expensive solution or by a sample-and-hold buffer followed by a multiplexer and a single analog-to-digital converter for all channels. In the case of, e.g., 20 channels and a sample frequency of 1 kHz, there will be a maximum delay of 20 ms between the first and the last channel if simultaneous sampling is not provided.

The resolution of signals is determined by their dynamic range. In the performed measurements, the highest resolution was required for the measurement of the

torque oscillations. Normally, 12 bits should be sufficient, which provides a resolution of approximately 0.5 ‰. At a maximum torque of 10 kNm to be measured, oscillations in the order of 10 Nm could be recognized with a sufficient resolution.

3.3 Oscillation analysis

3.3.1 Data processing

Considering the previously chosen sensors, there are three kinds of signals each requiring a specific data processing. First, there are slowly changing DC signals such as torque, speed, displacement and the inverter DC link voltage which are superposed with oscillatory signals. Second, there are switched signals, such as converter currents and converter AC voltages and, third, there are oscillatory signals containing peaks such as acceleration. Oscillation phenomena may be damped or undamped periodic, non-periodic, such as transients, and stochastic, such as excitation from the rails.

Here, the most important aspects of the signals acquired during the tests are discussed, in particular the chosen analysis methods and the errors made by using them.
Oscillation analysis has to extract the harmonic content of the acquired signals. As, during a traction cycle, the frequency of the drive changes continuously an approximation has to be found to quantify the phenomena. Mainly, two forms of data representation were chosen, time-domain plots and amplitude spectrum plots.
In cases where the signals will be sampled again, after being stored by the data-acquisition system, they require another anti-aliasing filter, in this case digital. Filtering may also be necessary in order to eliminate noise and frequencies which are beyond the frequency of interest. Further the offset of signals and spikes have to be removed.
A technique to analyze rotating machinery is the "waterfall" or "cascade" diagram [DIM92]. The spectrum of the measured signal is plotted as a function of rotational speed. Harmonic-order-related frequencies can in this way be distinguished from those related to structural natural frequencies. Here, this technique is extended to signals of the electrical drive. Instead of a function of speed, the amplitude spectra

are plotted as a function of time creating a relation to the time domain plots.
To compute a cascade diagram, the data set of a signal of a traction cycle has to be divided into equal parts. For each part the spectrum will be calculated. The cascade diagram is composed of the spectra as a function of time.
To be able to choose the right parameters the Fourier analysis is resumed. In digital signal processing, the Discrete Fourier Transform (DFT) is applied and use is made of an algorithm, the Fast Fourier Transform (FFT), which reduces computation time. Essentially, the DFT generates a discrete and a periodic spectrum from of a discrete and periodic signal. However, the signals to be measured are non-periodic and continuous. After sampling they become discrete. As discrete spectra cannot be obtained from non-periodic signals, the signal has to be assumed to be periodic. Considering a discrete signal

$$x(n) \ , \quad n = 0, 1, 2 \ ...$$

a data set of N samples $n_d = 0,1,2...N\text{-}1$ will is taken with a sample frequency of f_0. This data set is assumed to be a period of a periodic signal. Hence, the Discrete Fourier Transform can be calculated as

$$X(k) = \sum_{n=0}^{N-1} x_d(n) \ e^{\frac{-j \ n \ k \ 2\pi}{N}} \ , \quad k = 0, 1, ..., N-1 \ .$$

The spectrum is discrete and contains frequencies which are multiples of the frequency f_0/N. A finite number of samples can be interpreted as taking a rectangular window $w(n)$ with $n \leq N\text{-}1$, from the signal $x(n)$ so that the Fourier transform is calculated from the function

$$x^*(n) = x(n) \ w(n) \ , \quad n \leq N-1$$

when $x(n)$ is the data set of n data points and $w(n)$, with $n \leq N\text{-}1$, the window function with $N\text{-}1$ as the number of data points. The spectrum of the product of two signals is the convolution of their Fourier transforms so that the spectrum of $x^*(n)$ is influenced by the spectrum of the rectangular window. As a result, in addition to the spectral line of a sinusoidal signal, side lines are generated if the frequency of the signal is not a multiple of f_0/N. Special window functions have been developed in order to minimize this effect. The window has to meet the following requirements:

- minimum width of the window
- minimum width of the main peak of the window spectrum
- minimum side peaks of the window spectrum.

For the oscillation analysis, the Hanning window which is based on a cosine function was chosen as it meets these requirements [BES88].

The data to be analyzed describe a dynamic process, i.e., continuously changing frequencies. Within a data set of N samples the frequencies are not constant. Calculating the amplitude spectrum of a signal with increasing frequency, as seen in Figure 3.3.1 multiple peaks appear for every frequency component of the signal. It has to be noted that here and in all following spectra the envelope of the discrete spectrum is shown. Applying a Hanning window, the spectrum appears as shown in the figure. The window is weighing the data so that peaks are given of the frequency components around the samples $N/2$ of the data set. A sharper image of the system dynamics is obtained thus reducing the number of samples of the data set as seen in the figure. However, the resolution becomes poor. A remedy is the addition of a data set that consists of a number of zeroes to the data set as described by Schrüfer, which increases the resolution of the spectrum [SCH94].

For the composition of a cascade plot choices have to be made according to the following parameters:

- the number of spectra
- the number of samples per data set
- the number of samples of the Fourier transform
- the window function.

Considering a typical example of a data set of 60 seconds sampled with f_0 = 1 kHz and a number of 60 spectra, this results in a data set of 1 second or 1000 samples. Assuming a motor drive accelerating at 2 Hz/s stator frequency, e.g., a 6^{th} torque harmonic will change at a rate of 12 Hz/s. Taking a set of 100 samples, the harmonic will change at a rate of 1.2 Hz/s, which gives a reasonable resolution of the dynamics. However, maintaining the number of spectra, 90 % of the data will not be considered so that valid information may be lost. In the following, the full data sets are taken for cascade plots thus obtaining a minor resolution of dynamics. In the case of zooming on particular oscillation phenomena within a restricted time interval, reduced data sets may be chosen.

The Discrete Fourier Transform needs N^2 complex multiplications. In practice, faster algorithms are used, the Fast Fourier Transform (FFT). In the following, a radix 2 algorithm is applied, this reduced the number of multiplications of the

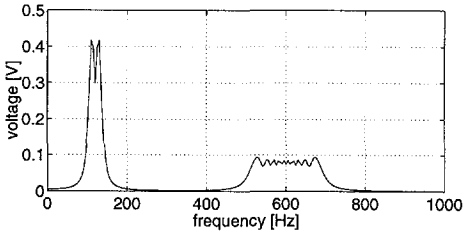

Fourier spectrum of 400 points of a 100 Hz signal with 5th harmonic at 2 kHz sample frequency with an increase of frequency of 44 %.

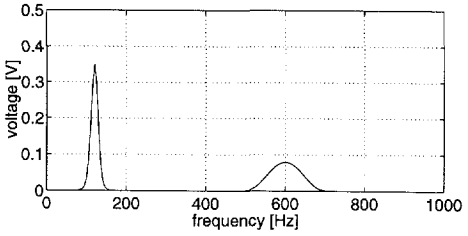

Fourier spectrum of the signal described above when applying a Hanning window.

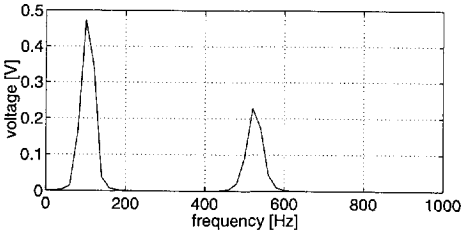

Fourier spectrum of 100 points of the signal described above when applying a Hanning window.

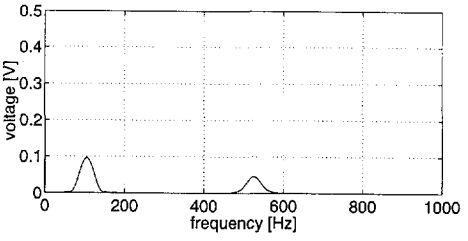

Fourier spectrum of 512 points of the signal described above with 100 data samples and addition of zeroes when applying a Hanning window.

Figure 3.3.1 Data processing for cascade plots.

algorithm to ^{2}log(N)N/2. For example, a Fourier transform of 1024 samples is reduced from approximately 10^6 to 5120 multiplications. Numerical errors of the FFT are discussed in literature [BES88]. The errors caused by noise of the analog-to-digital converter and the rounding error of the FFT have to be taken into account.

3.3.2 Oscillations during a traction cycle

To evaluate the oscillation characteristics of a traction cycle, a test with the electrical multiple unit has been chosen as an example to:

- evaluate the choices of sensors,
- evaluate methods of data analysis,
- detect oscillations under regular test conditions,
- locate oscillations within the bogie.

Test parameters of the chosen example are acceleration at maximum torque up to a vehicle speed of approximately 60 km/h and braking with maximum torque to standstill on a straight track with dry rails. The sensor configuration of the drive is shown in Figure 3.2.1.

Figures 3.3.2 to 3.3.4 show a cycle of the acceleration and braking of an electrical multiple unit in the time domain. The most significant signals which illustrate the dynamics of the drive are shown:

Inverter

- inverter DC voltage u_{cinv}
- inverter frequency f_{inv}
- inverter phase current i_u

Mechanical drive

- motor shaft acceleration α_m
- torques of motor side coupling and hollow shaft of the wheel side coupling T_{cpm}, T_{hsh}

Motor and gearbox suspension

- vertical displacement of motor and gearbox in bogie frame z_m, z_{gm}, z_{gw}.

Figure 3.3.2 shows the signals of the inverter which are the DC link voltage u_{cinv}, the inverter frequency f_{inv} and the inverter phase current i_u. The inverter frequency shows the dynamics of the traction cycle as described above. However, the drive is

braking at a low torque instead of coasting. The standstill period has not been displayed.

The DC link voltage is controlled at the two levels of 2300 V and 2400 V, depending on the value of the catenary current. The voltage dips and peaks during braking are due to the voltage control and were not investigated. The phase current plot gives only an indication of the current amplitude. Analysis has to be done in the frequency domain. Up to 1.2 seconds the current will build up the flux of the motor. After 1.2 seconds the current maintains the flux and generates the torque.

The signals derived from the mechanical drive, which are motor shaft angular acceleration α_m, motor coupling torque T_{cpm} and hollow shaft torque T_{hsh} are plotted in Figure 3.3.3. The acceleration of the motor shaft has been derived from the measurement of the angular velocity. The angular velocity ω_m multiplied by the number of pairs of poles of the motor is the inverter frequency minus the slip frequency of the motor. As the traction motor is a four-pole motor, the shaft rotation frequency is half the inverter frequency less half the electrical rotor frequency. Deceleration of the motor shaft reaches higher values than acceleration because the mechanical brakes are also operating.
The torque signals show the building up of flux up to 1.4 seconds and the building up of torque, which is followed by an overshoot. Field weakening during acceleration can be recognized by the decreasing torque. The transmission factor of 69/16 of the gearbox explains the difference of values between the torques. With a motor shaft torque

$$T_{cpm} = 2000 \text{ Nm},$$

a tare weight of a train which is equipped with four motors of

$$m_v = 92 \text{ t}$$

and a wheel diameter of

$$D_w = 0.92 \text{ m}$$

a motor shaft acceleration of

$$\alpha_m = 1.2 \text{ Hz/s}$$

is calculated according to the measured acceleration.
The time domain plot of the motor coupling torque T_{cpm} shows an oscillation with an amplitude of about 400 Nm and a frequency which increases with speed.

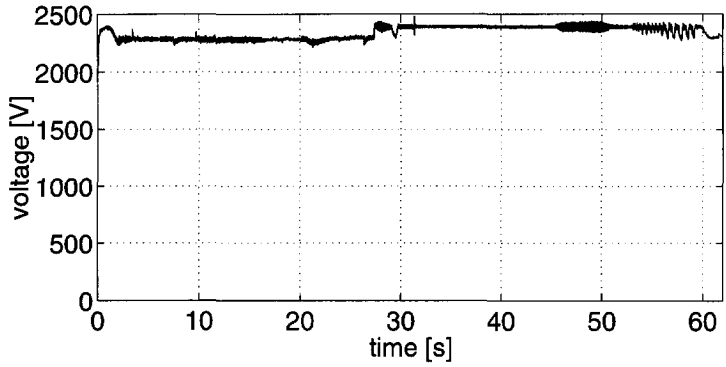

Inverter DC link voltage u_{cinv}

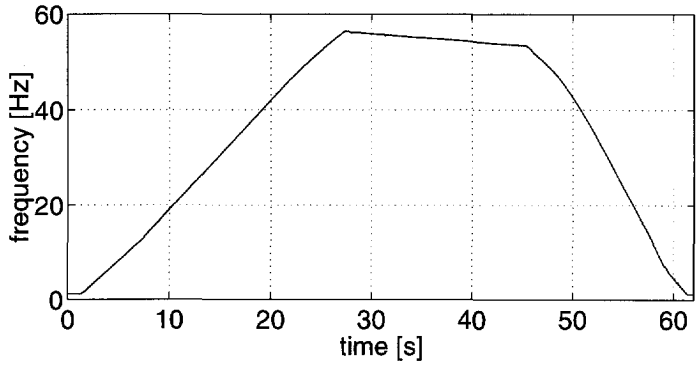

Inverter frequency f_{inv}

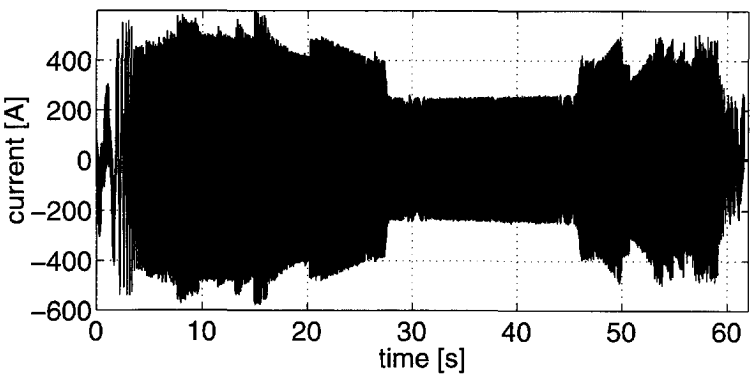

Inverter phase current i_u

Figure 3.3.2 Inverter signals of electrical multiple-unit drive.

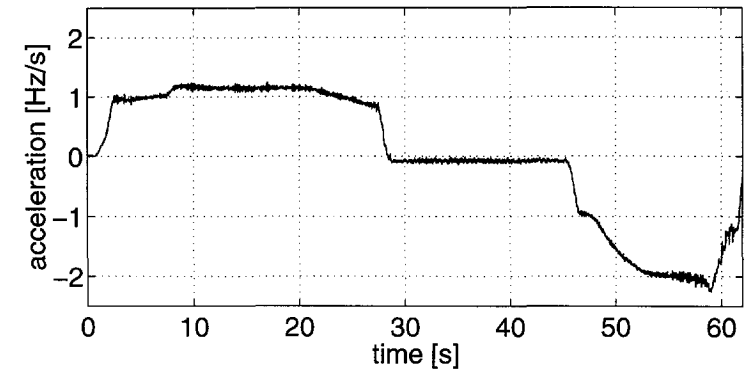

Motor shaft angular acceleration α_m

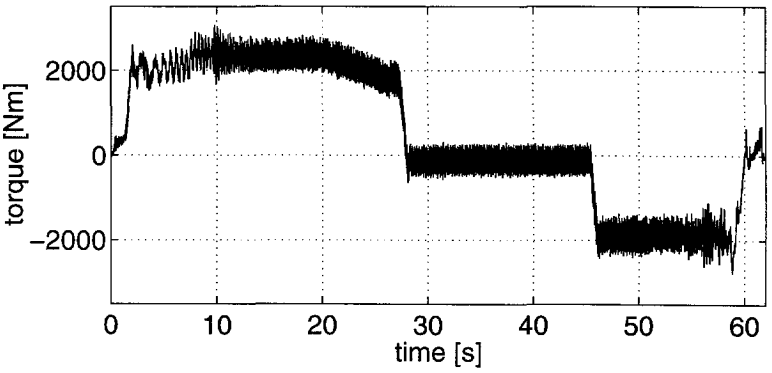

Motor coupling torque T_{cpm}

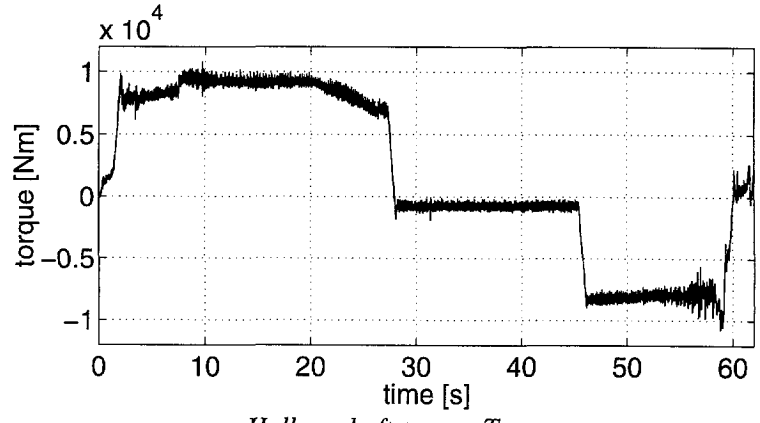

Hollow shaft torque T_{hsh}

Figure 3.3.3 Signals of the mechanical drive of the electrical multiple-unit.

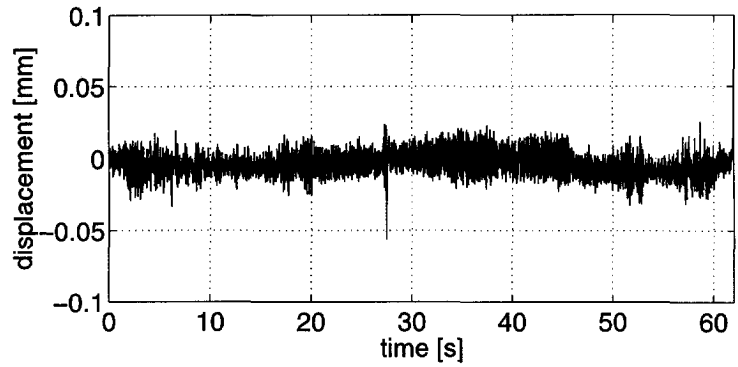

Displacement motor z_m (S_1)

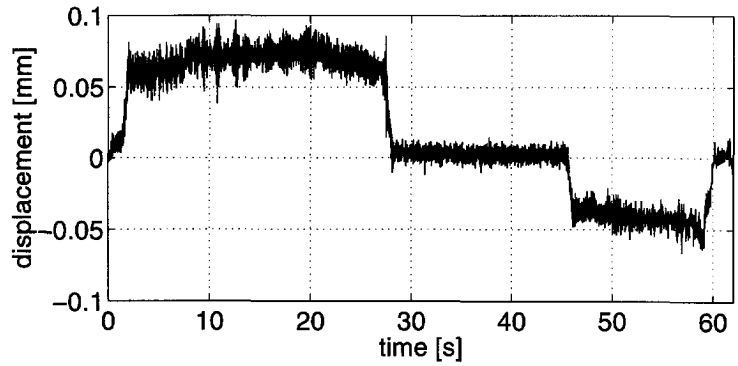

Displacement gearbox motor side z_{gm} (S_2)

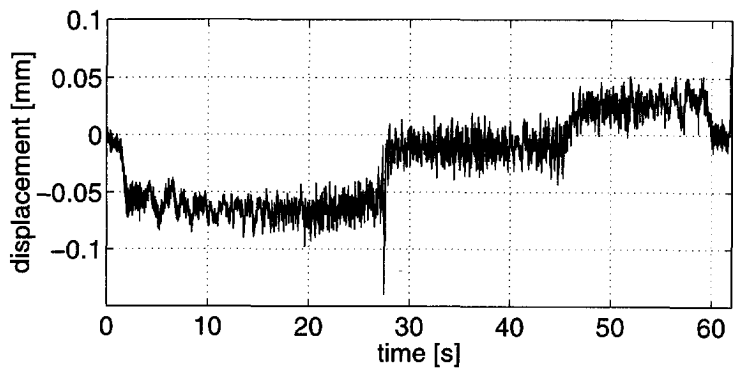

Displacement gearbox wheel side z_{gw} (S_3)

Figure 3.3.4 Vertical displacement of motor and gearbox of electrical multiple-unit.

The vertical displacement of motor and gearbox housing in the bogie frame, which is the most significant displacement, is plotted in Figure 3.3.4. Since there has been noise on the signals they were filtered using an 8th order Butterworth filter at a cut-off frequency of 100 Hz. A negative sign means displacement from the housing towards the rails. The resulting movement of the housing with respect to the fixed bogie frame during acceleration of the vehicle is schematically depicted in Figure 3.3.5. The dotted line indicates the displacement caused by the motor air gap torque T_e. The movement can be described by a rotation of the housing around the axial (y) and the horizontal (x) axis. At 28 seconds, when braking begins, a peak appears in the displacement due to the change of torque.

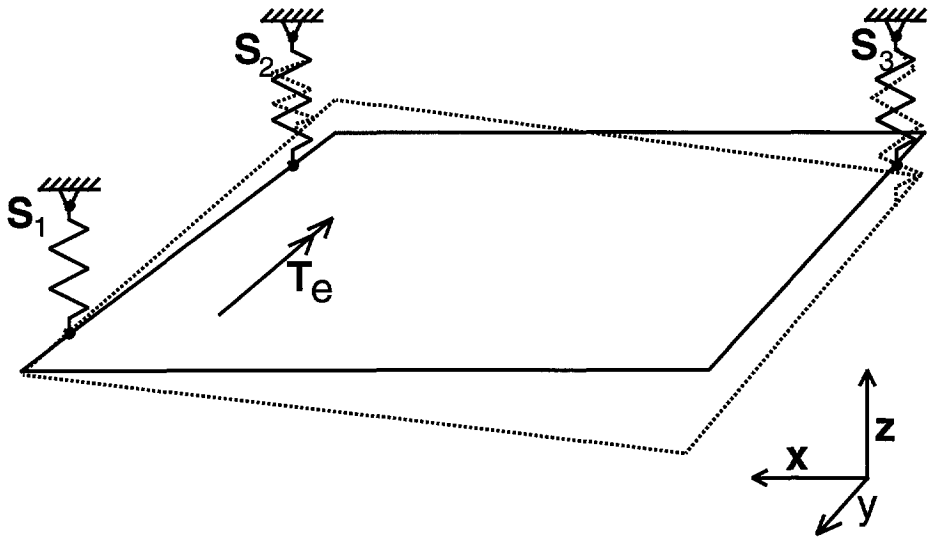

Figure 3.3.5 Displacement of drive in bogie frame during acceleration.

Time domain plots of signals of the electrical drive, the mechanical drive and the suspensions show:
- amplitudes
- peaks
- dynamics

of the signals thus giving an indication of the performance and the maximum stress of the drive by peak values.

Frequency domain analysis has to give information about harmonic oscillation sources which may be:

- the inverter which generates voltage harmonics. These harmonics cause current and flux harmonics in the motor. Hence the torque, as a product of flux and current, contains harmonics. However, voltage harmonics appear also in the DC link.
- the mechanical drive which may have unbalance or misalignment

and about sources of transients such as

- the wheel-rail contact
- the control system.

In the spectra, even and odd harmonics of the mechanical frequencies may be found while switched voltage waveforms in a symmetrical three-phase configuration generate only multiples of the sixth harmonic of the inverter frequency in the drive torques.

Modal analysis of the bogie and drive line leads to the natural frequencies of the drive including modes of the drive line, the drive in the bogie frame, the bogie itself and the car-body. In the case of the electrical multiple-unit, the most important natural frequencies were calculated between 0 Hz and 150 Hz [POE92]. Modal analysis of drive models is treated in Chapter 5.

Frequency domain analysis is done by means of cascade plots to obtain an insight into the traction cycle. The most significant plots of the signals plotted in the time-domain are shown in Figures 3.3.6 to 3.3.9.

In order to identify more accurately the frequency components of the measured signals and their correlation, spectra were computed at 30 seconds of the traction cycle and plotted in Figures 3.3.10 and 3.3.11. The main frequencies of the drive are:

f_{inv}	56 Hz	inverter
f_{m}	28 Hz	motor shaft, pinion wheel
f_{igw}	11.8 Hz	intermediate gearwheel
f_{gw}	6.5 Hz	gear wheel, wheel axle

when the slip of the motor is assumed to be zero, which can be done by approximation.

Figure 3.3.6 shows the cascade plot of the phase current in two different orientations, above to put into evidence the frequency dynamics, and below to show the amplitude dynamics. It has to be said that, due to windowing and the addition of

zeroes, the amplitude is less than the real value of the current amplitude, depending on the data processing parameters. The cascade plots of inverter current i_u show its frequency components. The fundamental frequency is equal to the inverter frequency f_{inv}. Further, the fifth and seventh harmonic of the inverter frequency, which are generated as a result of the pulse-width modulated inverter voltages can be recognized. The amplitude and appearance of the harmonics vary due to the applied pulse patterns of the converter pulse-width modulation. During braking at low torque the amplitude of the harmonics is maximum.

The cascade plot of the inverter DC link voltage shown in Figure 3.3.7 shows the sixth harmonic, which is a result of the product of the fundamental and the fifth or seventh harmonic of the phase voltage and current. Further, a 450 Hz component at 30 seconds and between 45 and 55 seconds and a 400 Hz component between 45 and 50 seconds appear. These frequencies are generated by the brake chopper which acts in the DC link bringing energy into resistors during braking. In the time domain plot of Figure 3.3.2 these oscillations can be seen as a ripple at the mentioned time periods. The cascade plot, however, shows the frequencies of the oscillations.

Frequency analysis of the motor side coupling torque T_{cpm} and the hollow shaft torque T_{hsh} reveals a harmonic content of the signal, which depends on axle speeds as seen in the cascade plots of Figure 3.3.8. The sixth harmonic of the inverter frequency can be recognized in the torques. The amplitude of the harmonic is lower in the hollow shaft torque than in the motor-coupling torque due to attenuation by the elastic couplings. At approximately 10 seconds of the cycle a peak appears. At this time instant the fifth current harmonic increases. This peak had already been noted in the-time domain plots of torques. Also, at approximately 57 seconds, a peak appears which corresponds with the fall of amplitude of the fifth harmonic of the current. Its frequency is lower than the frequency of the peak at 10 seconds, which indicates that it is no resonance.
The highest harmonic in the shown frequency band is equal to the tooth frequency of the gear wheels, which is 16 times the motor shaft frequency.
Cascade plots of the horizontal and vertical gearbox acceleration in Figure 3.3.9 show the sixth harmonic of the inverter frequency including the peaks at 10 seconds and 57 seconds. The gear tooth frequency can also be recognized.

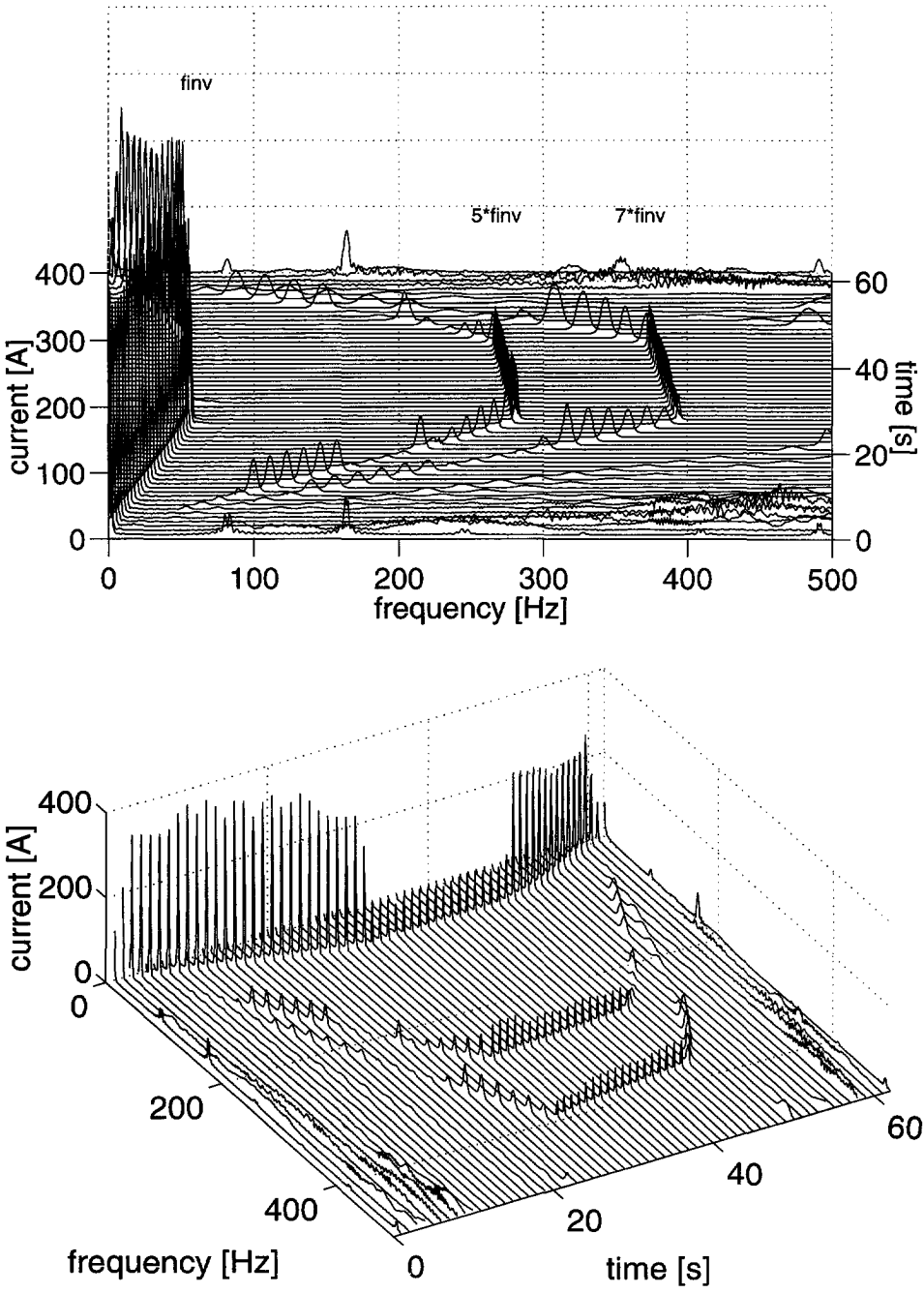

Figure 3.3.6 Cascade plots of inverter phase current i_u of electrical multiple-unit.

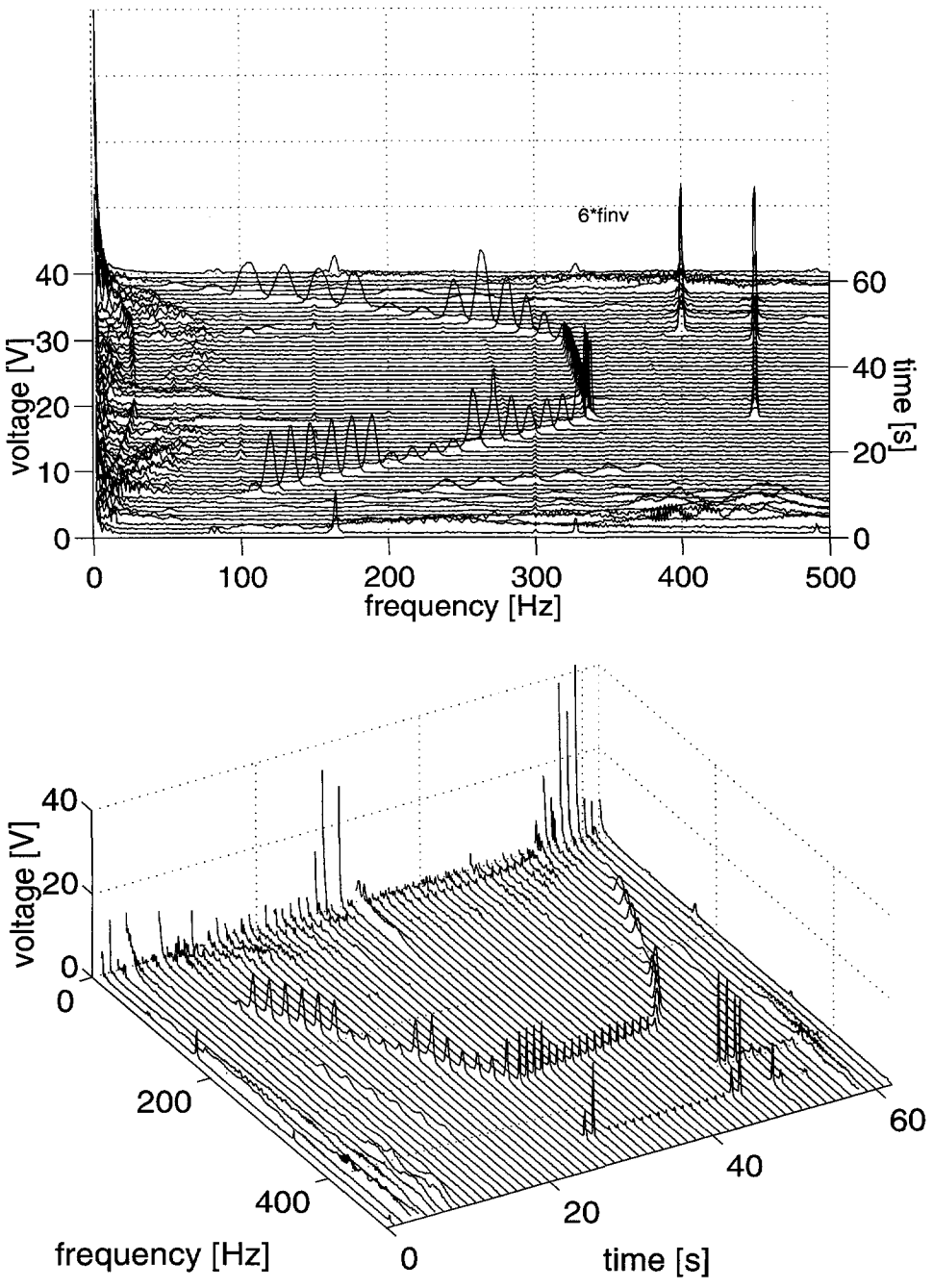

Figure 3.3.7 Cascade plots of inverter DC link voltage u_{cinv} of electrical multiple-unit.

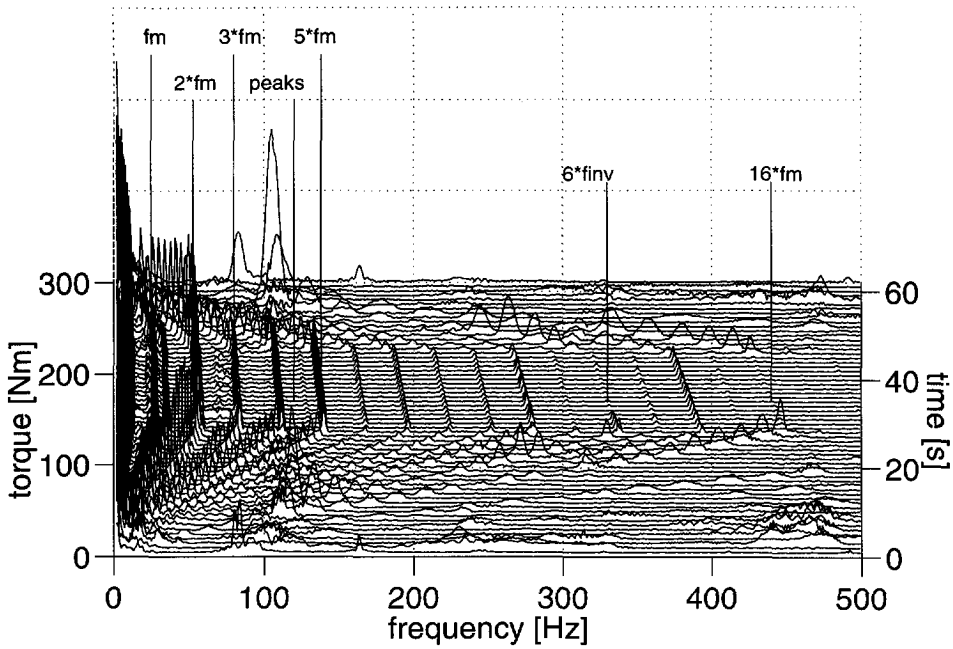

Motor side coupling torque T_{cpm}

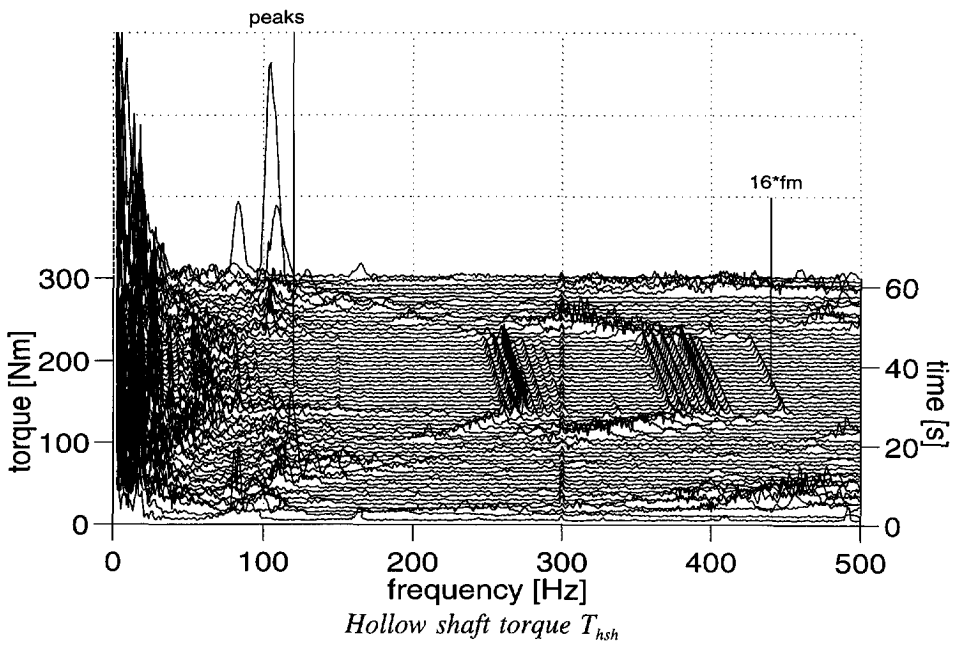

Hollow shaft torque T_{hsh}

Figure 3.3.8 Cascade plots of mechanical drive torques of electrical multiple-unit.

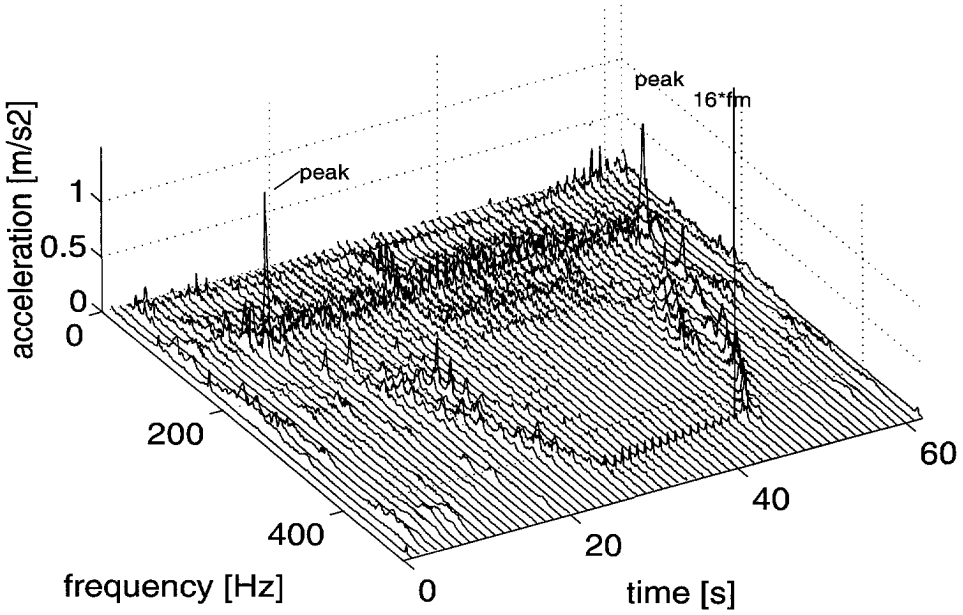

Horizontal acceleration ax_{gw}

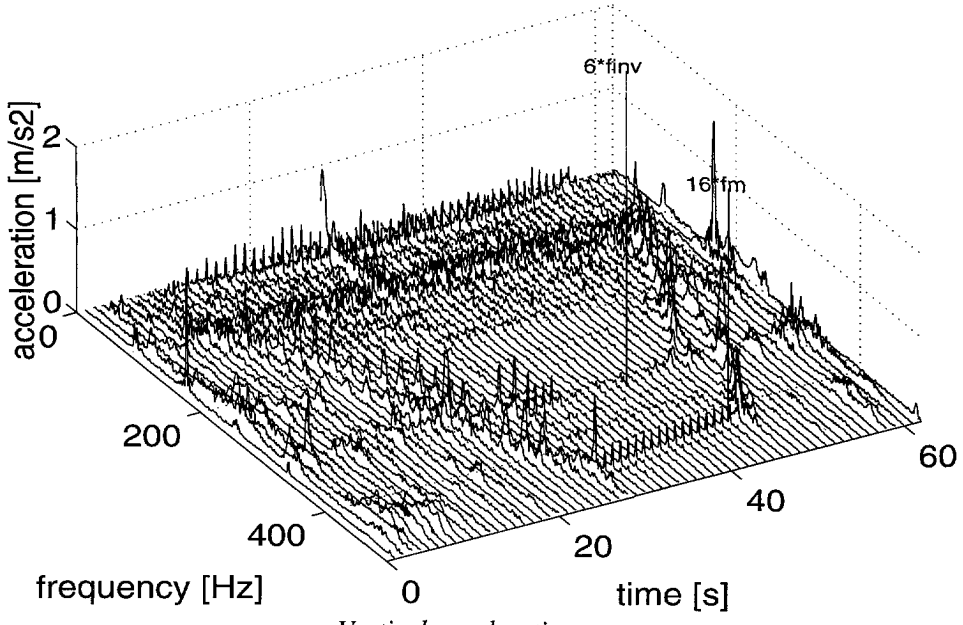

Vertical acceleration az_{gw}

Figure 3.3.9 Cascade plots of horizontal and vertical acceleration of the gearbox at the wheel side of the electrical multiple-unit drive.

Cascade plots give an overview of the frequency components of the entire drive during a traction cycle showing dynamics of frequency and amplitude. Within the example of Figure 3.3.6 to 3.3.9 there could be shown:
- converter switching frequencies
- converter waveform harmonics
- torque and acceleration harmonics due to converter harmonics
- torque and acceleration harmonics due to mechanical frequencies.

Figure 3.3.10 and 3.3.11 show the spectra of inverter signals, the shaft torques and signals of acceleration and displacement at 30 seconds of the cycle. The sixth harmonic of the inverter frequency can be recognized at a frequency of 336 Hz in both torques, but at a low level with respect to the other frequency components. The amplitude of the 336 Hz harmonic in the hollow shaft is 1/3 of the amplitude at the motor side. In both torques appears the gear tooth frequency $16*f_m$ = 448 Hz, also with a low amplitude.
The dominant frequencies in the spectrum of the motor side coupling torque T_{cpm} are multiples of the shaft frequencies of the mechanical drive. The multiples of the motor shaft frequency may be caused by a misalignment of the motor side coupling. The source of the intermediate gear wheel frequency is not known. The hollow shaft torque spectrum contains multiples of the gear wheel frequency which may be caused by a misalignment of the hollow shaft coupling.

The spectra of gearbox acceleration and displacement in the bogie frame are shown in Figure 3.3.11. The sixth harmonic of the inverter frequency is present in all spectra. The motor air gap torque acts on the stator and on the rotor. As the stator is rigidly coupled to motor and gearbox housing, torque harmonics are identified clearly in the spectrum of acceleration. The dominant mechanical frequencies are multiples of the gear wheel frequency. The acceleration spectra have a dominant peak at the gear tooth frequency.

The cross-correlation expresses the correlation between two signals. Time delays and correlation of harmonic contents can be detected. If two signals contain a common frequency component, a peak in the Fourier transform of the correlation function demonstrates the common component in spite of the other frequency components in either signal [HIG90].
The correlation between bogie and drive is illustrated by Figure 3.3.12, which shows the Fourier transform of the cross-correlation between horizontal acceleration

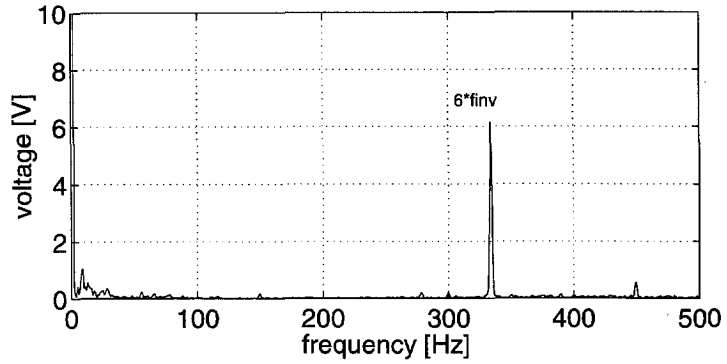

Inverter DC link voltage u_{cinv}

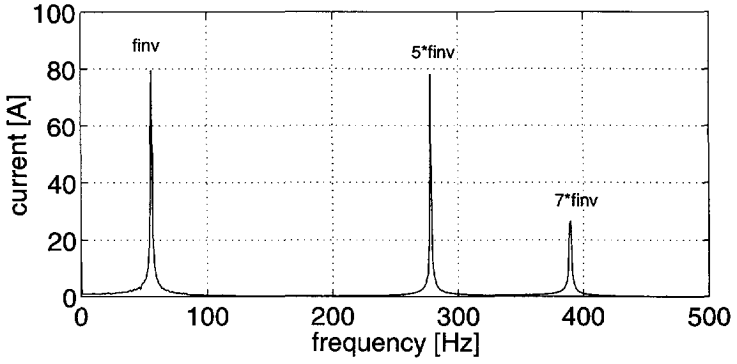

Inverter phase current i_u

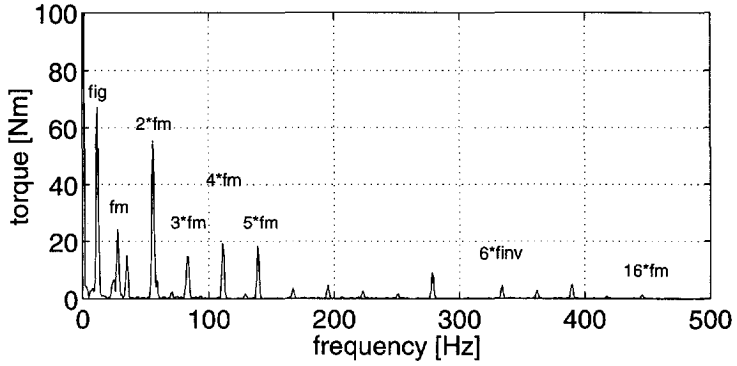

Motor side coupling torque T_{cpm}

Figure 3.3.10 Spectra of electrical multiple-unit drive at 30 seconds of the cycle.

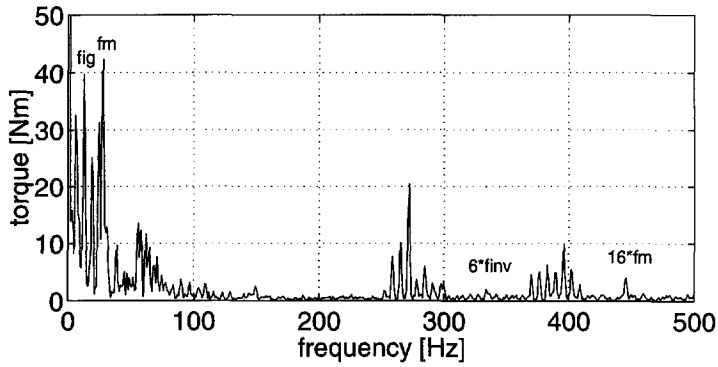

Hollow shaft torque T_{hsh}

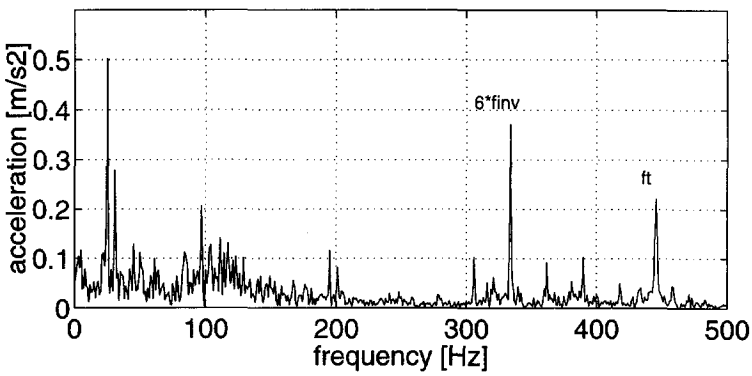

Vertical acceleration of gearbox at the wheel side az_{gw} (f_t=16f_m)

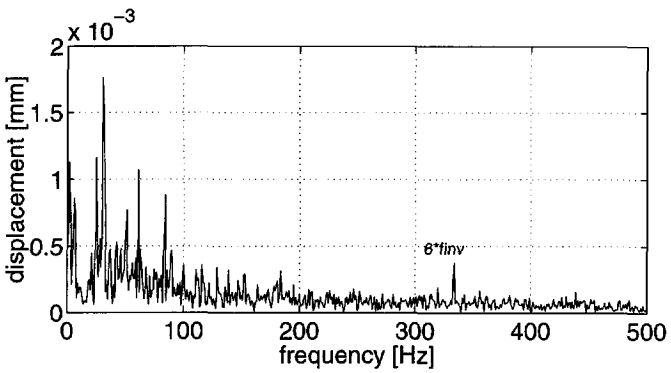

Vertical displacement gearbox motor side z_{gm}

Figure 3.3.11 Spectra of acceleration and displacement of electrical multiple-unit drive at 30 seconds of the cycle.

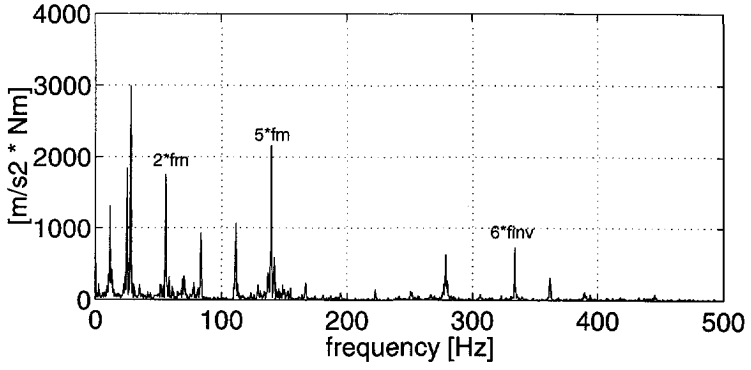

Figure 3.3.12 Fourier transform of the cross-correlation of the horizontal acceleration of the wheel axle bearing housing ax_{pg} and the motor side coupling torque T_{cpm}.

of the wheel axle bearing housing and the motor side coupling torque. Common harmonics are the sixth harmonic of the inverter frequency f_{inv}, e.g., the ripple torque generated by the motor, and harmonics of the shaft speed f_m.

This example has to be considered as a single case which has been used to illustrate the method to detect oscillations by measurements.
By this example it has been shown that:

- the main air gap torque harmonic generated by the inverter is propagated throughout the entire drive and bogie by the motor shaft and the motor housing.
- frequency components of mechanical origin with significant amplitudes have been measured only in the mechanical drive.

In order to determine the oscillation characteristics of the drive, analysis has to be carried out for a number of these cycles. Statistical methods have to be used to determine the deviation of signals. Then cycles with different torque and maximum speed have to be analyzed.
Various cycles were measured for different vehicle types and test parameters. Evaluation of the test results led to the insight that:

- An increased number of sensors and tests leads to an amount of data which is difficult to process and analyze within a reasonable amount of time and effort. [WIN94/3, WIN95/2]
- Every test has to be considered individually because rail conditions and the

action of the operator who gives the torque reference of the control system contain a reasonable degree of uncertainty [WIN94, WIN94/3, WIN95/2, WIN95/3].

The cycle discussed in this section was chosen because it provided most information concerning the number of signals and detected oscillation phenomena. Specific phenomena are analyzed in the following sections.

3.3.3 Converter harmonics

Converter harmonics which are contained by pulse-width modulated inverter voltage waveforms appear throughout the electrical and mechanical drive of a vehicle at varying frequencies according to vehicle speed and, therefore, inverter frequency. The torque harmonics caused by these converter waveforms are forced oscillations. They have to be attenuated by the mechanical drive on the one hand and kept in hand by the power converter on the other hand. However, resonances may occur when the harmonics meet a natural frequency of the system. Further, there are several pulse patterns which are applied during a traction cycle as a function of the motor's stator frequency. The change of pulse pattern may cause transients of the motor fluxes which affect the torque. Examples are given below to illustrate the influence of the converter harmonics

Attenuation of oscillations

Figures 3.3.13 and 3.3.14 show a detail of the traction cycle previously discussed. The 5^{th} and 7^{th} current and flux harmonic generate, together with the fundamentals, a 6^{th} harmonic in the torque. The time domain plots of the torque show only the ripple, which is a maximum of 13% peak to peak at a mean value of 2200 Nm on the motor side coupling and 1% peak to peak at a mean value of 9500 Nm on the hollow shaft. This illustrates the attenuation of the torque harmonic. The ripple amplitude is not constant because there are several frequency components below and above the torque harmonic as is shown in the cascade plot of Figure 3.3.8 and the spectra of Figure 3.3.14. Generally, the tests showed a low amplitude of the sixth torque harmonic in the stator frequency range up to 60 Hz which had earlier been investigated [WIN94/3, WIN95/2, WIN95/3].

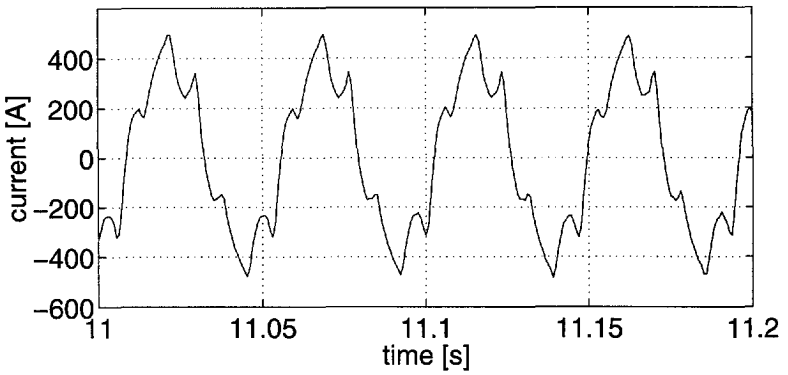

Inverter phase current i_u

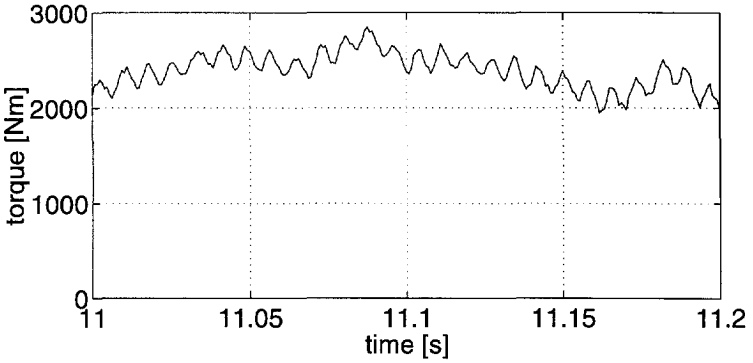

Motor side coupling torque ripple at T_{cpm} = 2200 Nm

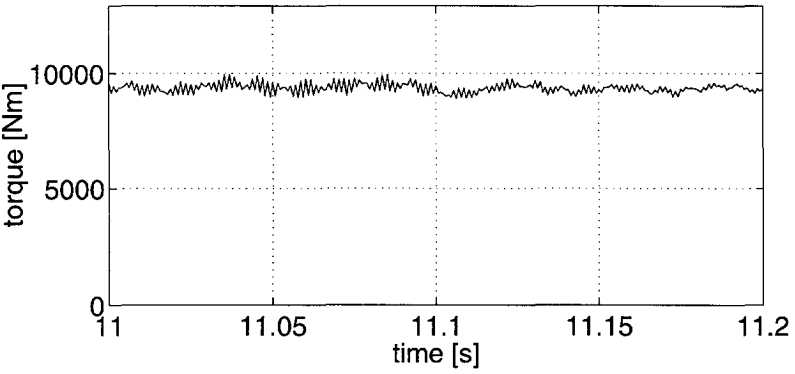

Hollow shaft torque ripple at T_{hsh} = 9500 Nm

Figure 3.3.13 Torque harmonic generation and attenuation of electrical multiple-unit drive.

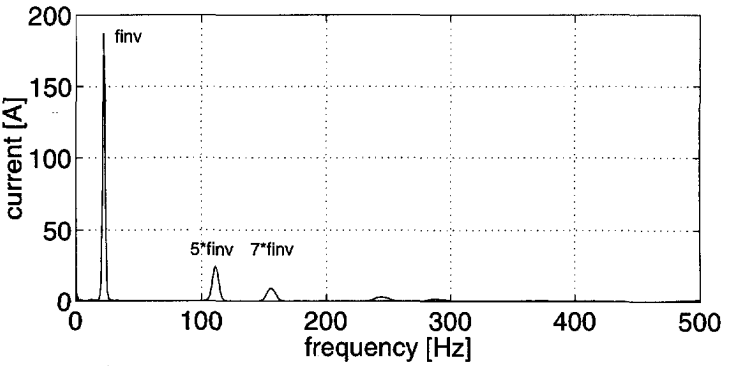

Inverter phase current i_u

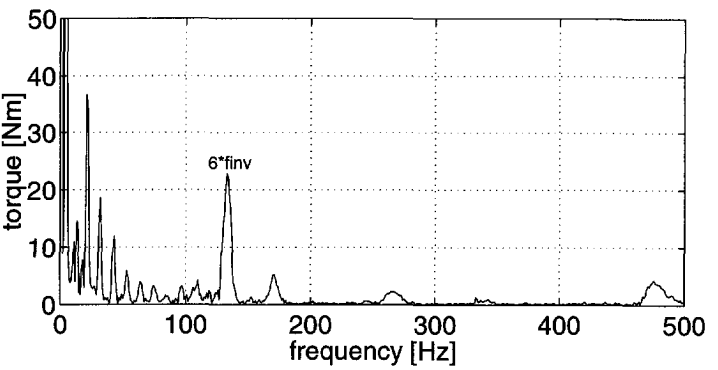

Motor side coupling torque T_{cpm}

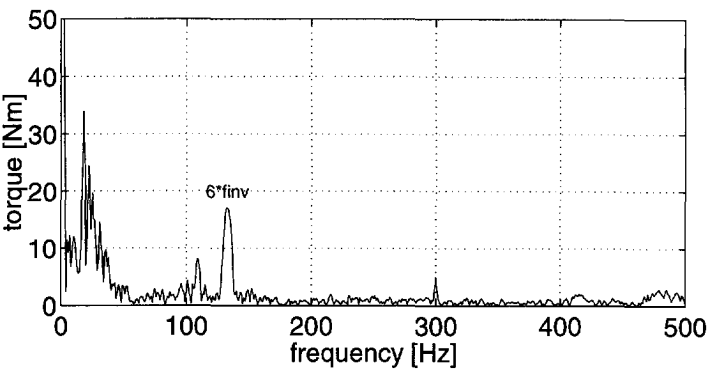

Hollow shaft torque T_{hsh}

Figure 3.3.14 Spectra of torque harmonic generation and attenuation of electrical multiple-unit drive.

Transients

The transient caused by a change of pulse pattern of the inverter is illustrated in figure 3.3.15. The transient was measured in the DC link voltage, torques, acceleration and displacement of the drive. It is a damped oscillation. The frequency of the torque oscillation is between 18 and 18.5 Hz while the frequency of the displacement oscillation is 21 Hz. The peak to peak value of the transient exceeds 10% of the torque [WIN94/3].

Resonances

Figure 3.3.16 shows the torque resonance of the cardan shaft of a metro vehicle in acceleration. A cardan shaft is a poorly damped component within a mechanical drive and therefore it is sensitive to resonances. The cascade plots in Figure 3.3.16 show the inverter current with a variety of pulse patterns during the first seconds; these cause torque peaks around 300 Hz. After 4 seconds the pairs of 5^{th} and 7^{th}, the 11^{th} and 13^{th}, and the 17^{th} and 19^{th} current harmonics appear. A 6^{th} harmonic of the torque, at a mean value of 700 Nm, appears with a resonance just above 300 Hz. Figure 3.3.17 shows one of the resonance peaks in the time domain. The resonant amplitude of the torque is nearly 400 Nm peak to peak, which is 57% of the mean torque. The resonance frequency of 310 Hz appears to be the switching frequency of the inverter.

Figure 3.3.18 shows a resonance in the inverter DC link of a locomotive drive during acceleration. The inverter line voltage spectra show the fundamental component and the pair of 5^{th} and 7^{th} harmonic in the cascade plot. Harmonics appear after 14 seconds of the cycle. The 6^{th} harmonic of inverter DC link voltage, at a DC value of 4200 V, can be recognized in the cascade plot. A resonance appears after 15 seconds at a frequency of 116 Hz. As the DC link of the inverter is a circuit composed of capacitors and inductances with low resistance there can be a natural frequency with low damping. The resonance was measured also in the catenary voltage, which can be seen in the spectrum of figure 3.3.19 [WIN95/3].

During the tests which were performed on the four vehicles described in section 3.2, the amplitude of the torque oscillations caused by the switching converter waveforms were found to be inferior to the amplitude of the measured torque oscillations which were generated within the mechanical drive. Exceptions are resonances and peaks of transients after the change of the inverter's pulse patterns. Converter harmonics cause current and voltage ripples in the DC link, which are propagated in the converter circuit with the possibility of resonances.

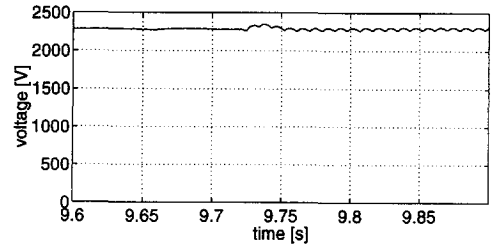

Inverter DC link voltage u_{cinv}

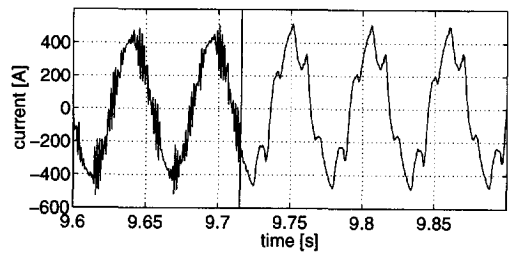

Inverter phase current i_u

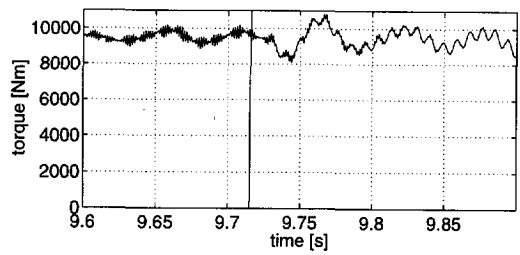

Hollow shaft torque at T_{hsh} *= 9500 Nm*

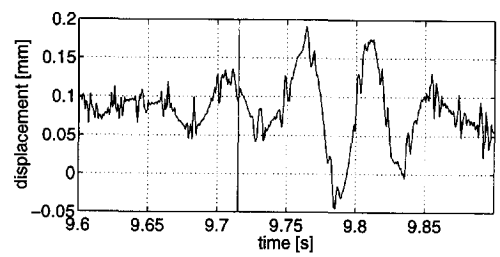

Horizontal displacement of motor housing suspension x_m

Figure 3.3.15 Transients at a change of PWM pulse pattern of electrical multiple-unit drive.

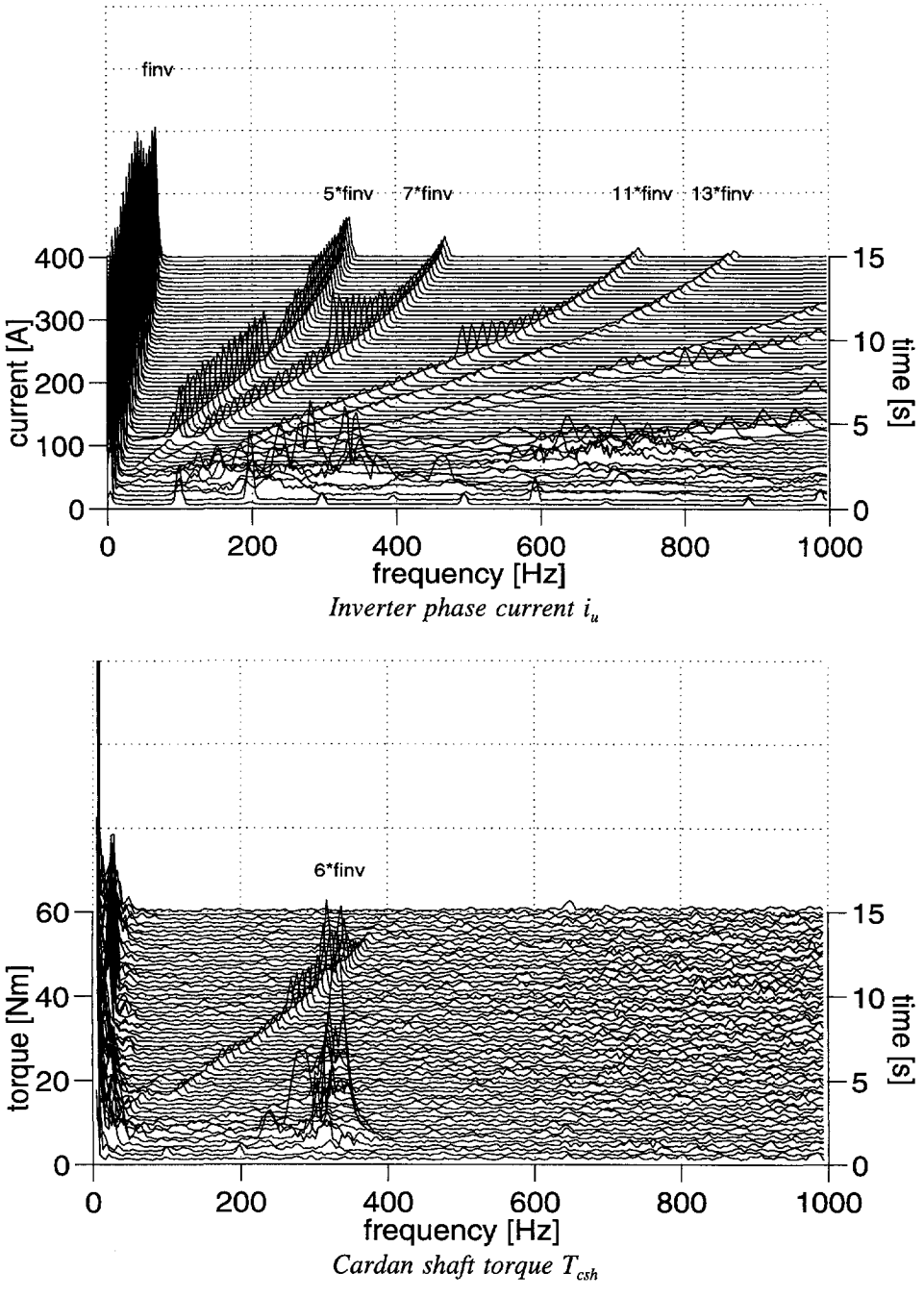

Figure 3.3.16 Cardan shaft resonance of metro vehicle drive.

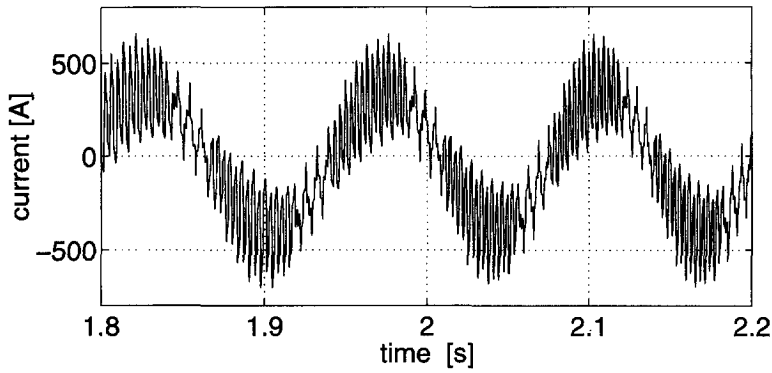

Inverter phase current i_u

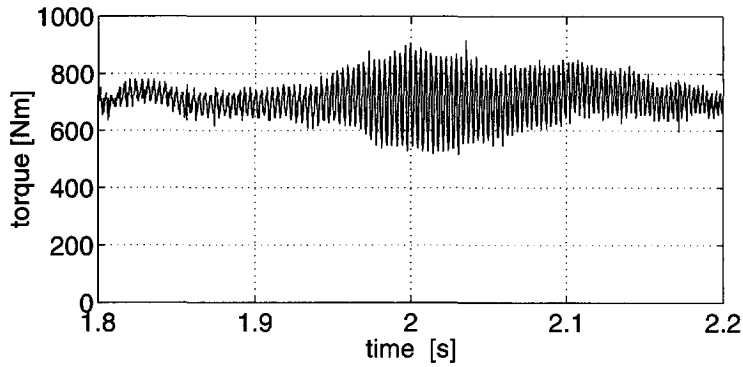

Cardan shaft torque T_{csh}

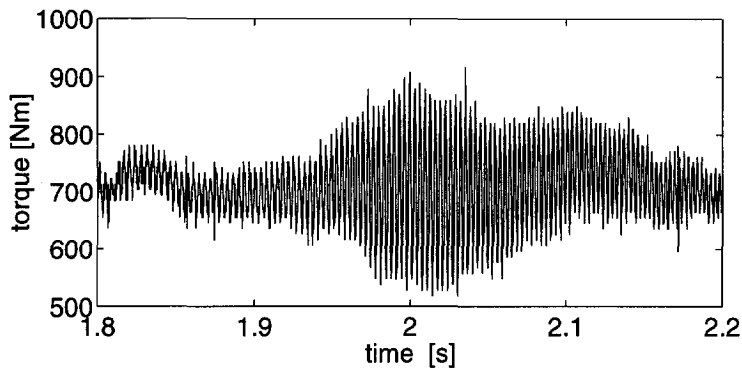

Cardan shaft torque ripple at T_{csh} = 700 Nm

Figure 3.3.17 Details of cardan shaft resonance of metro vehicle drive.

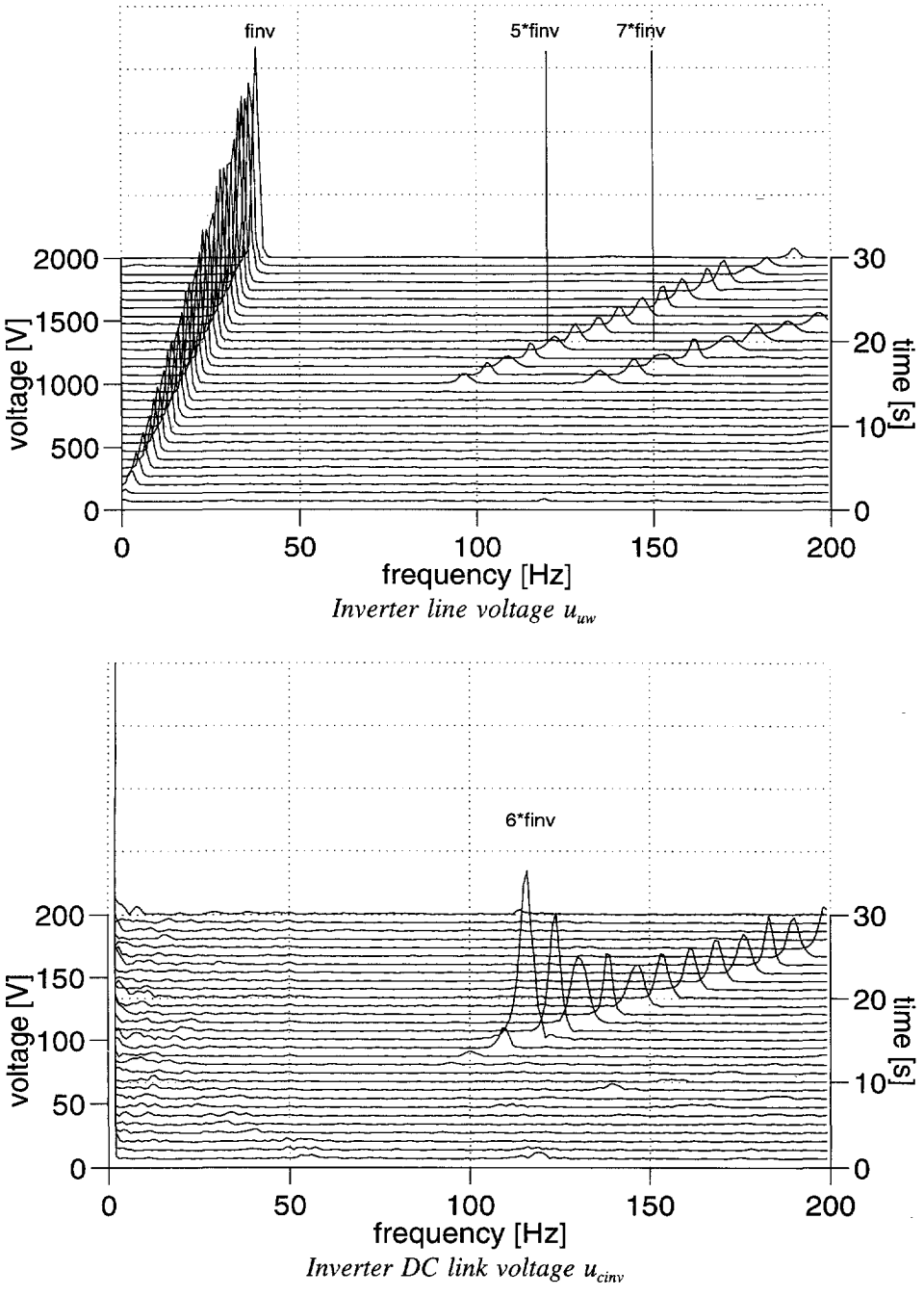

Inverter line voltage u_{uw}

Inverter DC link voltage u_{cinv}

Figure 3.3.18 Inverter signals at DC link resonance of locomotive drive.

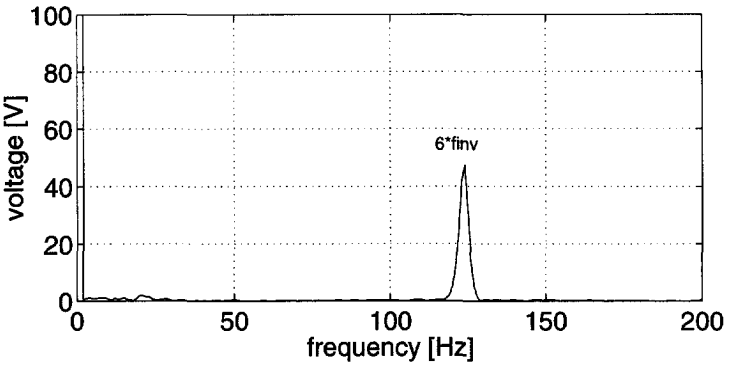

Inverter DC link voltage u_{cinv}

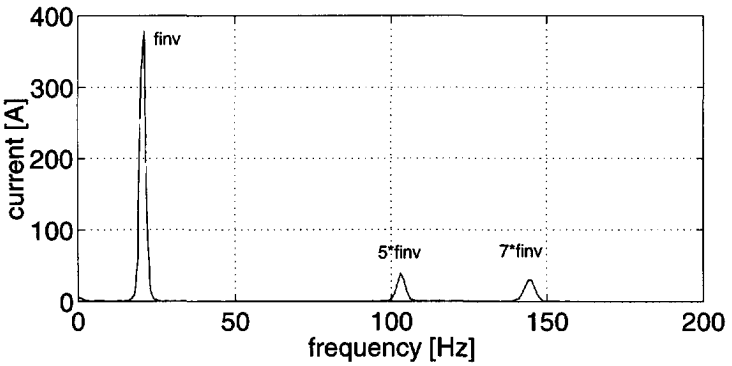

Inverter phase current i_u

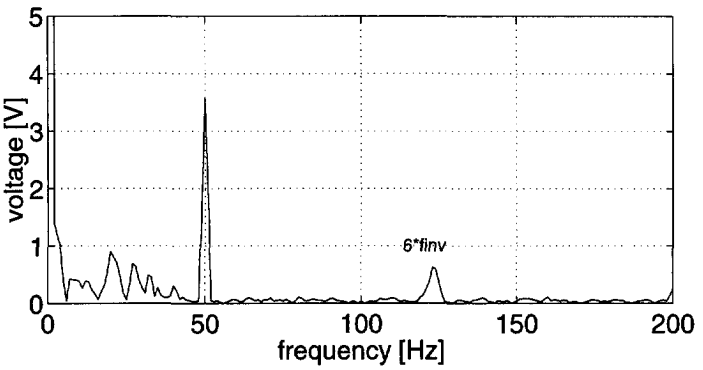

Catenary voltage u_{lin}

Figure 3.3.19 Spectra of locomotive drive signals at DC link resonance.

3.3.4 Rail influences

The rails may cause shock loads at, e.g., switches and crossings or any kind of irregularities. Oscillations excited by the wheel-rail contact may cause periodic excitation, e.g., transverse beams of the rails, or slip-stick phenomena. Of the performed tests, three examples have been taken which illustrate phenomena and their influence on the drive.

The responses of the low-floor tram bogie on a rail crossing and switch are shown in Figures 3.3.20 and 3.3.21 [WIN95, WIN92/2]. Passing the crossing, torque peaks appear which first accelerate then brake the wheel drive. The peaks have an amplitude up to three times the rated drive torque of 2000 Nm. The DC link voltage follows the torque. The transient has its effect also on the motor phase current. The crossing causes acceleration peaks of 6g in the vertical and 3g in the horizontal direction.
The rail switch which is met after 16 seconds causes higher acceleration but lower torque peaks which do not have an influence on the electrical drive.

Figures 3.3.22 and 3.3.23 show a torque oscillation of the low-floor tram bogie drive appearing before wheel slip of the drive [WIN95/2]. The oscillation lasts 600 milliseconds with a peak to peak torque of 4000 Nm, which is twice the rated torque of the drive. Its frequency of 45 Hz can be found in the inverter DC link voltage.

The examples have shown that rail excitation leads to torque oscillations and peaks which may.
- have an amplitude in the order of the rated torque of the drive
- affect the entire electrical and mechanical drive.

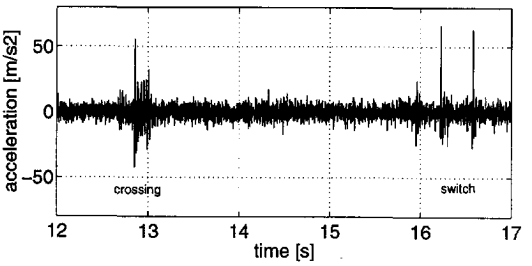

Vertical acceleration motor housing az_m

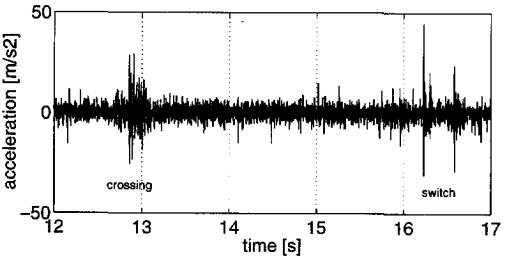

Axial acceleration motor housing ay_m

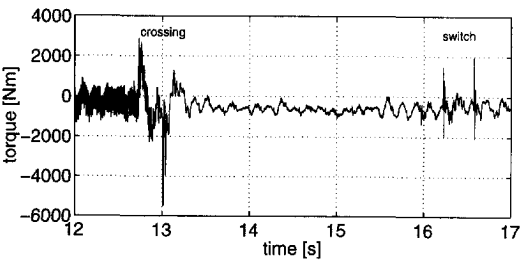

Hollow shaft torque T_{hsh}

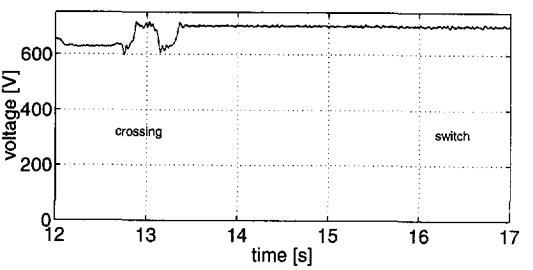

Inverter DC link voltage at u_{cinv} = 700 V

Figure 3.3.20 Response of low-floor tram bogie drive on rail crossing and switch.

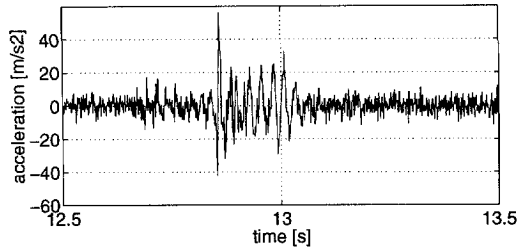

Vertical acceleration motor housing az_m

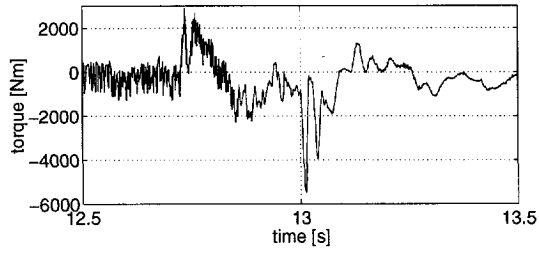

Hollow shaft torque T_{hsh}

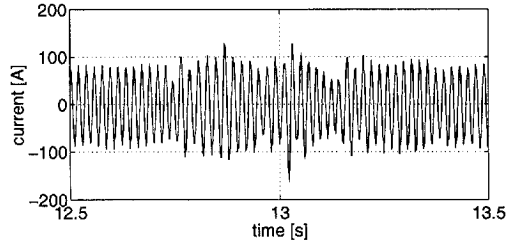

Inverter phase current i_u

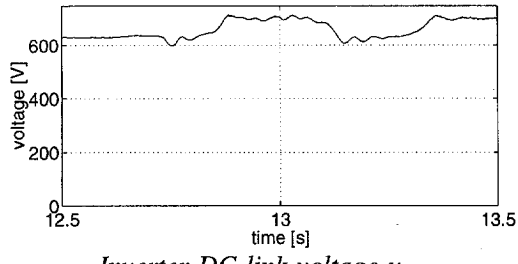

Inverter DC link voltage u_{cinv}

Figure 3.3.21 Detail of response of low-floor tram bogie drive on rail crossing.

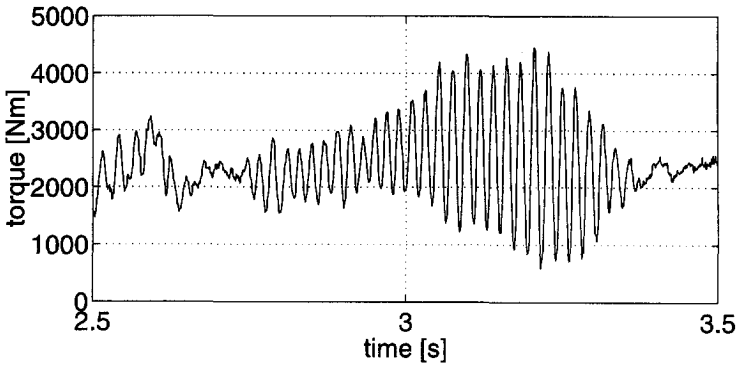

Figure 3.3.22 Hollow shaft torque oscillation of low-floor tram bogie drive.

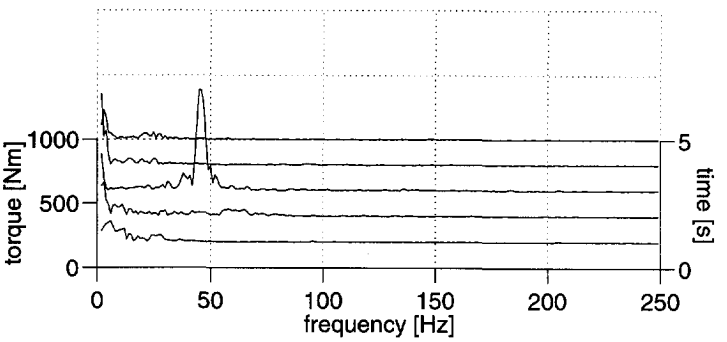

Hollow shaft torque T_{hsh}

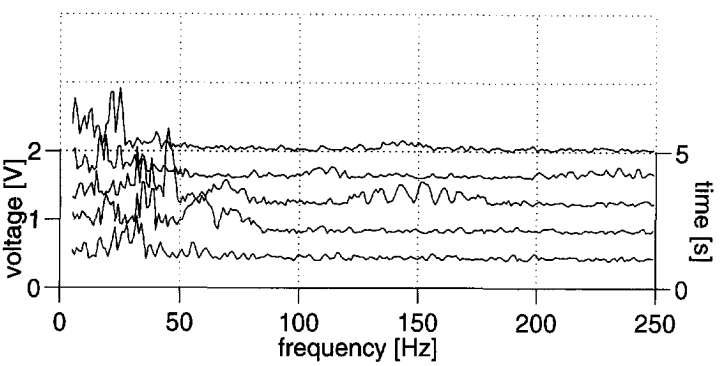

Inverter DC link voltage u_{cinv}

Figure 3.3.23 Spectra of torque oscillation of low-floor tram bogie drive.

3.4 Conclusions

The first problem statement of the thesis: -
Develop a test procedure including data processing which enables the detection of oscillations in traction drives -
has been treated in this chapter and has led to the following conclusions:

A procedure has been developed to perform experiments which enable the measurement and analysis of oscillations in traction drives in vehicles on track with a reasonable expenditure of effort.

- Before setting up any test the phenomena to be investigated have to be defined. The test parameters and the data acquisition parameters must be chosen appropriately for the phenomena which are to be investigated. This prevents us from obtaining incomplete data sets and an amount of data which cannot be processed and analyzed with a reasonable degree of effort.
- It is necessary to place sensors throughout the electrical and mechanical drive, including the control system, to detect oscillations and to analyze their propagation. Signals have to be acquired simultaneously.
- Tests contain two types of uncertainties, the actions of the operator and the rail conditions. Therefore, every test has to be considered as a single case. A number of tests will have to be analyzed statistically in order to evaluate seriously a vehicle drive. Test results presented in chapter 3 have to be seen exclusively as examples in the detection of oscillation phenomena.
- Tests on a vehicle test bench with fixed rollers eliminated rail influences, which increases the repeatability of tests but excludes a significant source of
- Since the bandwidth of oscillations to be investigated is limited, a relatively low sample frequency can be chosen for data-acquisition, which also helps to limit the data set size. Appropriate anti-aliasing filters are absolutely necessary.
- A traction cycle of acceleration, coasting and braking represented in the time domain and cascade plots provides an overview of a drive's system dynamics and oscillation characteristics.
- During the tests performed, four types of sources of oscillations were detected:

1. control system.
2. inverter.
3. mechanical drive.
4. wheel-rail contact.

- The measured torque oscillations generated by inverter harmonics had a low amplitude in comparison with the torque oscillations of mechanical origin. However, there may be transient high amplitudes in the case of resonances or a change of inverter voltage pulse pattern.
- Converter-excited oscillations were propagated throughout the entire drive while measured mechanical oscillations in general were limited to the mechanical drive.
- The highest oscillation amplitudes and peaks are caused by the rails. They can be propagated through the entire drive.

oscillations and shock loads.

4 Flexible Modelling

4.1 Introduction

After describing the traction drives to be investigated in Chapter 2 and discussing measured oscillations in Chapter 3, models derived to simulate oscillations are discussed below. The accent of modelling and simulation lies on the interaction between the electrical and mechanical drive. To be able to model the variety of mechanical drives that can be found in light-rail vehicles, modelling flexibility is important.

The point of departure for modelling is the phenomenon to be investigated. Depending on the phenomenon, the parts of the drive to be modelled and the order of the models have to be chosen. When investigating oscillations at low frequencies lumped parameter models were chosen. This means representation of motor windings by coils and representation of mechanical structures by rigid bodies connected by springs and dampers. Models are continuous in the time domain, which means that no switching devices are part of the models. All influences from switching converters are translated into voltage-source harmonics.

Drive modelling as discussed here is mainly white box modelling which means that the structure of the model and the parameters are known. Models will be derived as much as possible by deduction if the drive has been constructed or designed using physical laws. Causality has to be added to the model to indicate the cause of an oscillation.

There are different graphical representations of models. Specific model representations have been chosen, since one of the aims of modelling is the link to physical parameters. Motor or converter models are represented by circuit diagrams, the control systems by block diagrams and mechanical structures by rigid bodies, springs and dampers, with forces and torques which are acting on the bodies. From the model representations, ordinary differential equations are derived, ready for numerical integration or small signal analysis.

In section 4.2 the electrical drive model is derived, including motor, inverter and control. Section 4.3 treats the flexible modelling of mechanical drives by multi-body system modelling. A model of the wheel-rail contact is given in section 4.4. These models are subsequently integrated into a system model to be used for simulation. Integration and examples are described in section 4.5. Finally, the software implementation of the modelling is outlined in section 4.6. Section 4.7 gives the conclusions.

4.2 Electrical drive

4.2.1 Traction motor

Since the induction motor with squirrel cage rotor was exclusively used in the vehicles under consideration only this motor type is modelled. The supply of the motor is assumed to be a voltage source inverter which generates pulse-width modulated waveforms. Generally three types of oscillations appear with induction motors: torsional vibrations, radial vibrations and noise. Only the torsional oscillations are treated here. Oscillations may be free oscillations caused by machine transients or forced oscillations caused by supply voltages and machine asymmetries [BEL94]. The basic approach to modelling the motor is illustrated by the block shown in Figure 4.2.1.

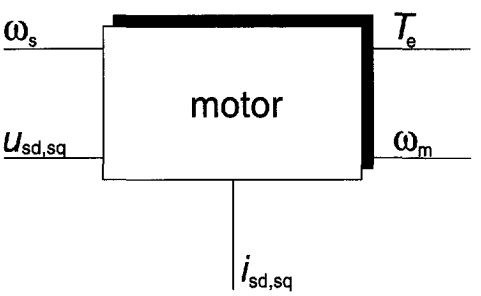

Figure 4.2.1 Block representation of induction motor

Finite-element calculation is used to the design of stator and rotor slots and provides the possibility to calculate the influences of geometry on field distribution. A lumped parameter model with an inductance matrix which is dependent on rotor position was derived from finite-element calculations by De Weerdt [WEE95]. He derived a model of the motor with $2p$ poles and N rotor bars which has three stator phases and $N/2p$ rotor phases.

Field harmonics are generated by the non-sinusoidal distribution of the motor m.m.f. which contribute to the motor torque. They have several causes:
- distribution of windings in stator and rotor slots
- non-constant air gap due to slotting or eccentricity
- saturation of the iron core.

The field harmonics may cause constant torques such as asynchronous torques or oscillating torques such as synchronous torques. Analytically, the field harmonics can be calculated separately by introducing separate windings for each field. Literature explains the torques at sinusoidal supply with the fixed frequency of mains, which in most cases is 50 Hz or 60 Hz [RIC54, JOR69].
Due to the non-sinusoidal distribution of the stator windings, the field distribution at a symmetrical sinusoidal three phase supply of stator currents with an angular frequency of ω contains space harmonic fields given by

$$B_{1,\nu}(\alpha_1,t) = \mu_0 \frac{3\ w_1}{\delta\ \pi\ p} I_1 \frac{\xi_{1,\nu}}{\nu} \cos(p\ \nu\ \alpha_1 - \omega\ t)$$

with

$$\nu = 1 + 6\ k_1\ , \qquad k_1 \in Z$$

and

$B_{1,\nu}$ flux density of the harmonic stator field
α_1 space coordinate
w_1 number of windings of the stator phase winding
δ air gap length
I_1 stator current amplitude
$\xi_{1,\nu}$ winding factor of the harmonic stator field.

The harmonic fields have a number of $2|\nu|p$ poles and their rotating frequency is $1/\nu$ of the frequency of the fundamental field. Each field induces a voltage in the rotor cage thus causing a rotor current and rotor field. Fields of stator and rotor with the same rotating frequency and the same number of poles generate a constant torque. Hence, for each harmonic stator field, a constant torque, an asynchronous torque, is generated.

In the case of inverter-fed motors these parasitic torques may not be neglected a priori because:

1. The supply frequency may assume values starting from very low frequencies. This means that the asynchronous torques may appear at a motor speed which is between synchronous speed and the speed at the pull-out torque.
2. Transients of harmonic fields due to variable frequency operation may have influence on the torque.
3. The supply voltage is superposed by harmonics which generate time harmonic fields. These time harmonic fields cause space harmonic fields, due to the winding distribution, which contribute to the torque.

The equivalent circuit for the steady-state of the induction motor with stator field harmonics is shown in Figure 4.2.2 indicating the harmonic fields by the index ν.

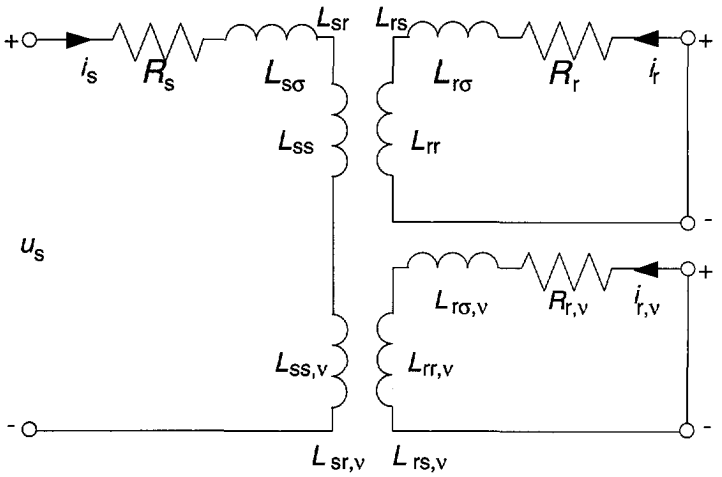

Figure 4.2.2 Induction motor model with stator field harmonics

The asynchronous torques of a traction motor at various supply frequencies in steady-state using the model depicted in Figure 4.2.2 have been calculated by Zijlstra [ZIJ94/2].
Figure 4.2.3 shows the example of asynchronous torques within the torque-speed characteristic of a voltage-fed induction traction motor at 60 Hz, 6 Hz and 1 Hz sinusoidal supply frequency. These calculations showed that in the steady-state the influence of asynchronous torques may be neglected within the stator and rotor frequencies of operation. At 60 Hz supply frequency, the asynchronous torques between -500 rpm and 500 rpm can be recognized. At 6 Hz supply frequency, the asynchronous torque is still beyond the slip frequency of operation of the drive. At synchronism of the asynchronous torque, the magnetizing current of the harmonic field is minimum. Hence, the flux of the machine decreases, thus a slight dip in the curve of the fundamental air gap torque can be noted. At a supply frequency of 1 Hz, the influence of asynchronous torques is negligible over the entire speed range. Hence, the influence of stator winding field harmonics may be neglected for the operation of the traction motor at variable stator frequency.

The investigation of torques caused by field harmonics has been restricted to this example, leaving time and space for investigation of system modelling rather than of component modelling.

The model of the traction motor was derived under the following assumptions:
- The induction machine has a three-phase stator winding and a squirrel cage.
- Both stator and rotor are symmetrical.
- The m.m.f. distribution is assumed to be sinusoidal.
- The air gap between stator and rotor is constant.
- Influence of slotting is accounted for by Carter's factor.
- Constant permeability of stator and rotor material. Thus inductances are constant.
- Skin effect is neglected.
- Iron losses are neglected.

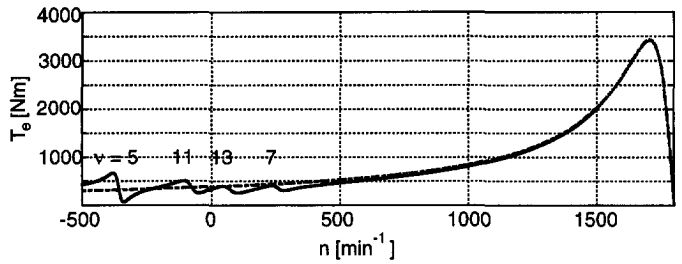

Air gap torque including asynchronous torques (solid line) and fundamental air gap torque (dotted line) at 60 Hz stator frequency

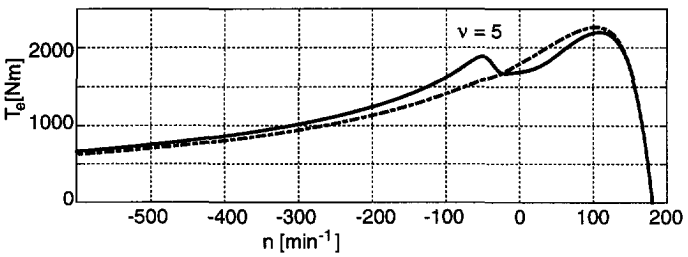

Air gap torque including asynchronous torques (solid line) and fundamental air gap torque (dotted line) at 6 Hz stator frequency

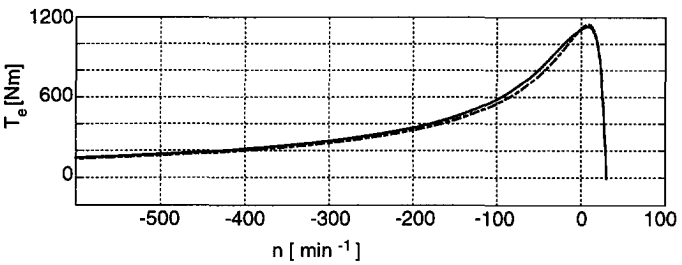

Air gap torque including asynchronous torques (solid line) and fundamental air gap torque (dotted line) at 1 Hz stator frequency

Figure 4.2.3 Torque speed characteristics of a traction motor including stator winding harmonics.

Model equations

The induction motor can be described by three-phase stator windings and three-phase rotor windings as shown in Figure 4.2.4.

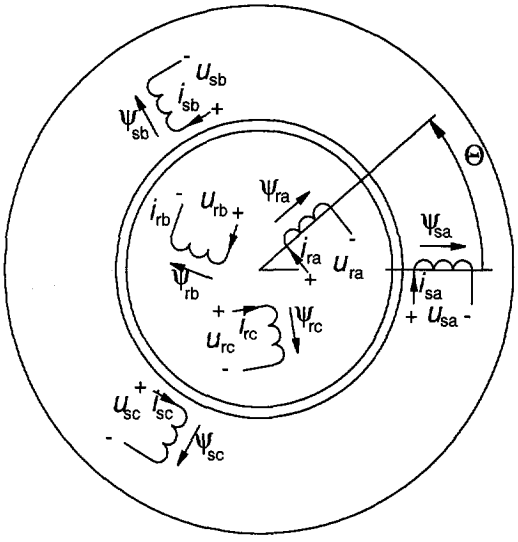

Figure 4.2.4 Schematic description of induction motor.

The voltage equations of the motor are given by:

$$\underline{u} = \underline{R}\,\underline{i} + \frac{\mathrm{d}\underline{\Psi}}{\mathrm{d}t} \tag{4.1}$$

with

$$\underline{\Psi} = \underline{L}\,\underline{i}$$

and:

$\underline{u}$ space phasor of phase voltages
$\underline{R}$ matrix of stator and rotor resistances
$\underline{L}$ matrix of inductances
$\underline{i}$ space phasor of stator phase or rotor currents
$\underline{\Psi}$ space phasor of flux per phase or rotor mesh.

As the machine is symmetrical it can be represented by two stator phases and two rotor phases. Equations are expressed in a rotating frame. The angular frequency of the rotating frame is chosen to be the angular frequency of the supply voltage. Hence, steady-state values of stator variables become DC values. The transformations of the equations are described in appendix A. Figure 4.2.5 shows the equivalent circuit of the induction motor. Rotor quantities have been referred to the stator by the winding ratio between rotor and stator. If stator and rotor fluxes are chosen as variables, the voltage equation 4.1 will become

$$\frac{d\underline{\Psi}_s}{dt} = -\frac{1}{\sigma\,\tau_s}\,\underline{\Psi}_s + \omega_s \begin{pmatrix} 0 & 1 \\ -1 & 0 \end{pmatrix} \underline{\Psi}_s + \frac{1-\sigma}{\sigma}\,\frac{1}{\tau_m}\,\underline{\Psi}_r + \underline{u}_s$$

$$\frac{d\underline{\Psi}_r}{dt} = -\frac{1}{\sigma\,\tau_r}\,\underline{\Psi}_r + \omega_r \begin{pmatrix} 0 & 1 \\ -1 & 0 \end{pmatrix} \underline{\Psi}_r + \frac{1-\sigma}{\sigma}\,\frac{1}{\tau_k}\,\underline{\Psi}_s \quad . \tag{4.2}$$

The torque equation is given by equation 4.3

$$T_e = p\,\frac{1-\sigma}{\sigma}\,\frac{1}{L_h}\,(\Psi_{sq}\,\Psi_{rd} - \Psi_{sd}\,\Psi_{rq}) \tag{4.3}$$

with the flux phasors

$$\underline{\Psi}_s = \begin{pmatrix} \Psi_{sd} \\ \Psi_{sq} \end{pmatrix}, \quad \underline{\Psi}_r = \begin{pmatrix} \Psi_{rd} \\ \Psi_{rq} \end{pmatrix}$$

and the stator voltage phasor

$$\underline{u}_s = \begin{pmatrix} u_{sd} \\ u_{sq} \end{pmatrix} \quad .$$

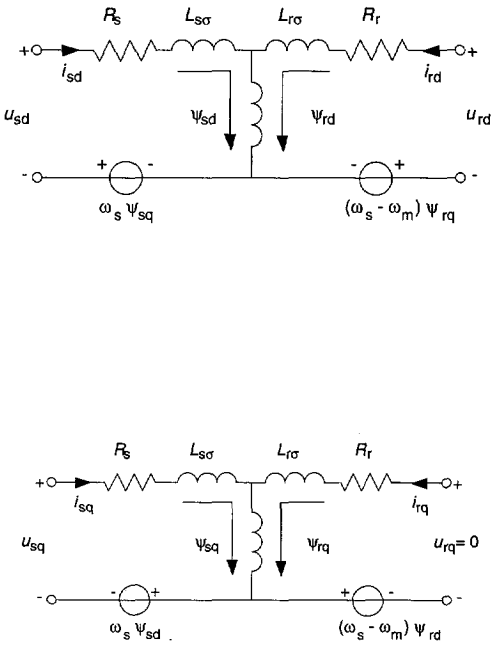

Figure 4.2.5 Equivalent circuit of induction motor.

The variables are:

ψ_{sd} stator flux d-axis
ψ_{sq} stator flux q-axis
ψ_{rd} rotor flux d-axis referred to the stator
ψ_{rq} rotor flux q-axis referred to the stator
ω_s electromagnetic stator angular frequency
ω_r electromagnetic rotor angular frequency

when

$$\omega_r = \omega_s - p\,\omega_m$$

with

p pair of poles

ω_m mechanical rotor frequency.

The parameters are:

$$\tau_s = \frac{L_s}{R_s}, \quad \tau_r = \frac{L_r}{R_r}, \quad \tau_m = \frac{L_h}{R_s}, \quad \tau_k = \frac{L_h}{R_r}$$

τ_s stator time constant

τ_r rotor time constant

τ_m air gap field stator time constant

τ_k air gap field rotor time constant

$$\sigma = 1 - \frac{L_h^2}{L_s L_r}$$

σ leakage factor.

Parameters

Motor parameters as derived from the equivalent circuit of figure 4.2.5. are

L_s stator inductance

L_r rotor inductance referred to the stator

$L_{s\sigma}$ stator leakage inductance

$L_{r\sigma}$ rotor leakage inductance referred to the stator

L_h mutual inductance for the machine with rotor parameters referred to the stator

R_s stator resistance

R_r rotor resistance referred to the stator

Stator and rotor inductances are defined by

$$L_s = L_h + L_{s\sigma}$$

$$L_r = L_h + L_{r\sigma} \quad .$$

Motor parameters can be determined by measurements of current, voltage and power with locked rotor and at no-load assuming a value of $L_{s\sigma}/L_{r\sigma}$. They can also be calculated by formulas found in literature by design parameters [NÜR63, SCH60]. In practice, the parameters depend on

- rotor position (slotting)
- saturation of the iron core
- stator and rotor frequency (skin effect)
- temperature.

Within the basic model the parameters are assumed to be constant.

Phase currents

The state variables of the motor model are fluxes in the d- and q-axis of a rotating frame. In practice, stator phase currents are measured. To obtain stator phase currents the following transformations have to be applied. First of all, stator currents in the rotating frame are calculated by

$$\underline{i}_s = (\underline{\Psi}_s - \underline{\Psi}_r \frac{L_h}{L_r}) \frac{1}{\sigma L_s} \quad .$$

Then currents are transformed to a frame fixed to the stator and are transformed from two-phase currents to three-phase currents. It has been assumed that there are no homopolar currents, i.e., the sum of the three phase currents is zero. Transformations are described in appendix A.

Linear model

Based on the model described in equations 4.2 and 4.3, a linear model for small variations in an operating point is derived. At a constant stator frequency small variations of flux and rotor frequency are considered. This assumption is valid for regular operation within a traction cycle when the variation of speed is negligible and fast flux and torque transients are absent. Instead of rotor frequency, the angular frequency of the motor shaft ω_m is be used in the equations in order to create a direct connection to the mechanical equations. Defining

$$\underline{\Psi}_s = \underline{\Psi}_{s0} + \Delta\underline{\Psi}_s$$

$$\underline{\Psi}_r = \underline{\Psi}_{r0} + \Delta\underline{\Psi}_r$$

$$\underline{u}_s = \underline{u}_{s0} + \Delta\underline{u}_s$$

$$\omega_m = \omega_{m0} + \Delta\omega_m$$

and introducing the equation of motion

$$T_l + J \frac{d\omega_m}{dt} + d\,\omega_m = p \frac{1-\sigma}{\sigma} \frac{1}{L_h} (\Psi_{sq}\,\Psi_{rd} - \Psi_{sd}\,\Psi_{rq}) \qquad (4.4)$$

with

J moment of inertia of rotor

d mechanical damping ratio (e.g. due to rotor bearings and fan)

T_l external load torque

equations 4.2 and 4.4 can be developed into the following equations assuming the mechanical damping ratio d and the external load torque T_l constant:

$$\frac{d\Delta\underline{\Psi}_s}{dt} = -\frac{1}{\sigma\,\tau_s} (\underline{\Psi}_{s0} + \Delta\underline{\Psi}_s) + \omega_{s0} \begin{pmatrix} 0 & 1 \\ -1 & 0 \end{pmatrix} (\underline{\Psi}_{s0} + \Delta\underline{\Psi}_s) +$$

$$+ \frac{1-\sigma}{\sigma} \frac{1}{\tau_m} (\underline{\Psi}_{r0} + \Delta\underline{\Psi}_r) + (\underline{u}_{s0} + \Delta\underline{u}_s)$$

$$\frac{d\Delta\underline{\Psi}_r}{dt} = -\frac{1}{\sigma\,\tau_r} (\underline{\Psi}_{r0} + \Delta\underline{\Psi}_r) + (\omega_{r0} - p\,\Delta\omega_m) \begin{pmatrix} 0 & 1 \\ -1 & 0 \end{pmatrix} (\underline{\Psi}_{r0} + \Delta\underline{\Psi}_r) +$$

$$+ \frac{1-\sigma}{\sigma} \frac{1}{\tau_k} (\underline{\Psi}_{s0} + \Delta\underline{\Psi}_s) \qquad (4.5)$$

$$T_l + J \frac{d\Delta\omega_m}{dt} + d\,(\omega_{m0} + \Delta\omega_m) =$$

$$= p \frac{1-\sigma}{\sigma} \frac{1}{L_h} ((\psi_{sq0} + \Delta\psi_{sq})(\psi_{rd0} + \Delta\psi_{rd}) - (\psi_{sd0} + \Delta\psi_{sd})(\psi_{rq0} + \Delta\psi_{rq}))$$

(4.6).

The steady-state is subtracted from equations 4.5 and 4.6 to obtain only the equations for small variations. Further there is set

$$\Delta\psi_{sd}\,\Delta\psi_{rq} = 0$$

$$\Delta\psi_{sq}\,\Delta\psi_{rd} = 0$$

$$\Delta\psi_{rd}\,\Delta\omega_m = 0$$

$$\Delta\psi_{rq}\,\Delta\omega_m = 0$$

so that the following equations are obtained; these are linear equations describing small variations of fluxes and rotor shaft frequency.

$$\frac{d\Delta\underline{\psi}_s}{dt} = -\frac{1}{\sigma\,\tau_s}\Delta\underline{\psi}_s + \omega_{s0}\begin{pmatrix}0 & 1\\ -1 & 0\end{pmatrix}\Delta\underline{\psi}_s + \frac{1-\sigma}{\sigma}\frac{1}{\tau_k}\Delta\underline{\psi}_s + \Delta\underline{u}_s$$

$$\frac{d\Delta\underline{\psi}_r}{dt} = -\frac{1}{\sigma\,\tau_r}\Delta\underline{\psi}_r + \omega_{r0}\begin{pmatrix}0 & 1\\ -1 & 0\end{pmatrix}\Delta\underline{\psi}_r - p\,\Delta\omega_m\begin{pmatrix}0 & 1\\ -1 & 0\end{pmatrix}\underline{\psi}_{r0} +$$

$$+ \frac{1-\sigma}{\sigma}\frac{1}{\tau_k}\Delta\underline{\psi}_s \qquad (4.7)$$

$$T_l + J \frac{d\Delta\omega_m}{dt} = - d\,\Delta\omega_m +$$

$$+ p \frac{1-\sigma}{\sigma} \frac{1}{L_h} (\psi_{sq0}\,\Delta\psi_{rd} + \psi_{rd0}\,\Delta\psi_{sq} - \psi_{sd0}\,\Delta\psi_{rq} - \psi_{rq0}\,\Delta\psi_{sd}) \quad . \tag{4.8}$$

A set of five linear equations has been obtained with the variables $\Delta\psi_{sd}$, $\Delta\psi_{sq}$, $\Delta\psi_{rd}$, $\Delta\psi_{rq}$ and $\Delta\omega_m$. Using these equations, stability analysis can be done but also system eigenvalues can be determined [TAE71, DEL82]. Transfer functions and frequency responses can be calculated. They, however, are state dependent as they depend on the fluxes and the speed of the chosen operating point. Transformation into the frequency domain is done by expressing the variations in

$$\Delta\underline{\psi}_s(\omega) = \hat{\underline{\psi}}_s\, e^{j\omega t}$$

$$\Delta\underline{\psi}_r(\omega) = \hat{\underline{\psi}}_r\, e^{j\omega t}$$

$$\Delta\underline{u}_s(\omega) = \hat{\underline{u}}_s\, e^{j\omega t}$$

with complex amplitudes indicated by the hat. If variables are described by a vector

$$\underline{x} = (\Delta\psi_{sd}\ \ \Delta\psi_{sq}\ \ \Delta\psi_{rd}\ \ \Delta\psi_{rq}\ \ \Delta\omega_m)^T$$

$$\underline{u} = (\Delta u_{sd}\ \ 0\ \ 0\ \ 0\ \ 0)^T$$

with

$$\Delta\underline{x} = \hat{\underline{x}}\, e^{j\omega t}$$

equations 4.7 and 4.8 become

$$j\omega \, \underline{E} \, \underline{x}(\omega) = \underline{A}(\omega) \, \underline{x}(\omega) + \underline{u}(\omega) \tag{4.9}$$

when $\underline{E}$ is the identity matrix and $\underline{A}$ is defined as

$$\underline{A} = \begin{pmatrix} \frac{-1}{\sigma \tau_s} & \omega_{s0} & \frac{1-\sigma}{\sigma} \frac{1}{\tau_m} & 0 & 0 \\ -\omega_{s0} & \frac{-1}{\sigma \tau_s} & 0 & \frac{1-\sigma}{\sigma} \frac{1}{\tau_m} & 0 \\ \frac{1-\sigma}{\sigma} \frac{1}{\tau_k} & 0 & \frac{-1}{\sigma \tau_r} & \omega_{r0} & -p \, \psi_{rq0} \\ 0 & \frac{1-\sigma}{\sigma} \frac{1}{\tau_k} & -\omega_{r0} & \frac{-1}{\sigma \tau_r} & p \, \psi_{rd0} \\ -\psi_{rq0} \, \kappa & \psi_{rd0} \, \kappa & \psi_{sq0} \, \kappa & -\psi_{sd0} \, \kappa & -\frac{d}{J} \end{pmatrix}$$

with

$$\kappa = p \frac{1-\sigma}{\sigma} \frac{1}{L_h} \frac{1}{J} \quad .$$

4.2.2 Inverter and control

A block representation of inverter and control is depicted in Figure 4.2.6. A reference torque T_{ref} is translated into a three-phase voltage $u_{u,v,w}$ with an angular frequency ω_s. The inverter phase currents are $i_{u,v,w}$. The inverter phase currents and the angular velocity of the motor ω_m are the feedback for control.

As the interaction between electrical drive and mechanical drive is the chosen subject, simple models for inverter and control have been derived. The models have to be sufficient to simulate a traction cycle including the stator voltage harmonics which are generated by the inverter.

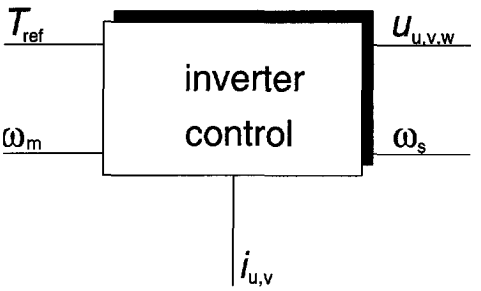

Figure 4.2.6 Block representation of traction inverter and control.

The fundamental inverter voltages are described by a three-phase sinusoidal voltage source expressed by the following equations:

$$\underline{u}_s = U_s \, e^{j\,2\pi\, f_{inv} t} \tag{4.10}$$

The fundamental of the inverter AC voltage has the inverter frequency f_{inv} and the amplitude U_s.

If these equations are transformed to rotating coordinates with the rotating frequency f_{inv} and expressed in the coordinates of the Cartesian reference frame d and q then the following equation is obtained.

$$\begin{aligned} u_{sd} &= \sqrt{\frac{3}{2}}\, U_s \\ u_{sq} &= 0 \qquad . \end{aligned} \tag{4.11}$$

Harmonics due to the switching behaviour are calculated separately. Amplitudes of the harmonics depend on the applied pulse pattern. A voltage harmonic of the stator voltage $\underline{u}_s$ is given by the equation

$$\underline{u}_{sv} = U_{sv} \, e^{2\pi\, v\, f_{inv}\, t \,-\, \phi_v}$$

The harmonics are calculated by the Fourier analysis of the stator voltages. Since the stator voltages are pulse-width modulated voltages odd harmonics appear. In a symmetric three-phase system the multiples of the third harmonic are eliminated. The harmonics generated by the symmetrical inverter are

$$\nu = -5,7,\ -11,13,\ -17,19\ ...$$

The three-phase system generates rotating fields in the motor. The sign of harmonics indicates the sense of rotation. In rotating coordinates the stator voltages are

$$\underline{u}_{sv} = \sqrt{\frac{3}{2}}\ U_{sv}\ e^{2\pi\ (\nu-1)\ f_{inv}\ t\ -\ \phi_v} \tag{4.12}$$

By superposition of fundamental and harmonics the required voltage waveforms can be described.

A way to simulate control dynamics is to measure the control system outputs during tests of the vehicle on track and to use them as inputs of the inverter and motor model. In the case of measurements on track, control system outputs were measured. In the case of the electrical multiple-unit the voltage reference u_{ref}, the inverter frequency f_{inv} and the DC link voltage u_{cinv} were measured. From these signals, the input of the motor model has been calculated by

$$\omega_s = 2\ \pi\ f_{inv}$$

$$u_{sd} = K\ \frac{u_{cinv}}{u_{ref}}\ f_{inv}$$

assuming a minimum frequency, which is not zero.
The data sets provide a simulation of a traction cycle for the vehicles under test including control system dynamics.

4.3 Modelling of mechanics

4.3.1 Multi-body system modelling

The mechanical structures to be modelled are mechanical drives, bogies or vehicles. Mechanical drives are composed of rotating shafts, gear wheels and couplings. Bogies are composed of drives which are suspended in the bogie frame and which allow rotation and translation. Vehicles are composed of car-bodies which are attached by suspensions on bogies. Modelling requires flexibility in order to be able to model various structures with different degrees of complexity. The block of the mechanical drive structure within the system is given in Figure 4.3.1. The motor air gap torque T_e and the motor shaft speed ω_m are the variables which couple the motor to the mechanical structure. The wheel torque T_w and wheel speed ω_w are the variables which couple the mechanical structure to the rails.
A rather accurate model is obtained by finite-element modelling of the mechanical structure. The number of elements may vary from a few to thousands. A simple model is obtained by a limited number of rigid bodies connected by springs and dampers. A classical multi-body system with rigid bodies is described by:

- its geometry,
- the degrees of freedom of the bodies with eventual constraints,
- the coupling of the bodies with masses and/or moments of inertia to each other and to ground by springs and dampers,
- external forces acting on bodies.

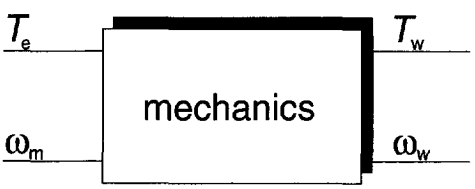

Figure 4.3.1 Mechanical structure block.

The differential equation of motion

$$\underline{M}\ \ddot{\underline{q}} = \underline{F} - \underline{K}(\dot{\underline{q}},\underline{q})$$

with

$\underline{M}$ mass matrix
$\underline{q}$ generalized degrees of freedom
$\underline{F}$ external forces and torques
$\underline{K}$ vector of internal forces

has to be derived from the system description.

There are several algorithms which lead to the differential equations. The choice of the algorithm used in this thesis was the principle of virtual power. The geometry of the system is described by reference frames whose origin lies in the centre of gravity of the body. Connections between bodies through springs and dampers are related to these reference frames. Each body may have six degrees of freedom, translation in the three directions of the reference frame and rotation around the three axes of the reference frame. Constraints caused by, e.g., a rigid connection between bodies may limit the degrees of freedom.
Each body of the mechanical structure has to be described by its degrees of freedom and centre of gravity, its mass and inertias. The external forces and torques which act on the body have to be specified and indicate the geometrical position of forces and torques. The reference frames generally are chosen to be inertia frames. Last, whether the body rotates around the principal axes of inertia has to be specified. General velocities of the bodies will be defined and velocities of points of reaction are calculated. Using the specifications above, the algorithm determines the virtual power of the inertial forces and the virtual power of the active forces. The power balance equation is:

$$F_r^*\ \delta v_r + F_r\ \delta v_r = 0$$

with

F_r^* generalized inertial forces of the system
F_r generalized active forces of the system, including external and internal forces
r index of degree of freedom
* index of inertial forces.

The algorithm has been described by Kane and Levinson [KAN80], while the theory has been outlined by Kane [KAN85]. Here, is given a short description in order to indicate how equations are derived from the geometrical structure. In the following sections equations of motion are derived for several models.

The assumptions made for modelling are
- The reference frames are defined as Cartesian frames with:
  positive x: direction of motion of the vehicle
  positive y: left from the direction of motion of the vehicle
  positive z: direction opposite of forces of gravity.
- The rotation axes are always the principal axes of gravity of each body.

A set of second-order differential equations is obtained

$$\underline{M}\,\ddot{\underline{q}} + \underline{C}\,\dot{\underline{q}} + \underline{K}\,\underline{q} = \underline{F} \tag{4.13}$$

which are transformed into the following set of first order differential equations by

$$\dot{\underline{q}} = \underline{u} \tag{4.14}$$

$$\dot{\underline{u}} = -\underline{M}^{-1}\,((\underline{C}\,\underline{u} + \underline{K}\,\underline{q}) - \underline{F}) \tag{4.15}$$

with

$\underline{q}$	vector of generalized degrees of freedom
$\underline{u}$	vector of generalized velocities
$\underline{M}$	mass matrix
$\underline{C}$	damping matrix
$\underline{K}$	stiffness matrix
$\underline{F}$	load vector.

This set of linear equations can be transformed into the frequency domain. Eigenvalues and eigenvectors can be calculated. The eigenvalues represent the natural frequencies and the eigenvectors represent the oscillation modes of the mechanical system.

4.3.2 Mechanical drive

The degrees of freedom of a model of the mechanical drive are chosen taking the following into consideration:
- which oscillation has to be simulated,
- which torques and forces have to be calculated,
- which frequency band has to be considered,
- how the wheel-rail contact has to be included.

Here, the modelling of a mechanical drive is illustrated by the example of the hollow shaft drive. Specific models are derived in Chapter 5 for the simulation of oscillations. The mechanical drive is composed of the motor shaft, the gear wheels and the wheel axle with their interconnections by hollow shafts, cardan shafts, quill shafts and couplings. The components to be modelled are:
- rotor with bearings
- cardan shaft, quill shaft or hollow shaft
- elastic couplings
- gearbox with bearings
- wheel-set.

The example of a model for practical use in Figure 4.3.2 shows a model representation of the mechanical drive with six degrees of freedom. It is composed of motor, gearbox and wheel-set. The two-stage gearbox is connected to the wheel axle by a hollow shaft and an elastic coupling. In this case the motor shaft is connected to the pinion shaft of the gearbox by an elastic coupling.

The six degrees of freedom are represented by those of the six rigid bodies: motor shaft (a), pinion shaft (b), intermediate gear wheel shaft (c), gear wheel shaft (d), coupling side wheel (e) and gearbox side wheel (f). The motor shaft is driven by the air gap torque (T_e). Motor and pinion shaft are connected by a flexible coupling which is modelled by a spring and damper (T_1). The inertia of the coupling has been added to the rotor and pinion wheel inertia. Gear wheel forces are transmitted by gear teeth which are modelled by springs (F_1 and F_2). The hollow shaft of the gear wheel is connected to the wheel axle near the wheel by a flexible coupling, again modelled by spring and damper (T_2). Here the stiffness of the hollow shaft and its flexible couplings is modelled as a single spring.

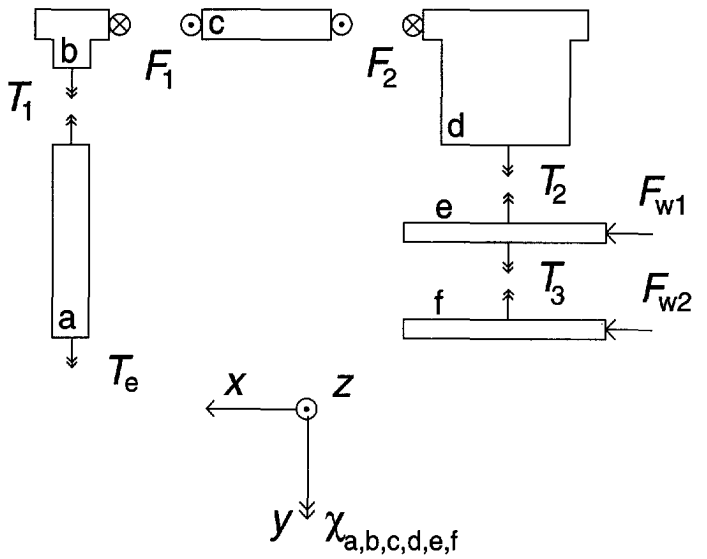

Figure 4.3.2 Model of mechanical hollow shaft drive.

The wheel axle is modelled by a spring and damper which is connected to the second wheel. The wheel axle has its torsional spring constant, so that a torque T_3 is transmitted to the gearbox side wheel. The bearings, cooling fans of the motor and the gearbox are assumed to be without losses. There are six reference frames, each in the centre of gravity of a body. Calculating inertia and active torques, the equations of motion are derived as follows.

According to equations 4.13 to 4.15 the following matrices and vectors are derived for the drive model: the mass matrix $\underline{M}$

$$\begin{pmatrix} J_{a\chi} & 0 & 0 & 0 & 0 & 0 \\ 0 & J_{b\chi} & 0 & 0 & 0 & 0 \\ 0 & 0 & J_{c\chi} & 0 & 0 & 0 \\ 0 & 0 & 0 & J_{d\chi} & 0 & 0 \\ 0 & 0 & 0 & 0 & J_{e\chi} & 0 \\ 0 & 0 & 0 & 0 & 0 & J_{f\chi} \end{pmatrix}$$

the stiffness matrix $\underline{K}$

$$\begin{pmatrix} k_1 & -k_1 & 0 & 0 & 0 & 0 \\ -k_1 & k_1 + r_b^2\, k_2 & r_b\, r_c\, k_2 & 0 & 0 & 0 \\ 0 & r_b\, r_c\, k_2 & r_c^2\,(k_2 + k_3) & r_c\, r_d\, k_3 & 0 & 0 \\ 0 & 0 & r_c\, r_d\, k_3 & r_d^2\, k_3 + k_4 & -k_4 & 0 \\ 0 & 0 & 0 & -k_4 & k_4 + k_5 & -k_5 \\ 0 & 0 & 0 & 0 & -k_5 & k_5 \end{pmatrix}$$

and the damping matrix $\underline{C}$

$$\begin{pmatrix} c_1 & -c_1 & 0 & 0 & 0 & 0 \\ -c_1 & c_1 & 0 & 0 & 0 & 0 \\ 0 & 0 & 0 & 0 & 0 & 0 \\ 0 & 0 & 0 & c_4 & -c_4 & 0 \\ 0 & 0 & 0 & -c_4 & c_4 + c_5 & -c_5 \\ 0 & 0 & 0 & 0 & -c_5 & c_5 \end{pmatrix} .$$

The damping of gear teeth has been neglected. The vectors of degrees of freedom $\underline{q}$ and the load vector $\underline{F}$ are given by

$$\underline{q} = \begin{pmatrix} \chi_a \\ \chi_b \\ \chi_c \\ \chi_d \\ \chi_e \\ \chi_f \end{pmatrix} \qquad \underline{F} = \begin{pmatrix} T_e \\ 0 \\ 0 \\ 0 \\ F_{w1}\, r_e \\ F_{w2}\, r_f \end{pmatrix}$$

with

$J_{a,b,c,d,e,f}$	inertia of bodies	[kg m^2]
$\chi_{a,b,c,d,e,f}$	degrees of freedom of bodies	[rad]
T_e	motor air gap torque	[Nm]
$k_{1,4}$	spring constants of couplings	[Nm/rad]
$k_{2,3}$	spring constants of gear teeth	[Nm/m]
k_5	spring constant of wheel shaft	[Nm/rad]
$c_{1,4}$	damping of couplings	[Nms/rad]
c_5	damping of wheel shaft	[Nms/rad]
$r_{b,c,d}$	radius of gearwheels	[m]
$r_{e,f}$	radius of wheels	[m].

Parameters

Inertia values can be derived from the dimensions and materials of bodies. Spring constants of shafts have been calculated and measured by the manufacturer. The spring constant of shafts can be calculated from the specifications of material and geometry [NES58].

Spring and damper characteristics of elastic couplings are found in coupling specifications. The most critical parameter in this model is the damping of the couplings as it is dependent on the frequency of the applied torque as described by Peeken [PEE86].

The damping factor c can be calculated from the relative damping by the equation

$$c = \frac{\Psi \, k_{Tdyn}}{2\pi \, \omega_b} \tag{4.17}$$

with

k_{Tdyn}	dynamic stiffness
ψ	relative damping
ω_b	angular frequency of applied torque.

For elastic couplings with damping by, e.g., rubber, values of $\psi = 0.6$ to $\psi = 2$ are usual [BEI94]. For steel couplings and shafts values of $\psi = 0.01$ or $\psi = 0.02$ are common.

The stiffness and damping of an elastic coupling are described by Figure 4.3.3. The static stiffness k_{Tstat} depends on the applied torque as indicated by the dotted curve. This characteristic is usually determined experimentally. Dynamic stiffness is defined in each point of operation, depending on the applied torque and frequency. Manufacturers give tables with the dynamic stiffness for a fraction of the rated torque at a defined temperature. When there is an increase in temperature the dynamic stiffness decreases.

The relative damping ψ is defined as the quotient of damping energy W_d and elastic energy W_e as indicated in Figure 4.3.3. An oscillating torque produces losses in the eoupling given by the hysteresis in the torque-angle characteristic. The damping c depends on the applied, constant torque and on the frequency of an oscillating torque superposed on the constant torque as given by equation 4.17.

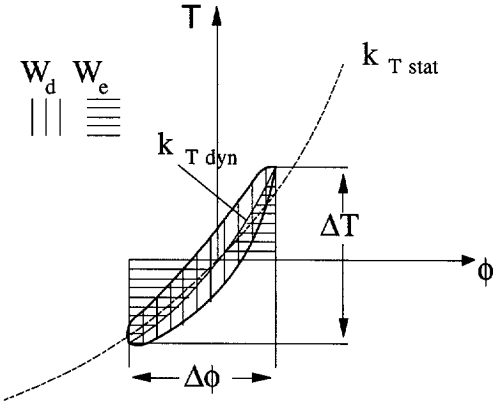

Figure 4.3.3 Dynamical stiffness and relative damping of flexible couplings.

Finally, the resistance of the vehicle on the track may be taken into account which is composed of:

- rolling resistance
- air resistance
- resistance of gradients
- curves.

Schwartz has given a formula to calculate the total resistance as a function of vehicle speed, vehicle mass and the gradient [SCH92].

4.3.3 Suspensions

In the preceding section modelling was described with exclusively rotational degrees of freedom and geometric linearity. For the modelling of suspension, translation and coupling of degrees of freedom are also introduced.

Motor suspension

Multi-body system modelling is applied to a suspended motor as shown in Figure 4.3.4. The geometrical configuration is shown, indicating the three suspensions S_1, S_2 and S_3 and their position with respect to the centre of gravity of the housing (0,0,0). The centre of gravity of the rotor is given by $(x_a,0,0)$. The active forces of the suspension F_{s1}, F_{s2}, and F_{s3}, which have been chosen for this example as reaction to the motor air gap torque, are shown in relation to the reference frame of the housing.

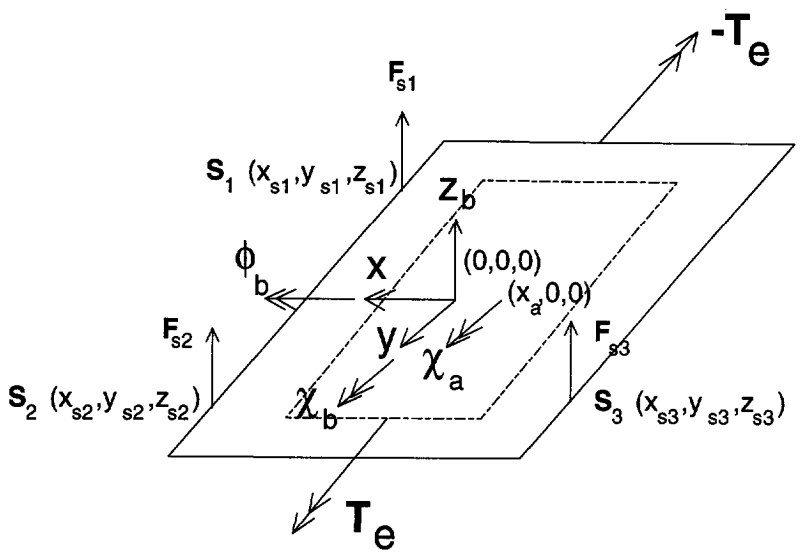

Figure 4.3.4 Model of a suspended motor.

The multi-body system can be described by two rigid bodies, the housing (b) and the rotor (a). Two reference frames are defined, the reference frame of the rotor

whose origin lies in the centre of gravity (x_a,0,0) and the reference frame of the housing whose origin lies in the centre of gravity of the stator (0,0,0). Both reference frames are fixed to ground. The degrees of freedom are defined as follows. The rotor may rotate around the y-axis with the angle χ_a and the housing has three degrees of freedom within its reference frame: vertical displacement z_b and rotation around the x-axis ϕ_b and rotation around the y-axis indicated by the letter χ_b. Defining the moments of inertia of the two bodies as $J_{a\chi}$, $J_{b\phi}$ and $J_{b\chi}$ and the masses as m_a and m_b, for each degree of freedom the generalized inertial and active forces can be formulated.

The equations of motion are given by (4.13) with the mass matrix $\underline{M}$

$$\begin{pmatrix} J_{a\chi} & 0 & 0 & 0 \\ 0 & m_a+m_b & 0 & -m_a x_a \\ 0 & 0 & J_{a\phi}+J_{b\phi} & 0 \\ 0 & -m_a x_a & 0 & J_{b\chi}+m_a x_a^2 \end{pmatrix} .$$

In the case where the centres of gravity of rotor and housing are identical and the reference frames of rotor and housing coincide, the matrix $\underline{M}$ becomes a diagonal matrix with the masses and inertias of the bodies as elements.

Assuming the same stiffness k for the three suspensions the stiffness matrix $\underline{K}$ is

$$\begin{pmatrix} 0 & 0 & 0 & 0 \\ 0 & 3k & k(y_{s1}+y_{s2}+y_{s3}) & -k(x_{s1}+x_{s2}+x_{s3}) \\ 0 & k(y_{s1}+y_{s2}+y_{s3}) & k(y_{s1}^2+y_{s2}^2+y_{s3}^2) & -k(x_{s1}y_{s1}+x_{s2}y_{s2}+x_{s3}y_{s3}) \\ 0 & -k(x_{s1}+x_{s2}+x_{s3}) & -k(x_{s1}y_{s1}+x_{s2}y_{s2}+x_{s3}y_{s3}) & k(x_{s1}^2+x_{s2}^2+x_{s3}^2) \end{pmatrix}$$

and the vector of degrees of freedom and the load vector

$$\underline{q} = \begin{pmatrix} \chi_a \\ z_b \\ \phi_b \\ \chi_b \end{pmatrix} \qquad \underline{F} = \begin{pmatrix} 0 \\ 0 \\ 0 \\ 0 \end{pmatrix} .$$

Motor and gearbox suspension

To model a mechanical drive in the bogie frame, the motor and gearbox housing and their suspension have to be modelled, extending, e.g., the model described in Figure 4.3.2.

If the traction motor and the gearbox are suspended by rubber suspensions in the bogie frame and the motor and gearbox housing are rigidly coupled, which is a common design for electrical multiple-unit and locomotive bogies, the housing is considered to be a single rigid body. Figure 4.3.5 shows the structure of the suspension model of the hollow shaft drive, assigning the index g to the additional body representing the housing.

The housing may have six degrees of freedom within its reference frame. Dependent on the modes to be modelled, constraints which limit the number of degrees of freedom are defined.

For the investigation of the influence of the electrical drive on the suspensions, following the major displacements which were measured, horizontal and axial displacement have been neglected, such as rotation around the vertical axis. Hence three degrees of freedom are added to the model of the mechanical drive: rotation of the housing around the horizontal (x) axis ϕ_g and axial (y) axis χ_g and displacement in vertical direction (z_g).

The reaction forces of the gear wheels on the gearbox (F_1 and F_2) and air gap torque of the motor on the stator (T_e) act on the housing.

The equations for the suspended drive are given in appendix B.

The parameters of the rubber suspension can be determined by finite-element modelling or taken from manufacturer's specifications. Using lumped parameter models the rubber suspensions are modelled by a spring and damper. As displacements are less than 1 mm the stiffness is considered to be constant.

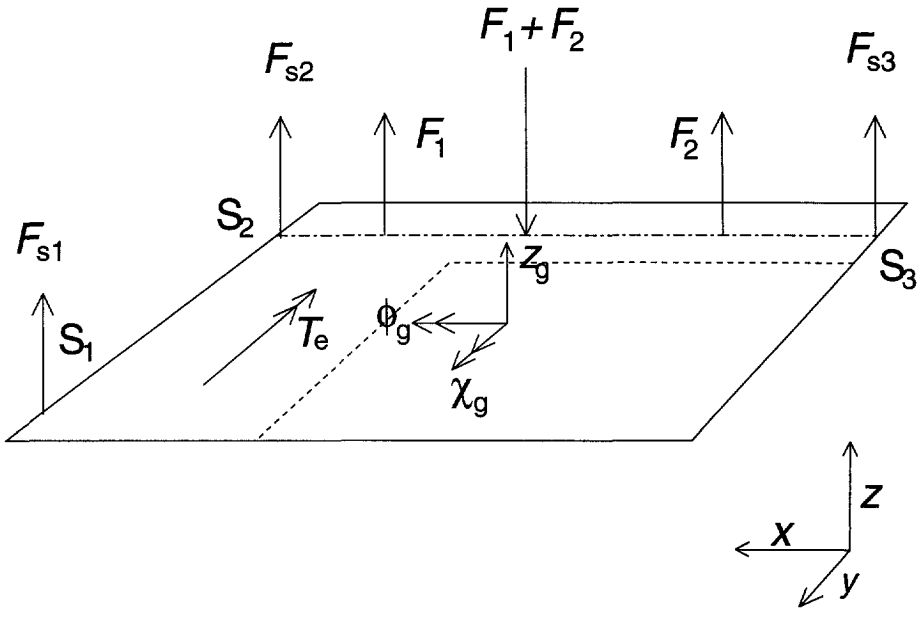

Figure 4.3.5 Model of motor and gearbox suspension.

Primary and secondary suspension

The primary suspension suspends the bogie frame from the wheel shaft bearing. To model the primary suspension, the ground reference frame is defined on the rails. Zeevenhooven gives an overview of bogie dynamics and oscillation modes. Degrees of freedom can be derived by the assumption of oscillation modes [ZEE89].

The secondary suspension suspends the car body from the bogie frame. In some cases, the secondary suspension is made up of two stages with a suspended beam between car body and bogie frame. The secondary suspension is modelled by introducing degrees of freedom of the car-body. The main degrees of freedom of the car body are described by Zeevenhooven [ZEE89]. The choice of modes to be simulated determines the degrees of freedom of the model [POE92].

4.4 Wheel-rail contact

4.4.1 Fundamentals

The wheel-rail contact can be described by the force transmitted from wheel to rail as shown in Figure 4.4.1

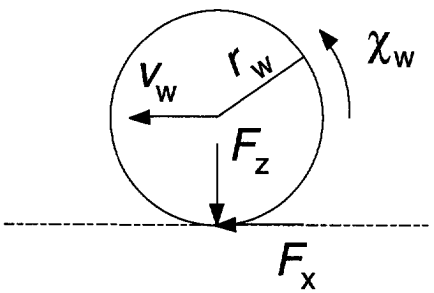

Figure 4.4.1 Forces of wheel-rail contact.

which is defined by

$$F_x = f\, F_z$$

with

F_x Tangential force on the wheel-rail contact point
F_z Normal force on the wheel-rail contact point
f Coefficient of friction.

The wheel-rail contact has been investigated by theoretical research and by measurements. Kalker developed a mathematical model, describing the elliptic contact area between wheel and rail [KAL67]. Kalker showed that a force from wheel to rail can only be transmitted in the case of a speed difference between wheel circumference and rail, the creepage. Kalker defined the creepage as the "sliding" of two elastic bodies at the rolling contact [KAL90].

The creepage can be divided into longitudinal and lateral creepage. Rotation of the wheel around the vertical axis against the rail causes spin. Kalker developed curves which describe the dependence between creepage, spin and transmitted forces and

torques [KAL90]. In the model derived for oscillation analysis, lateral creepage has not been modelled. Lateral movements of the wheel on the rails have a frequency of about 2 Hz while the natural frequency of the wheel shaft lies between 50 Hz and 100 Hz.

However, measurements have been done, which have been reported by Frederich [FRE83], Zeevenhooven et al. [FIE79], and Bauer [BAU86]. They tried to determine the dependence between creepage and transmitted force by measurements on locomotives. Their results can be summarized as follows:
All measurements showed that there is a maximum of transmitted force. If there is increase of the creepage the transmitted force will decrease. Frederich stated that the maximum of transmitted force lies at a constant difference of speed between wheel and rail of about 0.03 m/s up to a vehicle velocity of 15 km/h. Above 15 km/h the maximum lies at constant relative slip for all speeds [FRE83]. These characteristics are valid for dry rails. Bauer concluded that the maximum of transmitted force lies at a constant difference of speed of about 0.4 m/s for a wide speed range [BAU86], which is valid for wet rails. Generally, measurements showed a high friction coefficient up to 0.4 at a low speed difference for dry rails and a low friction coefficient, below 0.2, at a higher speed difference for wet rails.
The speed difference Δv is defined by

$$\Delta v = v_w - v_v \quad .$$

The relative slip is defined as

$$s = \frac{\Delta v}{\frac{1}{2}(v_w + v_v)}$$

with

Δv	difference of speed between wheel and rail
s	relative slip
v_w	wheel speed
v_v	vehicle speed.

Figure 4.4.2 shows a curve of the friction coefficient f versus speed difference Δv for acceleration of a vehicle.

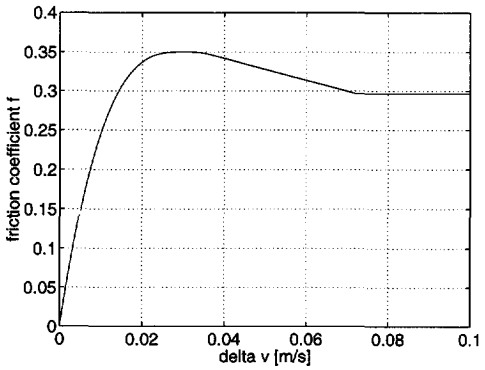

Figure 4.4.2 Friction coefficient as a function of speed difference.

4.4.2 A practical model

For a practical model only longitudinal forces and creepage are assumed. Lateral movement of the wheels is not added as a degree of freedom.
The transmitted force of an iron wheel on iron rails depends on various factors:
- dynamics of the normal force
- geometry of the contact area
- the surface quality of wheel and rail
- the lateral displacement between wheel and rail
- humidity
- temperature
- quality of wheel and rail material.

The ambient influences are considered through a stochastic distribution of parameters [SCH92].

To develop a practical friction curve, as shown in figure 4.4.2, choices have to be made via
- definition of the curve up to the maximum by:
    - the maximum value of transmitted force
    - the difference of speed or creepage at maximum transmitted force
    - the gradient at the origin of the curve
- definition of the curve beyond the maximum

- definition of the stochastic distribution of:
  - displacement on rails
  - speed difference or creepage
  - friction coefficient.

The curve used for simulation is documented in appendix C.

The wheel-rail contact can be represented by the block as shown in Figure 4.4.3.

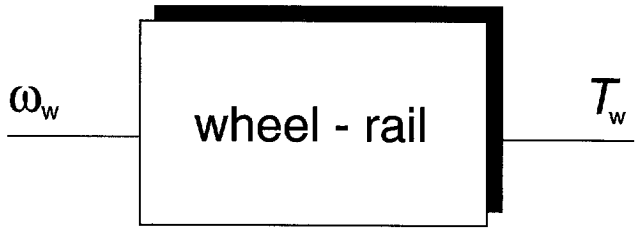

Figure 4.4.3 Wheel-rail contact model block.

A model of wheel-rail contact is depicted in Figure 4.4.4. It has been assumed that the wheel diameter is constant and that there is no flange contact. The friction coefficient f has been modelled as a function of speed difference.
The input of the model is the angular speed of the wheel under consideration. From the difference of the circumference speed of the contact point of the wheel and the velocity of the vehicle with respect to the rails, the friction coefficient f is calculated. The coefficient determines the force in the contact point which accelerates the vehicle on the one hand and which is the reaction force to the driving torque on the other hand. The reaction torque is the output of the model which enters into the mechanical model as external torque.
This model may be sufficient for a straight track at low speed. For higher speed, the speed difference has to be substituted by the relative slip. In order to simulate lateral displacements and spin, e.g., in curves and the sinusoidal oscillation of a wheel-set, taking the wheel profile into account, more complex models have to be derived.

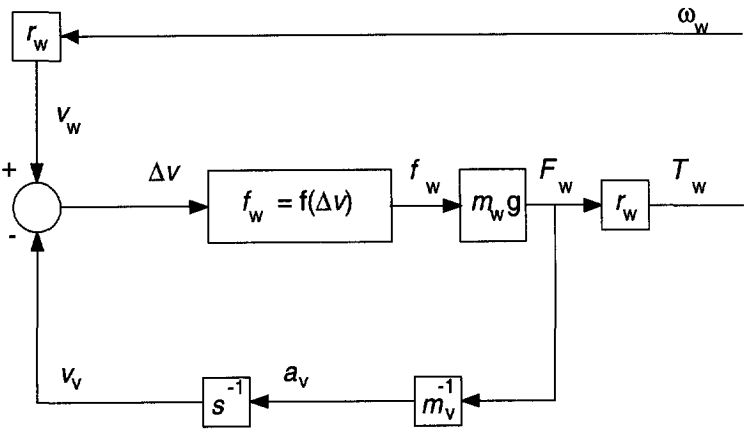

Figure 4.4.4 Wheel-rail contact model.

The symbols used are

ω_w	angular speed of the wheel
r_w	wheel radius
v_v	vehicle speed
a_v	vehicle acceleration
m_v	mass of the vehicle divided by the number of driven wheels
m_w	mass of the vehicle divided by the number of wheels
g	9.81 ms^{-2}
f_w	friction coefficient
Δv	speed difference between wheel and vehicle.

In the case of rolling wheels the wheel-rail contact is modelled by introducing the constraint

$$v_w = r_w \dot{\chi}_w \quad .$$

The equation of motion of the rolling wheel is given in appendix D.

4.5 System model

In the preceding sections, models of components of a rail vehicle drive have been derived, they yield sets of first-order nonlinear differential equations suitable for numerical integration.

$$\frac{d\underline{x}}{dt} = \underline{A}(\underline{x})\ \underline{x} + \underline{B}\ \underline{u} \tag{4.18}$$

with

$\underline{x}$ vector of variables
$\underline{A}(\underline{x})$ system matrix
$\underline{u}$ vector of excitation
$\underline{B}$ input matrix.

Forces, torques and currents can be calculated by

$$\underline{y} = \underline{C}(\underline{x})\ \underline{x} + \underline{D}\ \underline{u} \tag{4.19}$$

with

$\underline{y}$ vector of torques, forces and currents
$\underline{C}(\underline{x})$ output matrix
$\underline{D}$ matrix of transition.

An example of the equations of the drive described in section 4.3.2 is given in Appendix E.
The equations can be linearized at a point of operation, assuming small variations of the variables. Transformation to the frequency domain permits calculation of transfer functions and frequency responses. To calculate eigenvalues λ, the homogeneous equation is evaluated by

$$\det\ (\lambda\ \underline{E} - \underline{A}_{lin}) = 0 \quad . \tag{4.20}$$

Matrix $\underline{A}$ includes the motor parameters written in matrix $\underline{A}$ of equation 4.9 and the parameters of the mechanical structure written in the matrices $\underline{M}^{-1}\underline{K}$ and $\underline{M}^{-1}\underline{C}$ of equation 4.15. $\underline{E}$ is the identity matrix.
The matrix of transfer functions of the drive is defined as

$$\underline{H}(\omega) = (j\omega\ \underline{E} - \underline{A}_{lin})^{-1} \tag{4.21}$$

Frequency responses are calculated by

$$\underline{x}(\omega) = (j\omega\ \underline{E} - \underline{A}_{lin})^{-1}\ \underline{u}(\omega) \tag{4.22}$$

The frequency response of the fluxes and rotor speed can be calculated directly with equation 4.22. The response of currents and torque can be calculated by

$$\underline{y}(\omega) = \underline{C}(\omega)\ \underline{x}(\omega) + \underline{D}(\omega)\ \underline{u}(\omega) \quad .$$

Transfer functions and frequency responses are only valid for the chosen operating point, which means that each operating point is represented by its transfer function.
In the following, three examples are discussed: a drive of a wheel-set, a motor driven bogie and a vehicle with two motor driven bogies, in order to illustrate the system modelling. Only the first model has been used for simulations.
Figure 4.5.1 shows the model of a drive for a wheel or wheel-set composed of converter, motor, mechanics and wheel-rail contact. There is one wheel-rail contact block for each wheel.
The model equations are composed of
- the motor equations (4.2);
- the equations of the mechanical drive united with the torque equation (4.3).

The variables of the model are:
- the motor fluxes $\underline{\Psi}_s$, $\underline{\Psi}_r$
- the degrees of freedom of the bodies
- the first derivatives of degrees of freedom of the bodies

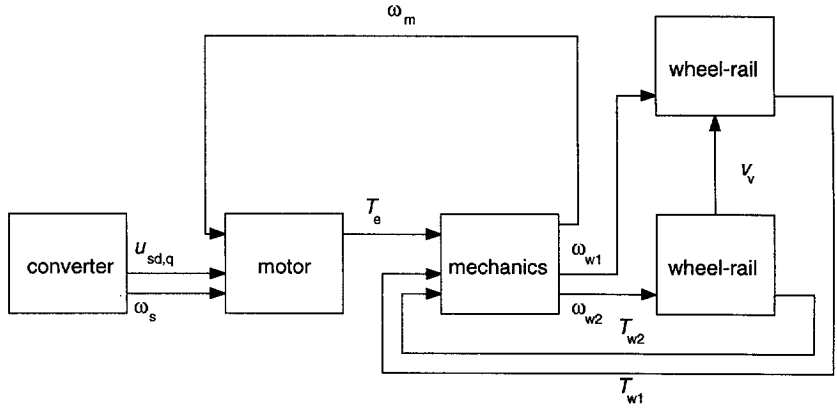

Figure 4.5.1 Model of a traction drive.

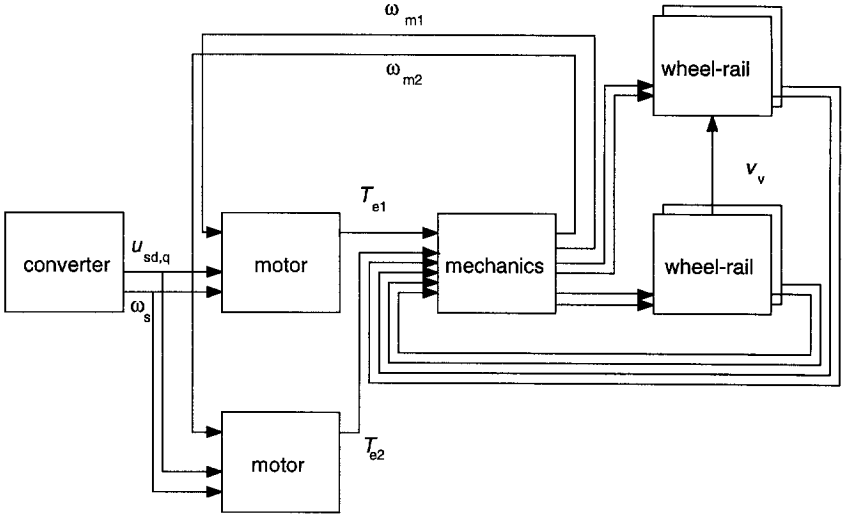

Figure 4.5.2 Model of a bogie.

If a bogie has to be modelled, the model will become more complex as shown in Figure 4.5.2. Here, a single converter feeds two motors in parallel which are placed in one bogie. The mechanical model contains the two drives which are mounted in the same bogie frame. There are four wheel-rail contact points to be considered. For the example of a bogie model of two motors, two drive lines and primary suspension, a system of ordinary differential equations can be derived which are composed under the assumptions given above and adding the following assumptions:

- Each of the motors is described by equations 4.2 and 4.3
- Both mechanical drives are described by the set of equations 4.13.
- The bogie frame introduces additional degrees of freedom.

The variables of the model are the variables mentioned above plus

- the motor fluxes, rotation angles and angular frequencies of the second drive
- the rotation angles and velocities of the drive housings and the bogie frame
- the displacement and speed of the drive housings and bogie frame.

A model of a vehicle car with two driven bogies with a single converter is obtained by extending the mechanical model of Figure 4.5.2. For the example of a vehicle model, a system of about 100 ordinary differential equations may be derived which are composed under the assumptions given above and adding the following assumption:

- Both bogies are supplied by a single converter
- Both bogies have the same degrees of freedom
- The car-body has additional degrees of freedom.

The variables of the model are the variables of two bogie models above with a single inverter current and voltage plus:

- rotation angles and angular frequencies of the car-body
- the displacement and speed of the car-body.

The examples have illustrated that basic models of vehicles are described by an extended set of differential equations. It requires an effort of several weeks to analyze oscillation modes and amplitudes of a single model. When several models and parameter variations have to be examined within a short time, models have to be as simple as possible. Hence, the reduction of model order is of great importance.

First the phenomenon to be investigated has to be defined by its sources, its frequency band and the range of operation of the drive. Formulating constraints will lead to a reduction of degrees of freedom. The frequency band of interest has to be limited thus leading to a further reduction of the model order.

4.6 Software implementation

The models have to be implemented into software which should meet the requirement of flexibility and also be user friendly. The software has several tasks:
- Implementation of a multi-body algorithm
- Building of component blocks including differential equations
- Building systems by means of component blocks
- Input by menu
- Graphical output.

Further, the software should meet the requirements of:
- Implementation on a Personal Computer
- Limited cost
- Suitability for measured data processing.

Various multi-body system algorithms have been applied in software for the modelling and simulation of dynamic systems [SCH90]. Some of them use Finite Elements to derive models such as SPACAR [JON90]. Others use rigid bodies with a limited number of degrees of freedom. During previous research on the modelling of traction drives, a dedicated program including a multi-body algorithm which uses the method of virtual work was developed [POE92]. Software dedicated to rail vehicle dynamics is described by Kortüm and Sharp [KOR93]. MEDYNA is widely used for rail vehicles, it contains a detailed model of the wheel-rail contact [WAL-91].

In order to fulfil the tasks a choice was made for the universal mathematical software, MATLAB®, which is suitable for modelling, simulation and data processing [MAT93]. The multi-body algorithm had to be integrated into MATLAB®. The program, AUTOLEV, written by Kane and Levinson which uses the virtual power method [SCH91] has previously been applied to the modelling of electromechanical systems [BON94]. As a low-cost software with an open structure it was well suited to be integrated into MATLAB® [OVE94].

The program AUTOLEV has been integrated into the software MATLAB® by use of the MATLAB® Extended Symbolic Toolbox [CHE93].
By using the SIMULINK® toolbox, system models can be composed of component

blocks which are part of a library [SIM93]. Figure 4.6.1 shows an example of a model in SIMULINK®.

There are blocks in the library for control system models, inverter models and wheel-rail contact models. The standard motor model is based on the equations 4.2 and 4.3. By using the menu various parameter sets can be created and used within the system model. The mechanical model block will be filled with the models created by input files. The software reads the input files, transforms them into files readable by AUTOLEV and starts AUTOLEV, which generates equations of motion. The equations of motion are rewritten automatically into a MATLAB® format which is loaded into the mechanical model block.

Systems with a maximum of 20 bodies can be created within the block. By composing systems with more than one mechanical model block, higher-order systems can be built. Parameters of mechanical models can be changed by menu.

The software provides simulation in the time domain, frequency domain and graphical output of variables [OVE94/2, OVE94/3]. Data sets acquired by measurements which have been discussed in Chapter 3 have been loaded and processed within MATLAB® [KRA94].

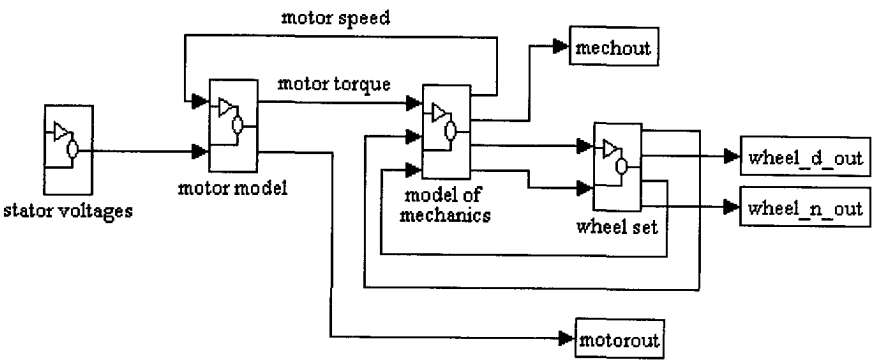

Figure 4.6.1 Model of a traction drive in SIMULINK®.

4.7 Conclusions

The second problem statement of the thesis -
Develop a method to model in a flexible and universal way traction drives including electrical and mechanical drive in order to describe and predict oscillations. -
has been treated in Chapter 4 which has brought us to the following conclusions:

A tool for modelling and simulation has been developed which enables the simulation and analysis of oscillations in traction drives. Due to the flexibility of the tool, a variety of drive types can be investigated in a short time.

- The goal of obtain the flexible modelling for oscillation analysis has been achieved by creating component models with a flexible structure which can be used to compose system models.
- The models include
  - switching harmonics of the inverter
  - mechanical degrees of freedom including rotation and translation
  - wheel-rail contact characteristics
- Models of components have to be simplified correctly to create system models for practical use, taking into consideration the frequency band to be investigated.
- System equations are first-order nonlinear differential equations that describe the dynamic operation of the system. The developed models are suitable for analysis by numerical integration in the time-domain and in the frequency domain by small signal analysis.
- The chosen software enables implementation of the models on a standard Personal Computer, using block diagrams from a library of components to compose systems.

5 Simulation and Analysis

5.1 Introduction

The system models discussed in the previous chapter are below used for the simulation and analysis of oscillations. The goal is to understand mechanisms of oscillations as a function of model structure and parameters.

First, we discuss the derivation of a model from a prototype or chosen design of a vehicle drive. With its parameter set, simulations are carried out in the time-domain and the frequency domain, thus indicating the frequencies and amplitudes of oscillations within the system. Next, the model is validated by measurements, if available. Last, the design is optimized in order to reduce oscillations by varying both structure and parameters. After having established the method of analysis, several sources of oscillations are investigated.

The accent of the investigations lies on the interaction between motor and mechanics, in particular on the analysis of couplings. The choice of couplings is discussed. The dynamics are simulated for acceleration of the vehicle, covering the frequency band, which contains the natural frequencies and excitation frequencies of interest.

The guidelines for simulation and analysis are given in section 5.2. In section 5.3, dynamics during acceleration are analyzed, taking the example of the hollow shaft drive with and without drive suspension. Frequency domain analysis of the traction motor and mechanical drive are first carried out separately, then, analysis of the drive is carried out in the time and frequency domains.

Section 5.4 examines oscillations of the mechanical drive, caused by inverter harmonics. Attention is focused on the attenuation of harmonics and on resonances.

Section 5.5 gives an impression of oscillations excited by the wheel-rail contact. Here, the accent lies on the determination of oscillation amplitudes and interaction of electrical and mechanical drives, taking the example of a fault condition, the stator short-circuit of the traction motor. The conclusion summarizes the analyses.

5.2 Methodology

5.2.1 Simulation

Model

The oscillation phenomenon and excitation source have to be defined first because they determine the bandwidth of the model and its parameters. Further, the system boundaries have to be defined, i.e., the part of the drive under investigation, which is relevant for the oscillation. The bandwidth is given by the maximum speed of the vehicle under consideration.

Depending on the oscillation to be investigated, a model has to be composed using the components described in Chapter 4. The basic model of the electrical drive has been chosen to be the two-axis motor model supplied by voltage sources and their harmonics, which values are determined by measured control outputs. Using this model, the dynamics of the torque-controlled drive can be simulated, including the voltage harmonics generated by the inverter.

The mechanical model may vary according to the phenomena to be simulated. The choice of models is discussed in the following sections. Generally, the model order is determined by modal analysis. The oscillation modes of the undamped mechanical system will be determined by computing the eigenvectors. By limiting the frequency band to be investigated, the model order can be reduced.

An approach to the reduction of the mechanical model order is its dynamic condensation, i.e., applying modal damping and reducing the model for the frequencies to within the desired bandwidth [MEIJ92]. This approach has been used by Poeze [POE92], who, however, assumed a Rayleigh damping, which implies that the damping matrix is a linear combination of stiffness and mass matrix.

However, one has to be aware of the dominant role the damping may play in the system. In particular, the frequency dependency of the damping of elastic couplings has to be taken into account.

Having determined the order of the model, the model's excitation has to be considered; this is made up of the fundamental inverter voltages including voltage harmonics. Additional disturbances may be external forces and torques.

When the excitation is known, in particular its frequencies, the damping can be

determined. Since parameters may depend on the frequency of excitation, they have to be represented as a function of frequency. Approximation tables are used for defined frequency bands.

Simulation in time-domain and frequency domain

Simulation can be done in the time domain by the numerical integration of the first-order differential equations derived in Chapter 4. The step size for explicit integration methods is determined by the highest natural frequency and the excitation of the model. Usually, explicit variable step size methods were chosen, suitable for systems with a limited frequency band [WAT82].

In the frequency domain eigenvalues, transfer functions and frequency responses can be calculated, assuming a linear model. Usually, frequency domain analysis is applied to control design. However, it can be used for system design, too, emphasizing open-loop model structures and the influence of system parameters on the critical frequencies of the drive and their damping.

The eigenvalues of the systems give an idea of the system's stability. The locus of the eigenvalues as a function of stator frequency represents the system during a traction cycle.

Usually, transfer functions that describe the system in the frequency domain are used for linear time-invariant systems by the amplitude and phase between a state variable or output variable and an input variable of the system.

In the case of the traction drive as described in Chapter 4, the model contains non-linearities of the motor and the mechanical systems. The model can be linearized in a point of operation, given by the stator frequency. For each point of operation, a transfer function can be calculated. Transfer functions give an insight into the frequency characteristics of the drive. The influence of stator voltage and torques and forces applied to the drive, on fluxes, speeds and displacement, can be calculated.

The advantages of frequency domain analysis are the high computation speed, the ease of analysis of parameter variation and the ease of control design. The disadvantage is the limitation to linear models in a point of operation.

Analysis has to give insight into the mechanisms of oscillation phenomena and particularly the interaction between the electrical and the mechanical drive. The dynamics of oscillations within a predefined traction cycle have to be simulated in the time-domain. The appropriate variables have to be visualized in order to explain

the mechanism of the oscillation and its dynamics. This means that, starting from excitation, the mechanical variables such as torques and speeds, forces and displacements, the electrical variables such as fluxes, currents and voltages have to be plotted. This can easily produce a great number of plots, but it is essential to capture the propagation of the oscillation throughout the drive.

Starting from the eigenvalues of the undamped mechanical drive, damping has to be incorporated and the mechanical drive has to be coupled with the electrical drive. The system eigenvalues of the open-loop drive as a function of parameters such as stator frequency and damping of couplings have to be evaluated. The relation between source and response has to be emphasized. Torques and forces can be related to specification values.

5.2.2 Validation

Validation of models can be done by
- comparison with a simplified model,
- comparison of a simulated and a measured time domain plot,
- identification of a model by measured data.

The first method has to be applied when no measured data is available, which occurs during the design process, before the prototype has been built. The simplified model can be obtained by a rigorous reduction of model order, such as done by Poeze, thus reducing the model to a few degrees of freedom [POE92]. Further, the dynamics of a mechanical system can be approximated by a static problem. The angles and displacements are then calculated by the equilibrium of forces and torques. To include the electrical drive, its steady-state operation has to be assumed.

The validation by comparison of simulated and measured plots is the "face" validation, which is a subjective validation. The weakness of this validation is the subjectiveness of the criterion to declare a model valid. However, there are methods to analyze the residuals which give criteria for validation, including analysis of the whiteness of residuals and analysis of the correlation between residuals and input [BOS94].

Identification of a model by measured data permits the estimation of models and their parameters; it is based on black box or grey box models. As a first and rough approach, the transfer functions may be estimated. The order of the system, its eigenfrequencies and the damping have to be identified.
Identification starts with a process analysis under operating conditions. During this analysis, signals are examined, the bandwidth of the process is estimated and sensors and data acquisition are tested. This analysis has been discussed in Chapter 3, where the bandwidth was limited to 500 Hz.
The identification experiment as defined by van den Bosch [BOS94] and van der Hof [HOF93] has to be done at constant stator frequency. Injecting a pseudo random binary sequence (PRBS), which guarantees persistence of excitation, the system variables are measured. The preferred signals chosen for injection are reference signals of the control system such as described by van Baars and Bongers [BAA94]. A remark has to be added as to the experiment design: Constant stator frequency is not easy to obtain with a torque controller that is commonly used in traction control. Therefore the experiment is carried out with coasting or minimum reference torque. If the experiment is short enough, the stator frequency variation can be limited.
The transfer functions may be estimated by the empirical transfer function estimate [LJU87]. The empirical transfer function estimate ETFE is defined as the quotient of the Fourier transforms of the measured output and input of the system.
Validation is done by comparing the identified transfer function to the transfer function of the physical model. Fitting of the model can be done by variation of parameters of the physical model.

5.2.3 Optimization

Two approaches to the optimization of the drive to reduce oscillations can be considered:
- control design and optimization,
- drive design and optimization, at component level and system level.

At the start of the design of a vehicle, specifications of components are subject of discussion. This aspect is treated in this thesis, in particular the choice of couplings. Optimization of the drive has to be done while taking into consideration a variety of possible oscillation sources such as those described in chapter 2 and measured in chapter 3. The choice of couplings includes the place within the drive and the type

and size of the coupling. The choice has to fit into the entire drive system while taking into account the bogie, motor, converter and control design.
Any choice of components should be examined within the system design. Depending on the results of analysis
- the drive structure has to be changed
- components and/or their parameters have to be changed.

Reduction of oscillation amplitudes and the oscillation time can be obtained by increasing the damping of the system. Increase of damping can be obtained by passive damping of components or by active damping by the control system, taking into account the fact that in the case of light-rail vehicles, traction drives are usually multi-motor drives.

Optimization is an iterative process which executes the procedure of simulation and analysis until the desired specification is met. At the start of the design process, the maximum of parameters can be changed with a minimum possibility of validation. Proceeding with the design, the freedom of parameter variation decreases with the increasing possibility of validation.
Validation of the models has to be done during all phases of prototype testing. This means that both the components and the entire system should be tested on oscillations. For example, tests on a test bench may help to optimize couplings and shafts as well as inverter pulse patterns and thus aid in obtaining an optimized system designed.

5.3 Drive dynamics

5.3.1 Traction motor

The dynamics of induction motors when operating at variable frequency have been investigated by various authors. Analysis in the frequency domain has been done, among others, by Kleinrath, Taegen and Novotny et al. [KLE80, TAE71, NOV78]. Transfer functions have been derived and stability analysis has been performed that indicate the motor's boundaries of stability.
Deleroi explained that, at constant rotor speed, the transients of the induction motor can be described by two transient rotating fields, one coupled with the stator, one coupled with the rotor [DEL82]. Kleinrath described the transient operation of the

induction motor by an electrical and a mechanical transient [KLE80]. These transients appear in an uncontrolled motor, i.e., a motor which is fed by voltage sources with imposed frequency and amplitude. In practice, the motor is controlled by a torque control system as described in section 2.3. In the following, however, the uncontrolled motor is considered in order to analyze the interaction between the motor and the mechanical drive.
An electrical multiple-unit motor is taken as an example in order to illustrate the transient operation of the motor.

It is known that at low frequencies the voltage-source-inverter fed motor may generate torque oscillations, known as "hunting" [UED92]; these occur in particular with motors with a high stator resistance. At low stator frequencies, the ratio of stator resistance versus main inductance increases. To illustrate the hunting phenomenon, Figure 5.3.1 shows the acceleration of an induction traction motor at no load up to a stator frequency of 18.8 Hz. At constant stator frequency, a torque oscillation is generated. Torque and rotor speed have been calculated by equations 4.2 and 4.4. The motor is fed by sinusoidal voltages with variable frequency and amplitude. Figure 5.3.2. shows a detail of the oscillation which has a frequency of 12.4 Hz. The oscillation is generated at *constant* stator frequency and voltage. It is an oscillation of stator and rotor fluxes which causes a torque oscillation. The chosen motor has a high stator resistance.

The transfer function of rotor speed divided by stator voltage has been calculated for stator frequencies of 10 Hz, 20 Hz, and 40 Hz with mean values of the motor flux. Eigenvalues have been calculated using equation 4.20. There are five eigenvalues of the system matrix $\underline{A}$. The first two eigenvalues have a frequency which is near the stator frequency. The third and fourth eigenvalues are weakly damped. Their frequency is constant for high stator frequencies but always lower than the stator frequency. The damping of this eigenfrequency may become negative so that self-excited oscillations may occur. The fifth eigenvalue is real and nearly constant. Figure 5.3.3 shows the transfer function at no-load, indicating the eigenfrequencies of the motor.
A traction drive can be modelled in the most simple case by adding an inertia to the motor's rotor inertia. A high inertia has a stabilizing effect on the motor, which can be illustrated by the transfer function of the traction motor of an electrical multiple-unit, shown in Figure 5.3.4. The frequency of the first two eigenvalues lies near the stator frequency. The damping of the third and fourth eigenvalue has increased,

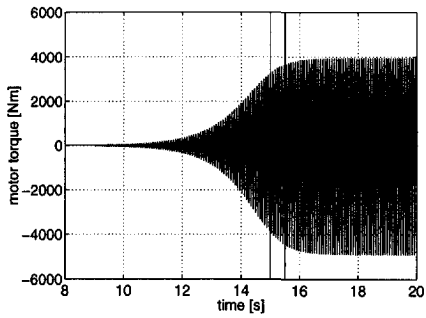

Air gap torque T_e

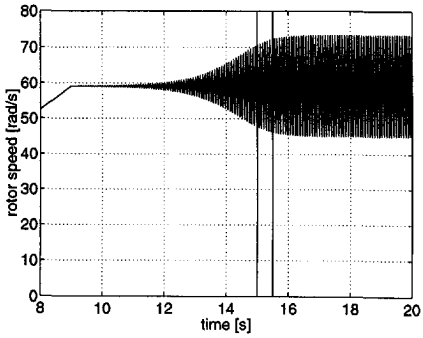

Rotor speed ω_m

Figure 5.3.1 "Hunting" phenomenon of the induction motor.

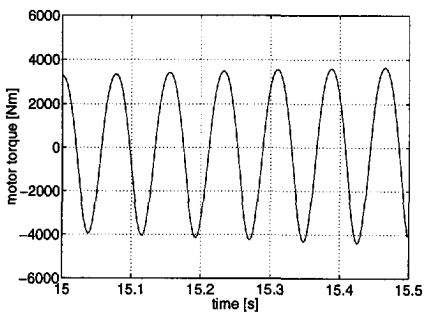

Air gap torque T_e

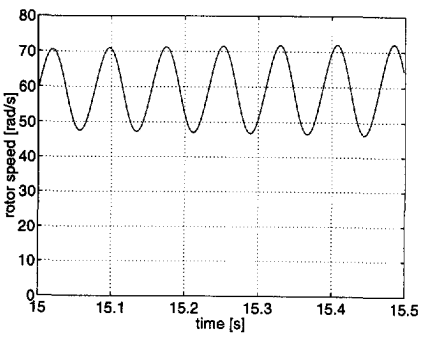

Rotor speed ω_m

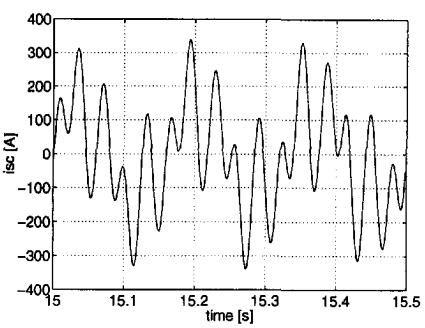

Stator current i_w

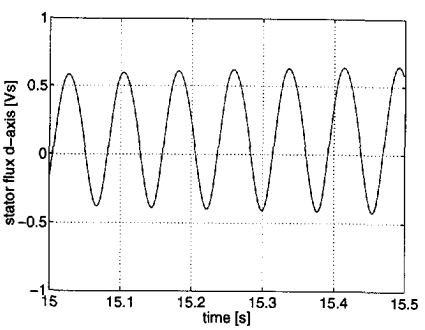

Stator flux ψ_{sd}

Figure 5.3.2 Detail of the "hunting" phenomenon.

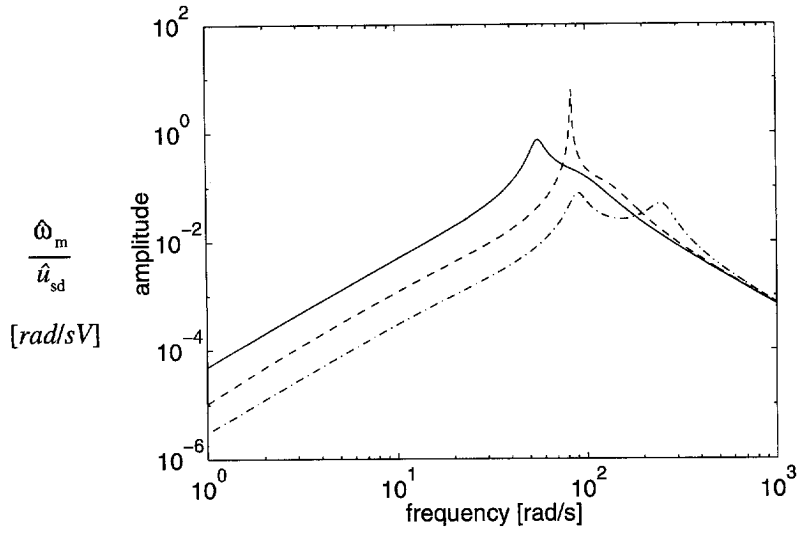

Figure 5.3.3 Amplitude of rotor speed divided by stator voltage of an induction motor for traction at no-load (- 10 Hz, -- 20 Hz, -. 40 Hz).

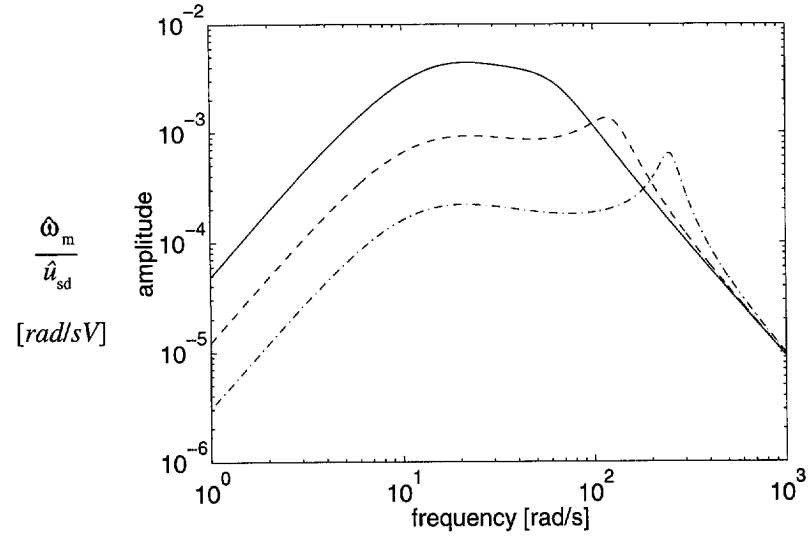

Figure 5.3.4 Amplitude of rotor speed divided by stator voltage of an induction motor for traction with the vehicle inertia added to the rotor inertia at no-load (- 10 Hz, -- 20 Hz, -. 40 Hz).

while their frequency is less than one tenth of the frequency at no load for high stator frequencies and increases at low stator frequencies. Self-excited oscillations will not occur.

The frequency characteristics of a traction motor with two different inertias, i.e., rotor inertia and the inertia representing the drive inertia plus mass of the vehicle have been illustrated by an example of a traction motor. Self-excited oscillations may occur if the motor operates in no load. The inertia of the drive, however, causes a decoupling of the mechanical and magnetical energy reservoirs of the motor. Here, the open-loop model of the motor has been examined. In the case of a controlled motor, the control system has an influence on the eigenvalues of the drive, which depends on the type of control. Within this thesis, the control system is excluded from investigation.

5.3.2 Mechanical drive

In section 4.3 the flexible modelling of mechanical structures was presented. In order to examine the oscillations of traction drives two examples were chosen. First, the electrical multiple-unit drive, since most parameters were available and measurements on track were done; second, a quill shaft drive of an electrical multiple-unit, whose parameters were available. In this section, models of the two drives are examined by means of modal analysis. Parameters of the models are listed in Appendix F.
Assumptions have been made in the first place to limit the complexity of the models by excluding degrees of freedom. Validation has to show whether the assumptions are correct.

Hollow shaft drive
A detailed model of the electrical multiple-unit drive including drive line, bogie and car body has been derived by Poeze [POE92]. Here, the attention is focused on the drive line, in particular the couplings, which are of major importance for the design of the electromechanical drive.
For the model of the drive line, the motor and gearbox are rigidly coupled to the bogie frame. The wheel-rail contact as described in section 4.4 determines the coupling between the rotation and the longitudinal displacement of the wheels. We distinguish two cases:

Rolling wheels

The wheel is rolling without difference between circumferential and translational wheel speed. This assumption is valid for pure rolling and for small variations at a point of operation when the difference between the circumferential and the translational speed of the wheel is negligible. In this case the rotation and the translation of the wheel are coupled, so that the model includes the longitudinal translation of the bogie frame and the car body as shown in Figure 5.3.5. The model consists of the rotor, the gear transmission, the wheel-set, the bogie and the car-body, which are flexibly coupled by springs and dampers. The translation of bogie and car body has been transformed into a rotation as described in section 4.4.4 and Appendix D. Since the wheels are rolling, the wheel shaft is assumed to be rigid. The gear teeth are considered rigid. This is permitted when the bandwidth of the model is limited to a maximum of 500 Hz. The rotation of the rotor has been transformed to the wheel side by the transmission factor of the gearbox. Table 5.1 shows the natural frequencies and eigenvectors and Figure 5.3.7 shows the oscillation modes. The mode of 0 Hz represents the rotation of the drive. The drive and bogie move with respect to the car-body at a frequency of 2.95 Hz. The drive moves with respect to the bogie at a frequency of 19.8 Hz with the car-body resting while the wheel-set rotates with respect to the drive at a frequency of 29.5 Hz. At the highest natural frequency of 192.65 Hz, rotor and gear wheels rotate with respect to each other. It is shown that the highest natural frequencies are close to the motor while the lowest frequencies involve the car-body and bogie.

When the bogie and the car-body are assumed to be rigidly coupled with the wheel-set, thus neglecting stiffness between wheel-set, bogie and car-body, the last two modes appear with a frequency of 24 Hz and of 192 Hz.

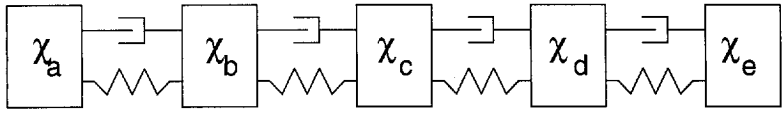

	rotor	gear wheel	wheel set	bogie	car body	
J =	72.5	20.9	410	667	3990	kgm^2
k =		$2.2\ 10^7$	$2.4\ 10^6$	$2.56\ 10^6$	$3.15\ 10^5$	Nm/rad

Figure 5.3.5 Model of hollow shaft drive with rolling wheels.

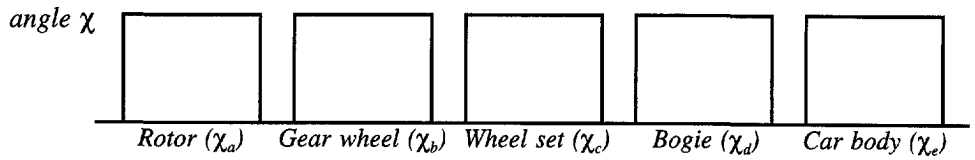

Oscillation mode of 0 Hz

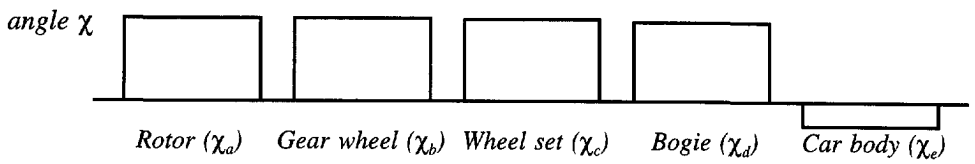

Oscillation mode of 2.95 Hz

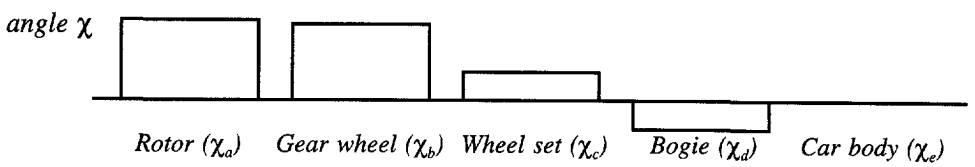

Oscillation mode of 19.8 Hz

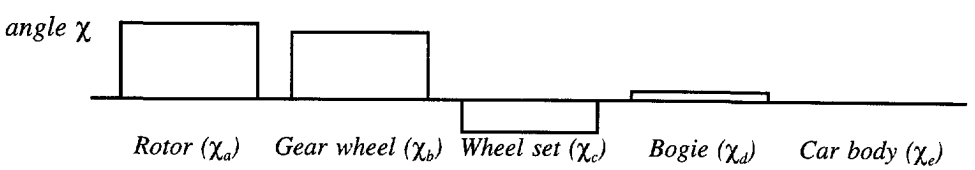

Oscillation mode of 29.5 Hz

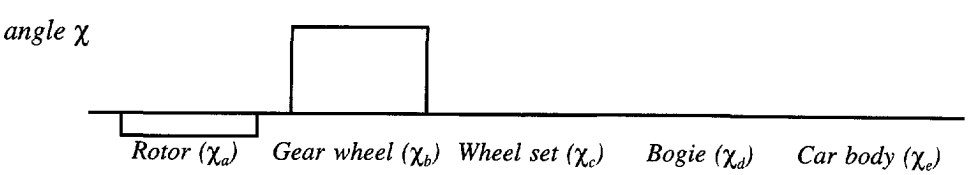

Oscillation mode of 192.6 Hz

Figure 5.3.6 Oscillation modes of hollow shaft drive with rolling wheels.

frequency	χ_a	χ_b	χ_c	χ_d	χ_e
0 Hz	1	1	1	1	1
2.95 Hz	1	0.999	0.986	0.952	-0.284
19.8 Hz	1	0.949	0.352	-0.366	0.002
29.5 Hz	1	0.888	-0.418	0.103	0
192.6 Hz	-0.266	1	-0.004	0	0

Table 5.1 Natural frequencies and modal angular displacement of hollow shaft drive with rolling wheels.

Slipping wheels

At the maximum of transmitted force from wheel to rail, the force is nearly independent of variation of the speed difference between wheel and rail. Translation and rotation of the wheel can be considered to be decoupled. The elasticity of the wheel shaft has to be included because of the variation of the speed of the wheels. Figure 5.3.7 shows the model. In Table 5.2 and Figure 5.3.8 the natural frequencies, eigenvectors and oscillation modes are given.

The mode of 0 Hz again describes the rotation of the drive. The mode of 32 Hz describes the rotation of the rotor and gear transmission against the wheel-set. In the mode of 73.2 Hz, the wheels are twisted against each other with rotor and gear transmission resting, while the mode of 192.8 Hz shows the torsion of the rotor against gear transmission. The second and fourth mode correspond to the fourth and fifth mode of the model with rolling wheels. The second mode has a higher frequency due to the decoupling of the drive from the bogie.

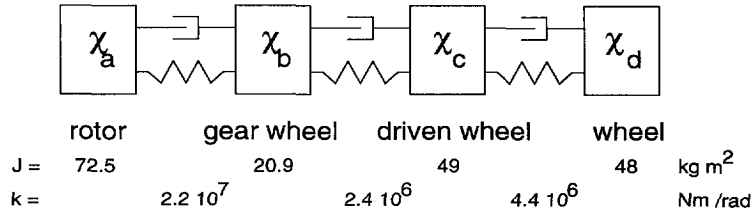

Figure 5.3.7 Model of hollow shaft drive with slipping wheels.

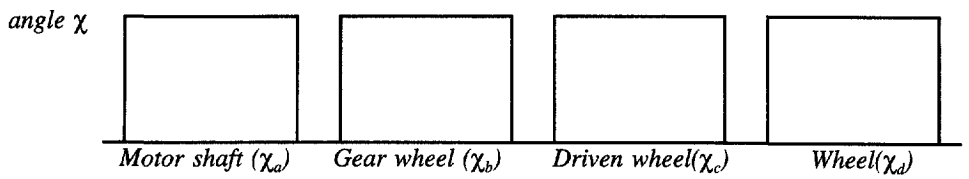

Oscillation mode of 0 Hz

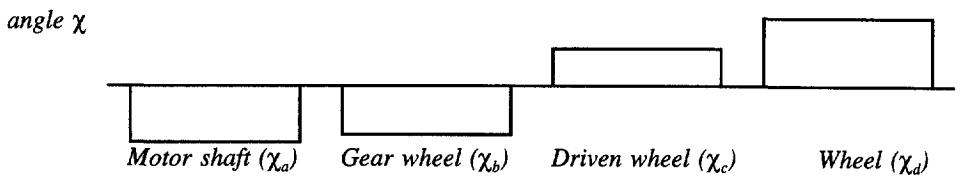

Oscillation mode of 32 Hz

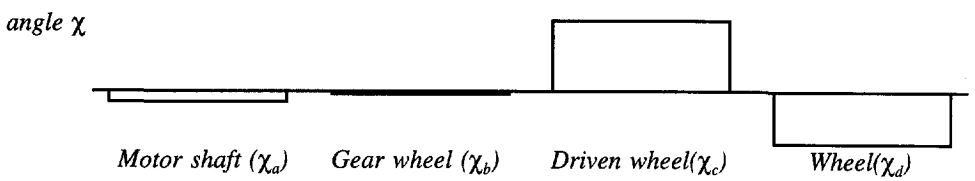

Oscillation mode of 73.2 Hz

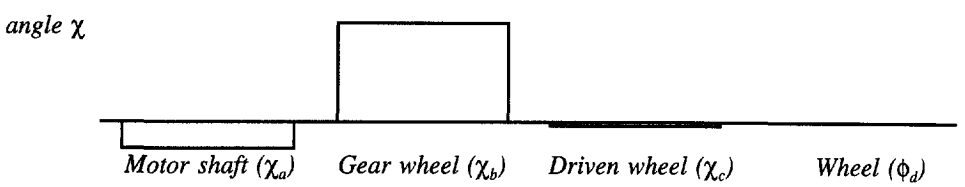

Oscillation mode of 192.8 Hz

Figure 5.3.8 Oscillation modes of hollow shaft drive with slipping wheels.

frequency	χ_a	χ_b	χ_c	χ_d
0 Hz	1	1	1	1
32 Hz	-0.83	-0.72	0.55	1
73.2 Hz	-0.15	-0.05	1	-0.74
192.8 Hz	-0.27	1	-0.069	0.0

Table 5.2 Natural frequencies and modal angular displacement of hollow shaft drive with slipping wheels.

Quill shaft drive

Models of the quill shaft drive can be derived like models of the hollow shaft drive. Here, only one simple model is examined which has been defined due to the parameters available. The model as depicted in Figure 5.3.9 and Figure 5.3.10 consists of the rotor, the quill shaft with couplings and an inertia which represents the drive line, bogie and car-body. The wheels are considered to be rolling so that the wheel shaft has been assumed to be rigid. Here, also the connection between wheel-set and car-body has been assumed to be rigid, which limits the validity of the model. Only the dynamics of the connection between the motor and the gearbox transmission, which will be used to investigate coupling parameters, has been modelled.

In Table 5.3, natural frequencies and eigenvectors are shown, while in Figure 5.3.10 the oscillation modes are depicted. The first mode describes rotation of the drive, the second mode shows the torsion of the drive line. The mode of the third natural frequency shows the torsion of the quill shaft against rotor and gear wheel transmission, while the fourth mode shows the torsion of the quill shaft.

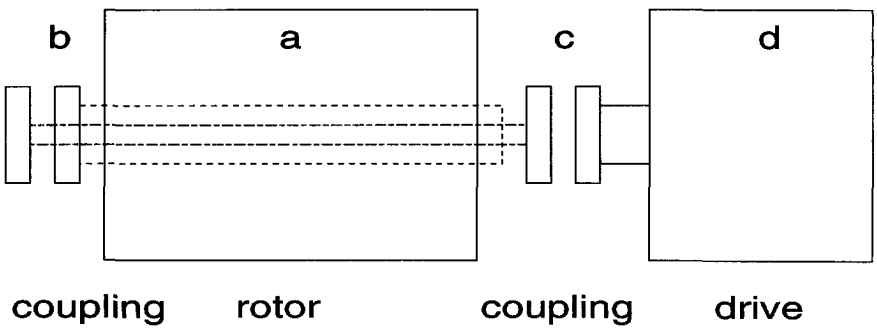

Figure 5.3.9 Schematic description of the quill shaft drive.

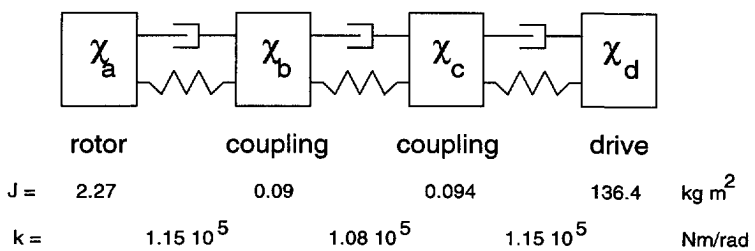

Figure 5.3.10 Model of quill shaft drive with rolling wheels.

Frequency	χ_a	χ_b	χ_c	χ_d
0 Hz	1	1	1	1
20.4 Hz	1	0.676	0.32	-0.017
179.7 Hz	-0.04	0.956	1	0.0
302 Hz	-0.014	1	-0.928	0.0

Table 5.3 Natural frequencies and modal angular displacement of quill shaft drive.

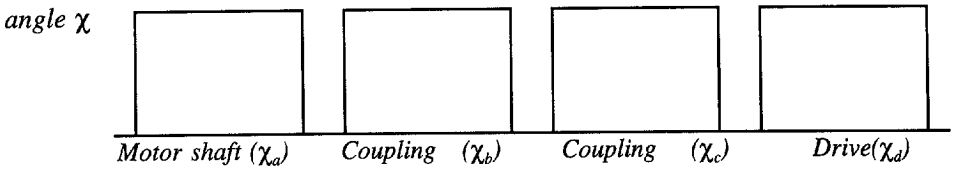

Oscillation mode of 0 Hz

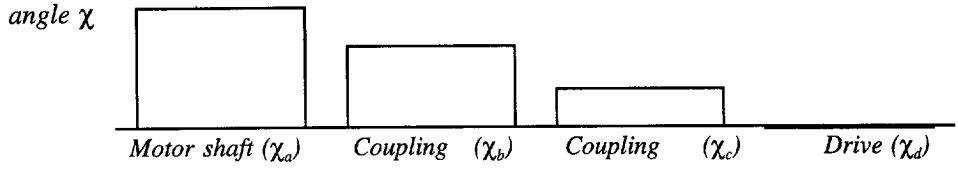

Oscillation mode of 20.4 Hz

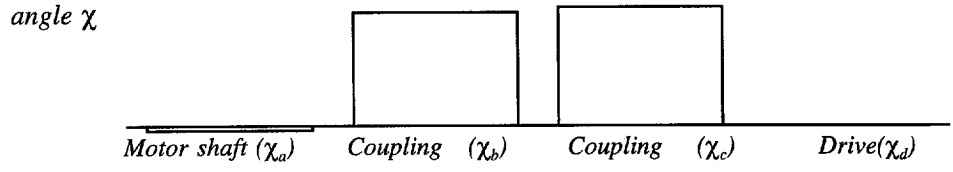

Oscillation mode of 179.7 Hz

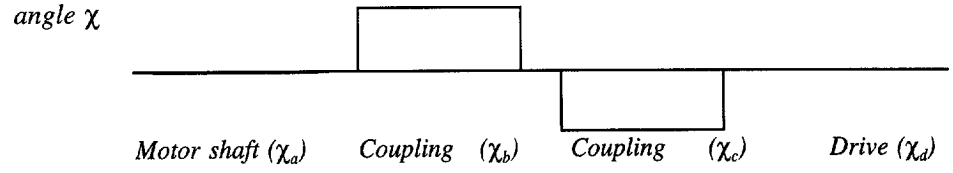

Oscillation mode of 302 Hz

Figure 5.3.11 Oscillation modes of quill shaft drive with rolling wheels.

5.3.3 Electromechanical drive

In order to investigate the dynamics of a traction drive during a traction cycle, several assumptions have to be made. First, the appropriate model has to be chosen. Then the damping of the flexible couplings and connections has to be calculated. Simulations in the time-domain show the drive dynamics, while transfer functions give an overview of the natural frequencies of the drive and their damping.

Acceleration of the electrical multiple-unit drive was simulated with the two models described in section 5.3.2. Further, simulations were done with a simplified model with rolling wheels, by assuming a rigid connection between wheels, bogie and car-body. The simulated torques, speeds and motor currents were similar for the three models.
Figure 5.3.12 shows the acceleration of the electrical multiple-unit drive when using the simplest model. The time responses of the three models do not differ significantly. The measurements described in Chapter 3 were used for the validation of the model.
The vehicle has been accelerated with maximum torque starting from zero flux of the motor and zero speed of the vehicle. Excitation is imposed by the stator voltages of the traction motor by means of variation of the frequency and amplitude of sinusoidal voltage sources. The first six seconds of simulation are shown.
The time axis in the simulation can be divided into three phases: building up of motor flux (1), building up of torque (2), and acceleration with maximum torque (3). After building motor flux up to 1.2 seconds, acceleration starts with increasing stator frequency. Building up torque gives an overshoot. After the overshoot the shaft is driven by a constant torque of about 8000 Nm. Overshoot and the following transient can also be recognized in the phase current.

The measured gradient of the inverter frequency is lower than simulated. The simulation neglects the resistance of the track, so that the maximum torque of the drive is simulated at a higher acceleration.
The measured current is the inverter current which feeds two motors, so its value is twice the motor phase current, assuming identical drives. Obviously, current waveforms include all harmonics caused by PWM voltage waveforms. However, frequency and amplitude of fundamentals correspond with simulated values.
The measured torque includes harmonics caused by PWM voltage waveforms, parasitic torques of mechanical origin and measurement noise. However, rise time,

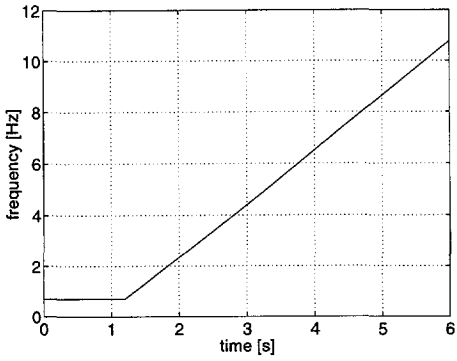

Simulated inverter frequency f_{inv}

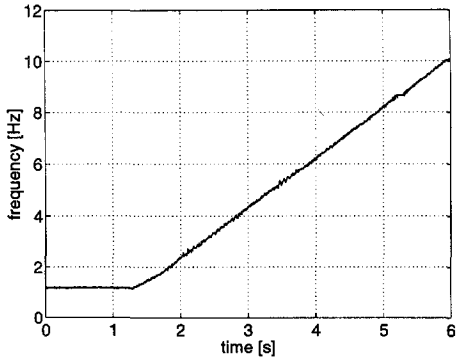

Measured hollow shaft torque T_{hsh}

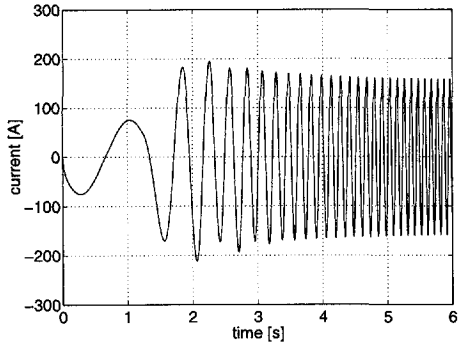

Simulated motor phase current i_w

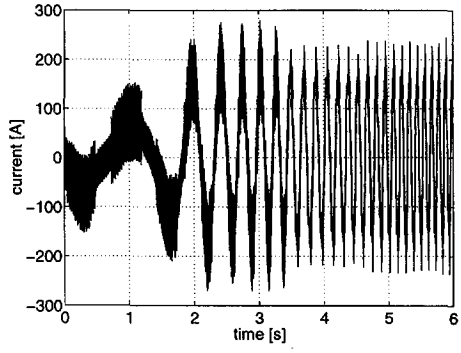

Measured inverter phase current i_w

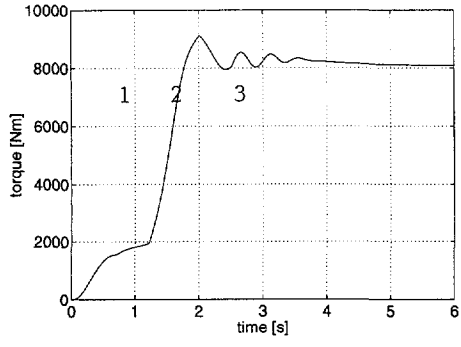

Simulated hollow shaft torque T_{hsh}

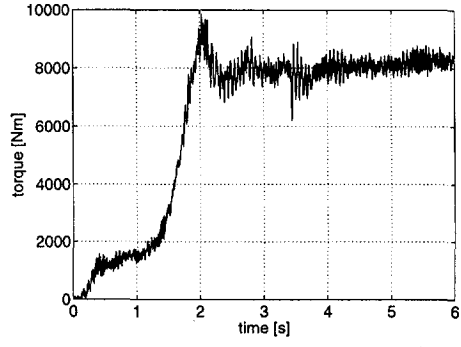

Measured hollow shaft torque T_{hsh}

Figure 5.3.12 Acceleration of hollow shaft drive.

overshoot and constant torque value correspond with the simulated torque.
It can be seen that with a simple model, a part of a traction cycle of a traction drive within a vehicle can be simulated quite properly. How requested torque will be generated by the motor and transmitted within the traction drive can thus be verified.
Figure 5.3.13 shows the vertical displacement of the motor and gearbox as described in sections 3.3.2 and 4.3.3. Simulation was performed with excitation by sinusoidal voltages. Torque and current waveforms correspond to waveforms obtained with the previous described models. Here, the vertical displacement of the silent blocs is discussed in simulation and measurement. The figure shows the displacement of the three silent blocs S_1, S_2 and S_3 as depicted in Figure 3.3.5, as shown in section 3.3.2. The simulated displacement of the motor in its silent bloc is close to zero. The gearbox has a vertical displacement moving upwards from the rails in the silent bloc on the motor side, while it moves downwards to the rails on the wheel axle side. The resulting movement is a rotation around the lateral (y) and longitudinal (x) axes of motor and gearbox.
Measured displacement signals as plotted in Figure 5.3.13 are noisy, with a low resolution. The displacement signal of the silent bloc of the gearbox at the wheel axle side is disturbed for between four and six seconds. However, the displacements can still be recognized. First of all, the simulated motion was found in the measurements, which indicates that the chosen model structure is valid. Critical parameters are the characteristics of the rubber silent blocs which are assumed to be linear springs with estimated stiffness. Since the measured displacement values are lower than the simulated values, the estimation of the spring constants of the silent blocs was too low.

The interaction between motor and mechanical drive was investigated by calculating the eigenvalues of the damped system. The eigenvalues show that the motor has a damping influence on the drive. The damping influence of the induction motor has already been stated by Poeze [POE92]. The eigenvalues show further that the damping of the motor itself has decreased with respect to the motor values with high inertia as shown in Figure 5.3.4.
A frequency characteristic of the drive is shown in figure 5.3.14 by the transfer function of wheel speed divided by stator voltage as a function of frequency. The natural frequency of 32 Hz has a relatively low damping while the frequency of 192 Hz is strongly damped. The frequency of 73.2 Hz of the wheel shaft is poorly damped.

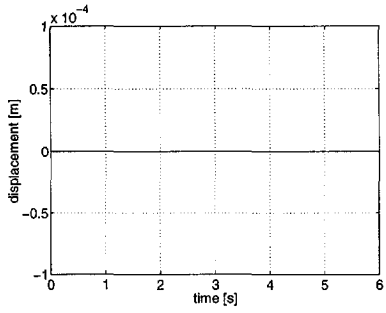

Simulated vertical displacement of the motor in silent bloc S_1

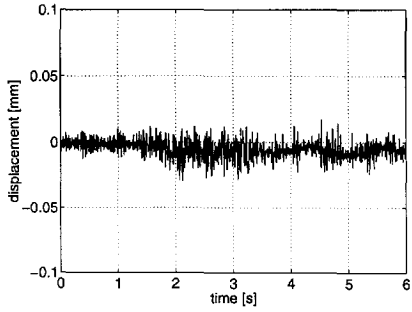

Measured vertical displacement of the motor in silent bloc S_1

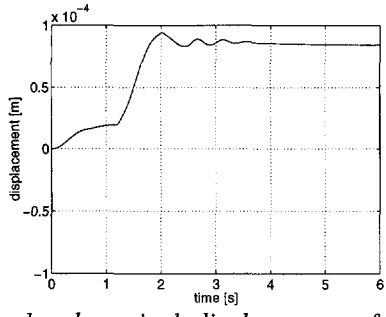

Simulated vertical displacement of the gearbox in silent bloc S_2 at the motor side

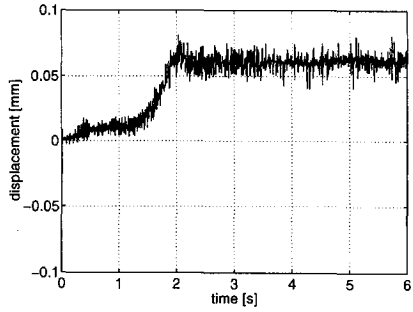

Measured vertical displacement of the gearbox in silent bloc S_2 at the motor side

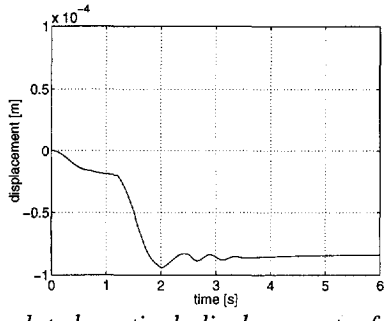

Simulated vertical displacement of the gearbox in silent bloc S_3 at the wheel axle side

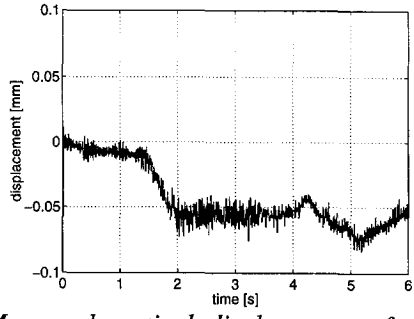

Measured vertical displacement of the gearbox in silent bloc S_3 at the wheel axle side

Figure 5.3.13 Motor and gearbox displacement during acceleration of hollow shaft drive.

An example of a transfer function of the quill shaft drive is shown in Figure 5.3.15 for a 10 Hz stator frequency of the motor. The figure shows the example of a poorly damped drive line with the natural frequencies calculated in section 5.3.2.

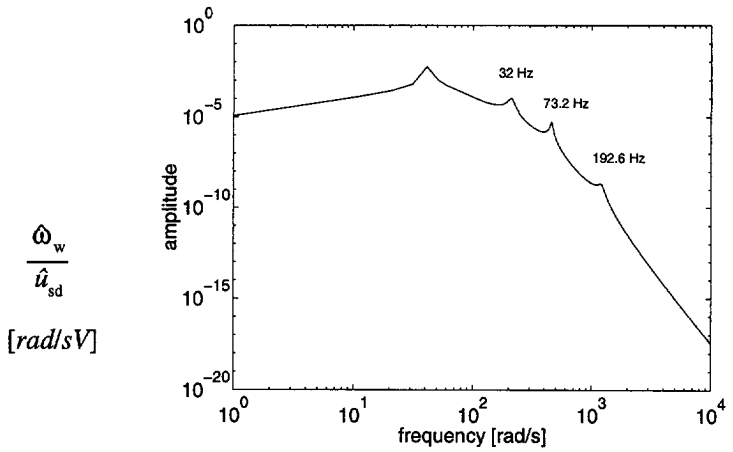

Figure 5.3.14 Amplitude of wheel speed divided by stator voltage of hollow shaft drive at 10 Hz stator frequency.

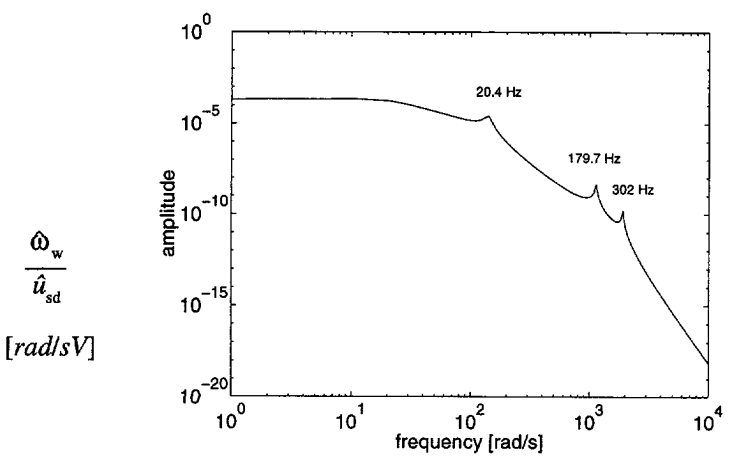

Figure 5.3.15 Amplitude of wheel speed divided by stator voltage of quill shaft drive at 10 Hz stator frequency.

5.4 Inverter harmonics

The stator voltage of the motor is generated by an inverter by switching a DC voltage. The principle of the inverter was described in section 2.3. A simple derived model of the inverter was discussed in section 4.2.2. The switching action of the inverter generates voltage harmonics, these harmonics cause current and flux harmonics. In section 4.2.2 it was stated that the order of the voltage harmonics is given by

$$\nu = -5,7, \ -11,13 \ -17,19...$$

Since the torque is the product of motor currents and fluxes, the torque harmonics are mainly the product of the fundamental and harmonics generating multiples of the sixth harmonic of the stator frequency. The stator phases of the motor are y-connected without neutral conductor.
In this section, the attenuation of these torque harmonics in the drive for the hollow shaft drive and the quill shaft drive is investigated.

5.4.1 Oscillation amplitudes

During acceleration of the drive, the frequency of voltages rises and so does the frequency of the harmonics. As a result, couplings will transmit torques with superposition of harmonic torques with variable frequency. The damping of elastic couplings depends on the frequency of the applied torque, as mentioned before. Thus damping parameters have to be chosen according to the frequency of torque harmonics.
Figure 5.4.1 shows the acceleration of the electrical multiple unit drive from standstill up to 11 Hz stator frequency. Making use of the models described in section 5.3.2, time response of the torques was simulated. Simulated torques and currents were similar for the these models. The excitation of the model is done by stator voltages varying in frequency and amplitude. Values are derived from measurements on track. The 5^{th} and 7^{th} harmonics of the stator voltage are superimposed thus simulating the pulse-width modulated voltage waveforms. Up to the inverter frequency of 18 Hz, the fifth and seventh harmonic of the stator voltage were assumed to be 2% and 3% of the fundamental, above f_{inv} = 18 Hz, these

harmonics were set to 20% and 10% of the fundamental.
The damping of the couplings was determined by equation 4.17. The frequency of the applied torque is the 6th harmonic of the stator frequency. The stiffness of the couplings was derived from specifications of manufacturers.

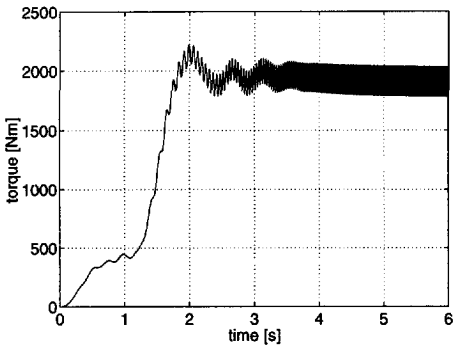

Simulated air gap torque T_e

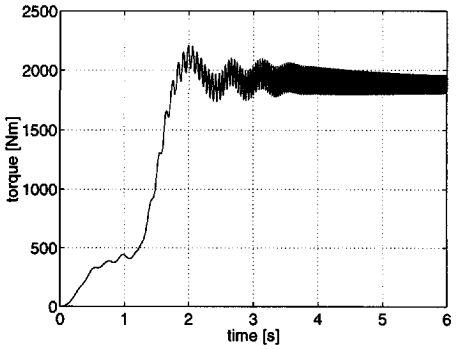

Simulated torque T_{cpm} of elastic motor-coupling

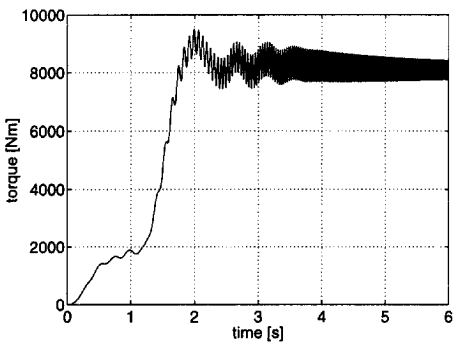

Simulated torque T_{hsh} of elastic wheel side coupling

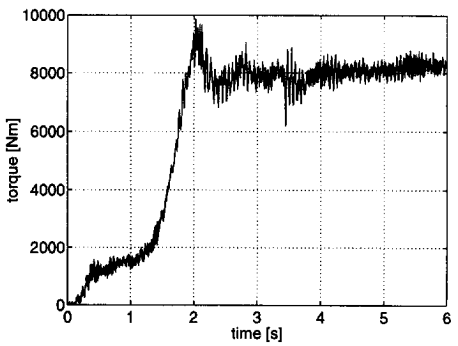

Measured torque T_{hsh} of elastic wheel side coupling

Figure 5.4.1 Acceleration of drive with torque harmonics.

Figure 5.4.1 shows simulated torque responses of the air gap torque T_e, the torque in the elastic coupling between motor and gearbox T_{cpm}, and the torque between gearbox and wheel axle T_{hsh}. The measured torque response shows a lower harmonics amplitude. Validation of the amplitudes by this comparison, however, is not permitted because voltage harmonics had been estimated and had not been measured during the experiments on track.

A detail at nearly 20 Hz stator frequency is shown in Figure 5.4.2. Only a short time period has been chosen to illustrate the influence of harmonics. Figure 5.4.2 shows the motor phase current which is no longer sinusoidal due to voltage harmonics. The motor side coupling torque T_{cpm} and the hollow shaft torque T_{hsh} show a 6th harmonic ripple torque at a constant acceleration torque of the drive. Measured waveforms show that the peak values of currents correspond to the simulated values, taking into account the fact that one inverter supplies two motors. Further, it can be seen that the measured current contains more harmonics than the 5th and 7th harmonic.

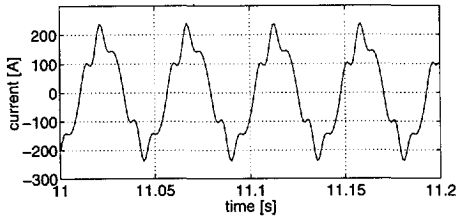

Simulated motor phase current i_u

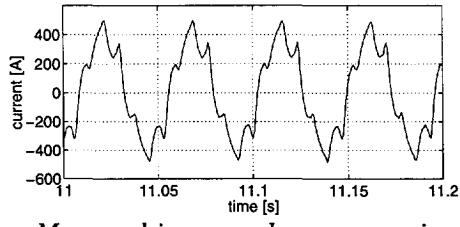

Measured inverter phase current i_u

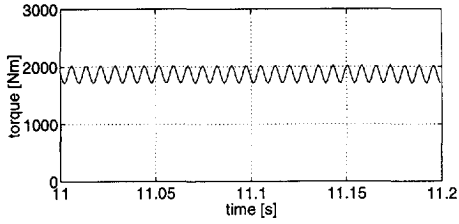

Simulated motor coupling torque T_{cpm}

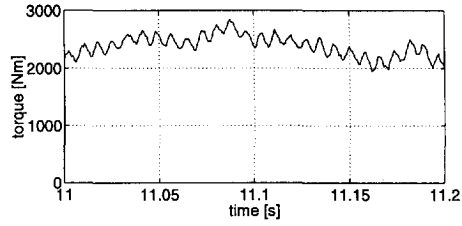

Measured motor coupling torque T_{cpm}

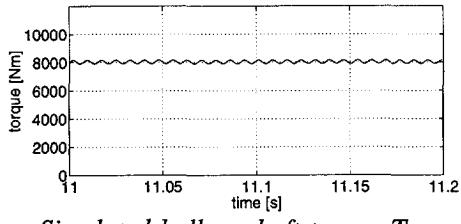

Simulated hollow shaft torque T_{hsh}

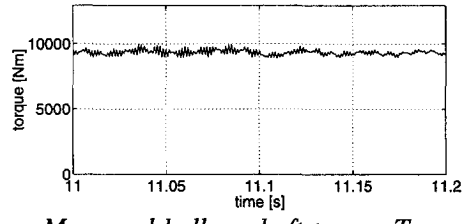

Measured hollow shaft torque T_{hsh}

Figure 5.4.2 Simulated and measured torque ripple in hollow shaft drive.

The simulated torque ripple amplitude differs from the measured amplitude. In addition, the motor model also has the limitation that current redistribution in the rotor have been neglected. Thus, a lower air gap torque ripple may be calculated than appears with the skin effect [VEL94]. However, the attenuation of the harmonics between the simulation and the measurement corresponds. The amplitude of the air gap torque ripple within the chosen time span is 800 Nm, so that the ripple torque has been significantly attenuated by the rotor inertia.

Changing pulse pattern may cause transients in torque. Figure 5.4.3 shows simulated and measured transients after the change of pulse pattern. The damped transient can be recognized. Again, the difference between values of simulation and measurement lies in the approximation of pulse patterns.

Rondel et al. and de Beer have shown how to minimize transients by choosing the right switching vector phase angle [RON92, BEE94]. An optimized transient was obtained by changing more slowly the stator voltage vector at the moment of change of pulse pattern, so that the flux remains nearly constant as shown in Figure 5.4.4.

In practice, minimization of transients is obtained by a minimum variation of amplitude and phase angle at the change of pulse patterns.

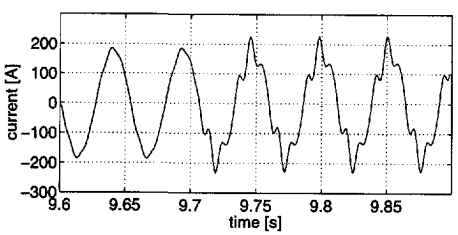

Simulated motor phase current i_u

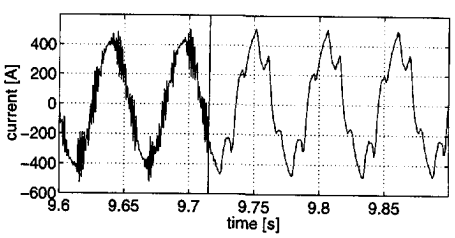

Measured inverter phase current i_u

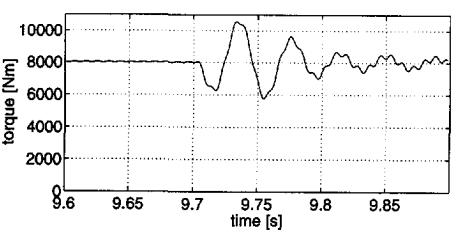

Simulated hollow shaft torque T_{hsh}

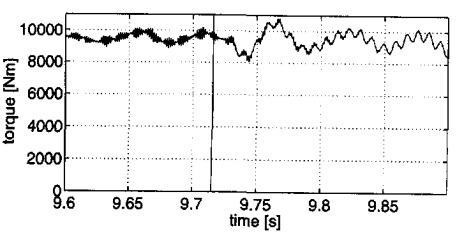

Measured hollow shaft torque T_{hsh}

Figure 5.4.3 Simulated and measured current and torque transient in hollow shaft drive.

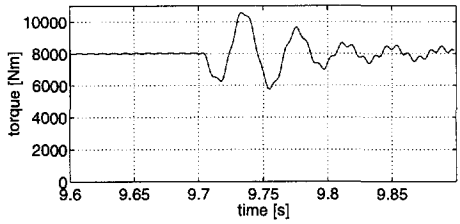

Hollow shaft torque transient

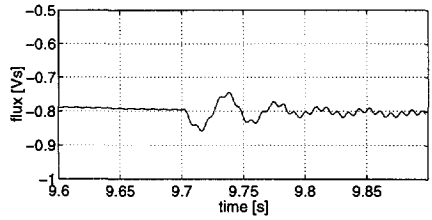

Rotor flux transient

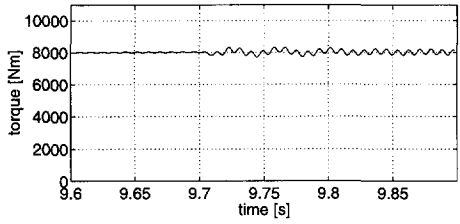

Optimized hollow shaft torque transient

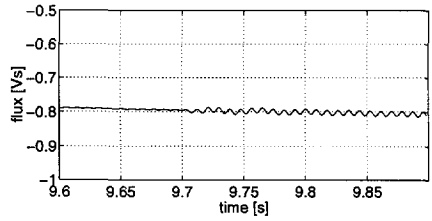

Optimized rotor flux transient

Figure 5.4.4 Optimization of torque transient in hollow shaft drive.

Generally, simulations have shown that the motor inertia, which is dominant between the inertias of the drive line, attenuates most of the torque ripple. This attenuation increases with the motor speed. At high inverter frequencies, the number of switched stator voltage pulses is relatively low, which causes a high torque ripple. In practice, this high ripple is attenuated well by the motor inertia.
At low speeds, the torque ripple is lower, due to the high number of switched stator voltage pulses. However, the ripple is less attenuated at low speed.
Investigation of torque harmonics caused by the inverter is of special interest at low frequencies, because the damping of the couplings is dominant and there are possibilities of resonances.

5.4.2 Hollow shaft drive

The hollow shaft drive has two couplings, the wheel shaft to gear wheel coupling and the motor to pinion wheel coupling. The influence of variation in the stiffness and damping of the couplings is shown by time domain responses and transfer functions.

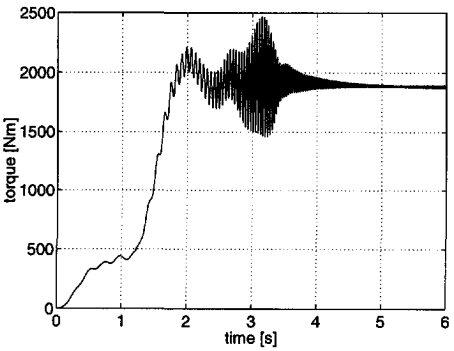

Simulated torque T_{cpm} of elastic motor coupling with reduced damping

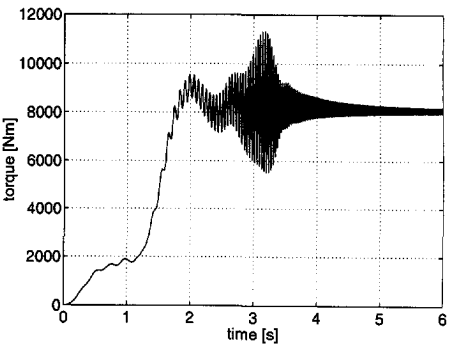

Simulated torque T_{hsh} of elastic wheel side coupling with reduced damping

Figure 5.4.5 Simulated torque with reduced damping of hollow shaft coupling.

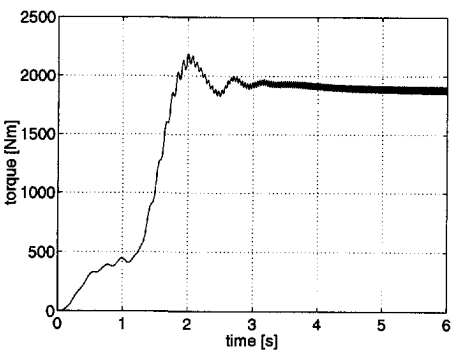

Simulated torque T_{cpm} of elastic motor coupling with reduced stiffness

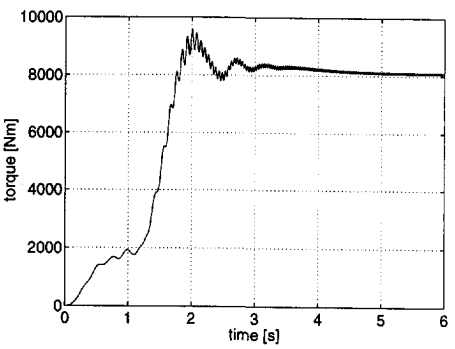

Simulated torque T_{hsh} of elastic wheel side coupling with reduced stiffness

Figure 5.4.6 Simulated torque with reduced hollow shaft coupling stiffness and damping.

The torques of the hollow shaft drive at the beginning of acceleration of the vehicle have been shown in section 5.4.1. The torque response, assuming a wheel-side coupling with the same stiffness but a tenth of the relative damping ψ, has been simulated. The torque shows a resonance between two and three seconds as seen in Figure 5.4.5.

Assuming a wheel-side coupling with a tenth of the stiffness and the same relative damping, responses are simulated as shown in Figure 5.4.6. Torque responses show major attenuation of harmonic torques.

Figure 5.4.7 shows transfer functions of the hollow shaft drive for the three simulated cases of rated damping, reduced damping of the hollow shaft coupling and reduced stiffness of the same coupling. Reduced stiffness causes a lower natural frequency of the drive against the wheel set.

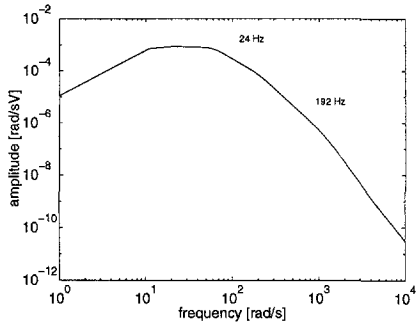

Wheel axle speed divided by stator voltage with rated damping

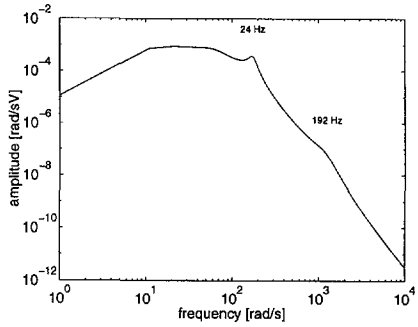

Wheel axle speed divided by stator voltage with reduced damping of wheel side coupling

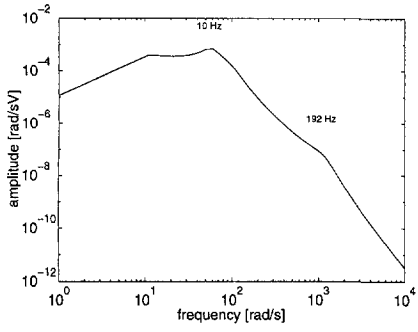

Wheel axle speed divided by stator voltage with reduced stiffness of wheel side coupling

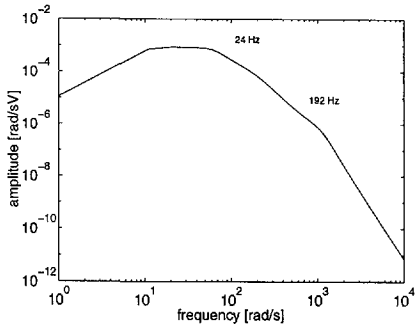

Wheel axle speed divided by stator voltage with reduced damping of motor side coupling (steel coupling)

Figure 5.4.7 Transfer functions of the hollow shaft drive (ω_w/u_{sd} [rad/sV]) with variation of coupling parameters at 10 Hz motor stator frequency

In the case under consideration, the motor is coupled with the pinion wheel of the gearbox by a flexible coupling with a damping of $\psi = 0.4$. In other drive concepts, the coupling between pinion wheel and motor is a steel coupling with a low damping. The transfer function of a drive with a steel coupling is also shown in Figure 5.4.7.

The transfer functions were calculated with a reduced model of the hollow shaft drive with rolling wheels, assuming elasticity only in the two couplings of the drive. The ripple torques have most influence on the couplings and gear transmission of the drive line. With respect to the model depicted in Figure 5.3.5, section 5.3.2, the frequency of 192 Hz remains while the frequency of 28 Hz has decreased to 24 Hz in the reduced model.

When including finite stiffness of the gearwheels, two natural frequencies are added to the drive model:

$f_4 = 1256$ Hz

$f_5 = 2500$ Hz.

Comparing the figures, the main difference is the addition of the eigenvalues due to the stiffness of the gear teeth. The transfer function is shown in the frequency range of up to 10^5 rad/s. The poorly damped gear teeth can be recognized. Resonances may occur at this frequency.

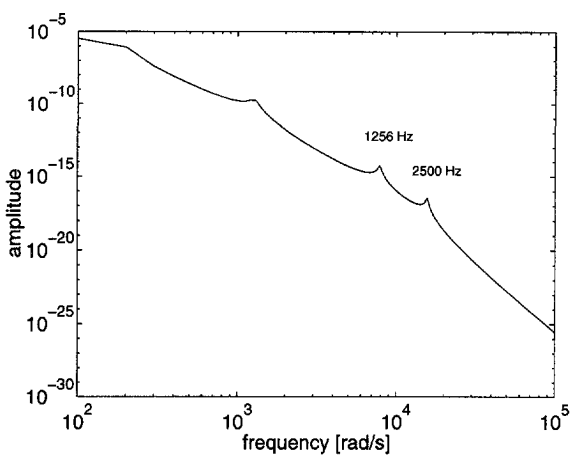

Figure 5.4.8 Transfer function of hollow shaft drive including gear teeth stiffness.

The hollow shaft drive under investigation is a drive with high torsional stiffness. With respect to a drive with lower torsional stiffness there will be higher natural frequencies and less attenuation of ripple torques.

In practice, the wheel side coupling of a hollow shaft drive always has a sufficient damping, so that resonances as shown in the illustrative example above will not occur. The motor coupling is less critical and therefore for this type of drive, ripple torques will not cause problems.

5.4.3 Quill shaft drive

The torsional stiffness of the quill shaft drive as described in section 5.3.2 is determined by quill shaft and couplings. Compared with the hollow shaft drive, the motor is less rigidly coupled with the gear transmission. In practice, the ripple torques of the motor are well damped by the rotor inertia so that the couplings are not critical. There is a possibility of resonances when the couplings are poorly damped. Elastic couplings of the quill shaft may be rubber couplings with relatively high damping or steel couplings with low damping.

The choice of couplings for the quill shaft drive is again illustrated by transfer functions and time responses. The drive has three natural frequencies, at 20.4 Hz, 179.7 Hz and 302 Hz. The eigenfrequency of the quill shaft has the highest damping. The first two frequencies are more critical. Two cases have been simulated, in the first case, elastic rubber couplings were chosen. In the second case steel couplings are modelled with a damping which is 2.5 % of the rubber coupling damping at 180 Hz. Figure 5.4.9 shows the transfer functions which evince the well-damped drive with rubber couplings in contrast with the poorly damped drive line with steel couplings.

Figure 5.4.10 shows the detail of a simulated quill shaft drive traction cycle with rubber and steel couplings. The traction cycle was simulated with acceleration with a rated torque of 1400 Nm and a rate of rise of the inverter frequency of 3.25 Hz/s. The figure shows the pinion side coupling torque at the time span between 4.3 s and 4.6 s during acceleration. The inverter frequency is 13 Hz at 4.5 s. The ripple torque was generated by an 11^{th} and 13^{th} stator voltage harmonic with an amplitude of 2% of the fundamental. The air gap torque ripple at the shown time span is 30

Nm. The torque of the rubber coupling shows a strong attenuation of the ripple torque while the steel coupling torque shows a resonance of 179.7 Hz. At this frequency, the quill shaft is twisted against the rotor and pinion wheel, which means a high dynamic load on the couplings.

Resuming discussion of the simulations of the quill shaft drive, ripple torques were mostly absorbed by the rotor inertia which is coupled with a relatively low stiffness to the gear transmission. The application of steel couplings in this type of drive may lead to resonances.

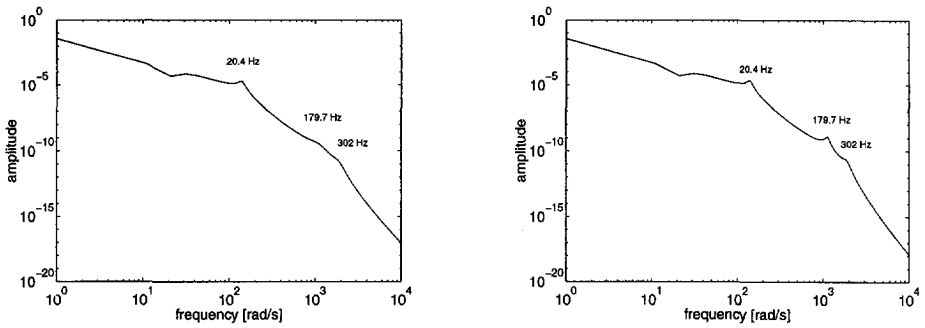

Elastic rubber couplings *Elastic steel coupling*

Figure 5.4.9 Wheel-set speed divided by stator voltage ω_w/u_{sd} [rad/sV] for the quill shaft drive with rubber and with steel couplings.

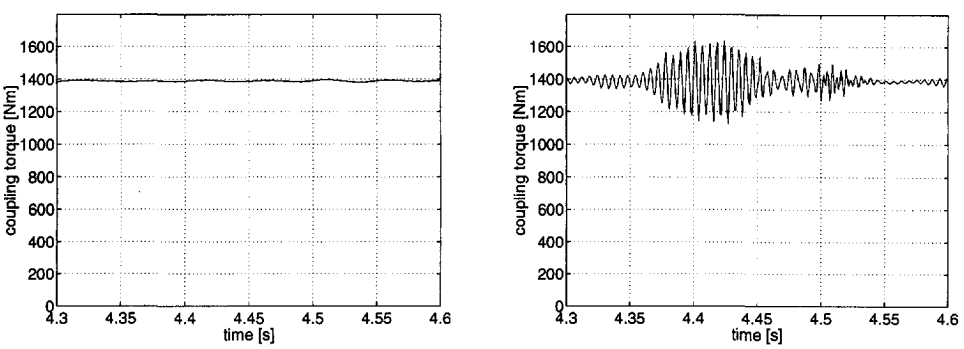

Elastic rubber coupling torque *Elastic steel coupling torque*

Figure 5.4.10 Resonance and damped ripple torque of quill shaft drive.

5.5 Influence of the wheel-rail contact

In the preceding sections, we reported on simulations with rolling wheels and with the wheel-rail model as described in section 4.4. The required friction coefficient of the hollow shaft drive at maximum torque was 0.16 so that on dry rails with a friction coefficient maximum of 0.3, the wheels will not slip. In some cases, however, wheel slip occurs, which has influence on oscillations of the drive.

5.5.1 Slip-stick oscillations

When the drive operates at the maximum of transmissible force, which occurs with, e.g., wet rails or with high power drives, the wheels may slip. Traction drives are equipped with wheel slip control, which detects the slip of the wheel-set by the variation of the speed of the drive at a given inverter frequency. The drive is then operating within the descending part of the friction curve, as has been depicted in Figure 4.4.2, section 4.4. Wheel-slip control reduces the demanded torque so that the drive returns to operate in the rising part of the friction curve.

When operating near the maximum of the curve, "slip-stick" oscillations may occur. Such oscillations are generated when the force of one wheel is transmitted to the rising part of the adhesion curve while the other wheel transmits the force to the falling part of the curve. The poorly damped wheel shaft is excited and the wheels oscillate while twisted against each other with the frequency of the wheel set, in the case of the hollow shaft drive 73.2 Hz.
Figure 5.5.1 shows the acceleration of the hollow shaft drive when slip-stick oscillations occur between 2 s and 4 s. Since the drive is modelled in an open-loop system, the slip-stick oscillation is followed by a motor transient of 5 Hz, which would be damped much faster in the case of simulation of a controlled motor.
The highest amplitude of the torque appears in the wheel shaft. In practice, the slip-stick oscillation may cause damage in components such as couplings, or even the wheel shaft. Several control concepts have been proposed to minimize slip-stick oscillations [SCH92, ENG96].

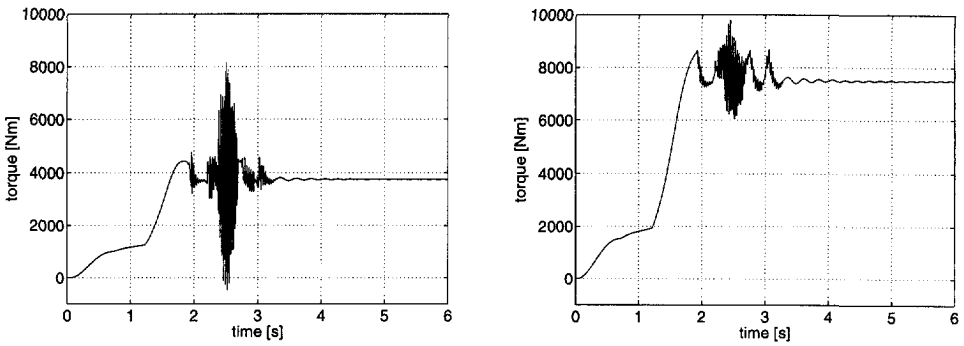

Wheel axle torque *Hollow shaft torque T_{hsh}*

Figure 5.5.1 Simulation of acceleration of the hollow shaft drive near the maximum of transmissible force between wheel and rail.

5.5.2 Motor short-circuit

Simulation of fault conditions is important in order to be able to estimate the torques and forces on mechanical components. In particular, fault conditions of the electrical drive may cause peak torques or the excitation of oscillations which may damage the mechanical drive. High torque peaks are generated in the case of short-circuit of the stator such as depicted in Figure 5.5.2, or the loss of the speed probe of the motor.

One of the most critical fault situations is the short-circuit of the stator phases. Although short-circuit occurs very rarely, the situation has to be taken into account in order to foresee eventual damage to the drive and suspension.

Various studies have been done on this subject, such as that by Pittius and Seinsch [PIT89]. They concluded that the two-phase short-circuit generates the highest torques and that the dynamics of mechanical load may not be neglected. Other studies investigated the influence of eddy currents in rotor bars on the short-circuit torques.

Validation of these simulations is not impossible but might be very costly, as severe damage to the drive may occur. However, tests on a test bench made it possible to validate the chosen motor model [JAC92]. On the test bench the motor was rigidly coupled with a rotating mass and was short-circuited.

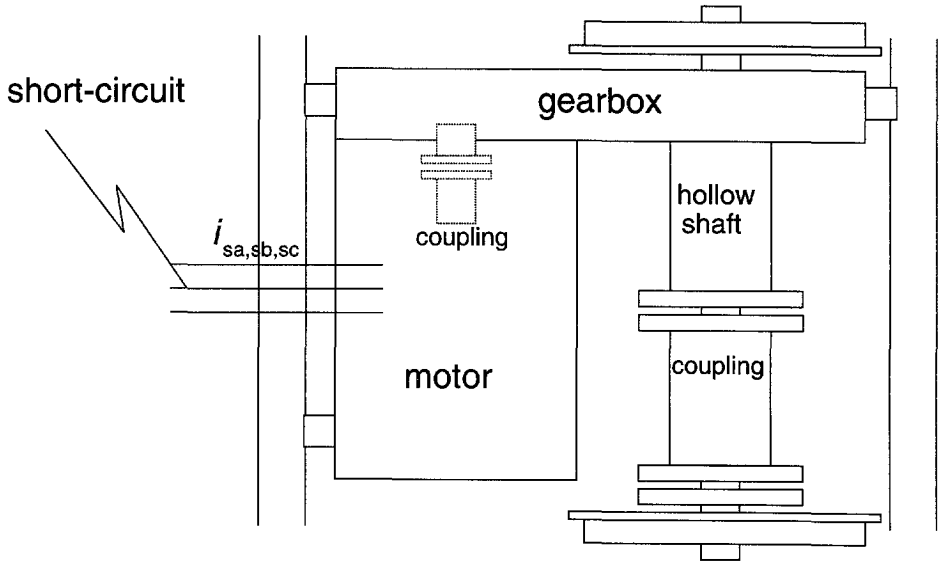

Figure 5.5.2 Bogie and drive configuration at motor short-circuit.

Short-circuit of the stator windings occurs in the case of inverter switch failure. Since the mechanism of short-circuit depends on the type of inverter protection, here, a generalized example has been taken. A comparison between two models has been made. In engineering practice, models of a drive line with rolling wheels are in use; these neglect springs between wheel-set, bogie and car-body. Simulations were done for the hollow shaft drive as described in section 5.3.2. The bogie and car-body inertia were added to the wheel-set inertia, which yielded a model with three natural frequencies, 0 Hz, 24 Hz and 192 Hz.

In order to include the possibility of wheel slip, simulations were repeated with the model of the hollow shaft drive for slipping wheels as depicted in Figure 5.3.7, section 5.3.2, including the wheel-rail model as depicted in Figure 4.4.4, section 4.4.2.

Figure 5.5.3 gives an example of a three-phase short-circuit of the stator by plotting phase current, motor speed and drive torques both excluding and including wheel slip.

The stator is short-circuited during acceleration of the drive with an air gap torque of 2000 Nm at a stator frequency of 11 Hz.

When wheel slip is excluded, the braking torque peak of the motor is amplified by the transmission factor to obtain the hollow shaft torque. The torque peak, which is a

Rolling wheels

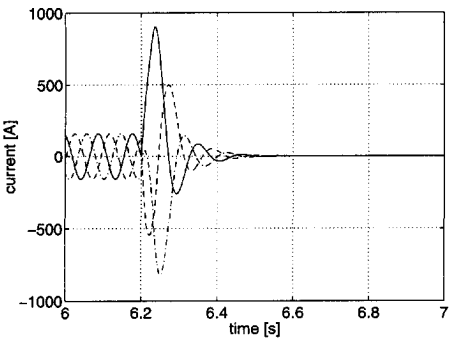

Stator currents, i_a (__), i_b (--), i_c (_.)

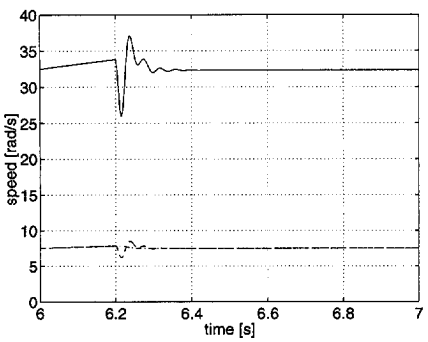

Shaft speeds, motor shaft (__), gear wheel (--), wheel set (_.)

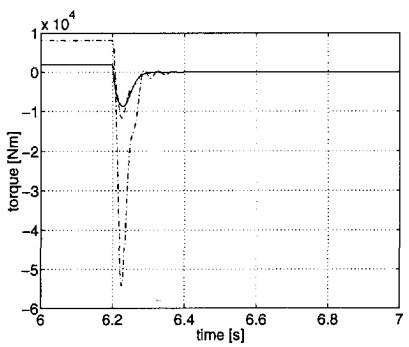

Torques, air gap motor (__), motor side coupling (--), hollow shaft (_.)

Slipping wheels

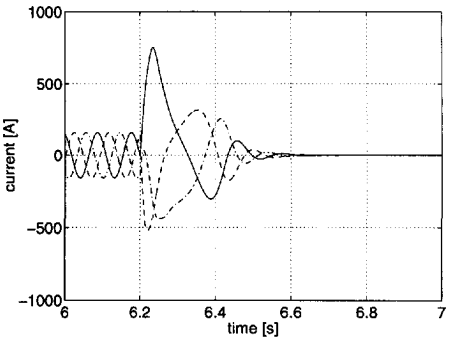

Stator currents, i_a (__), i_b (--), i_c (_.)

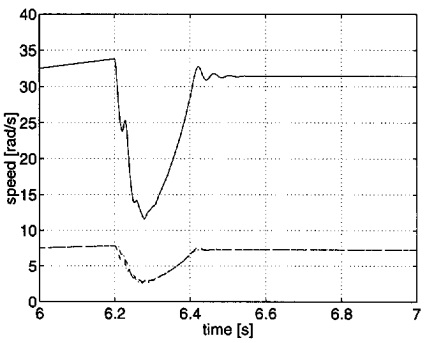

Shaft speeds, motor shaft (__), gear wheel (--), driven wheel (_.)

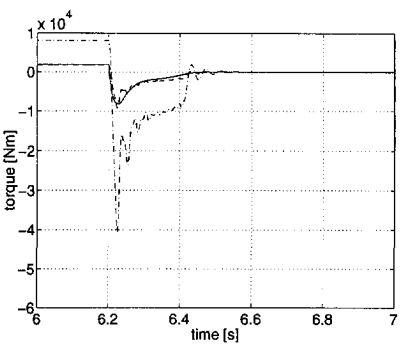

Torques, air gap motor (__), motor side coupling (--), hollow shaft (_.)

Figure 5.5.3 Simulation of three phase stator short circuit neglecting (left) and including (right) wheel slip.

multiple of the rated torque, is propagated throughout the entire drive. The peak value increases with motor speed at rated flux. In the case of wheel slip, the hollow shaft torque peak is significantly lower, because the friction coefficient limits the maximum transmissible force from wheel to rail. After short-circuit, a braking torque appears which rises until the wheels begin to slide. A damped transient with the frequency of 73.2 Hz can be recognized during wheel slide. At 6.4 seconds, the wheels stop sliding, which is followed by a 24 Hz transient. The frequency of 24 Hz is a natural frequency of the drive model with rolling wheels.
The peak value of the torque at a given motor parameter set increases with the stator frequency at rated flux and the maximum transmissible force between wheel and rail. In the simulation shown in Figure 5.5.3, a friction coefficient of 0.3 has been assumed at rated torque of the drive in acceleration. During coasting and braking, the wheel slide will occur faster so that the torque peak will decrease.
The damping of the drive line is essential to shorten transients and limit torque amplitudes. In the example shown, the damping of the drive was high. Poorly damped drive lines may oscillate at high torque amplitudes, even leading to slip-stick oscillations.

Simulation of fault conditions of the electrical drive which cause torque peaks are essential, in order to design properly an electromechanical traction drive that obviates damage of mechanical components. The wheel slip determines the maximum torques in the mechanical part of the drive. The worst-case conditions are maximum stator frequency at rated flux and torque in acceleration with dry rails.

5.6 Conclusions

The third and fourth problem statements of the thesis -
Apply the developed methods to traction drives in service and test the validity.
Apply the developed methods to minimize oscillations. -
have been treated in Chapter 5, which has brought us to the following conclusions:

Analysis of oscillations has to include the electrical drive, the mechanical drive and the wheel-rail contact. In order to investigate sufficiently oscillations in traction drives, traction cycles have to be simulated, including control dynamics, inverter harmonics, slip-stick phenomena and fault situations of the drive.

Elastic couplings have to provide damping to obviate resonances and limit transient amplitudes. Inverter pulse patterns have to minimize torque ripple and transients.

The oscillation characteristics of traction drives have been examined by means of time-domain simulations and frequency domain analysis. It has been shown that the traction motor is a damping component in the open-loop drive system. Further, the damping of elastic couplings plays a determining role in the attenuation of oscillations. Ripple torques generated by the motor, which is supplied with pulse-width modulated inverter waveforms, may cause resonances when the damping of the drive line is not chosen properly. The wheel-rail contact may cause slip-stick oscillations, but is also a damping factor for, e.g., torque peaks generated by motor short-circuit.

The results have to be seen as qualitative. To determine the amplitudes of oscillations by simulations, certain parameters have to be estimated with the aid of measured data. Transfer functions give an insight into system dynamics. When analysing transfer functions guidelines have to be followed:

- The stator frequency has to be chosen.
- The stiffness of the elastic couplings has to be determined.
- The damping of the elastic couplings has to be determined.

By combining the motor model and the mechanical model, the influence of the motor on mechanics and vice versa can be analyzed directly. Transients and resonances can be estimated and parameter influences can easily be investigated. Hence, discussions about the choice of drives and components such as couplings and gearboxes are provided against a background of modelling and simulation.

6 Conclusions

6.1 Results

The questions we asked in the introduction:
Which oscillation occur ?
How are they generated ?
How can they be described ?
Hoe can they be measured ?
How can they be avoided ?
have been answered only for a small part. The mechanical part of the drive and the uncontrolled motor have been considered. Oscillations have been measured and simulated by taking into account the inverter harmonics and the wheel-rail contact. However, the basics have been created by measurement, modelling and simulation of the drive as a system. The interaction of components, including the control system will have to be first investigated. In the following the results are discussed in detail.

A procedure has been developed to perform experiments which enable the measurement and analysis of oscillations in traction drives in vehicles on track with a reasonable expenditure of effort.

The simultaneous measurement of electrical and mechanical drive signals is essential in the analysis of oscillations and their causality. Cascade plots, i.e., Fourier spectra at subsequent moments of time, provide an overview of the oscillations of a drive during a traction cycle of acceleration, coasting and braking.

During the performed tests, four types of oscillation sources were detected, the control system, inverter voltage harmonics, mechanical drive sources such as misalignment of shafts or unbalance, and the wheel-rail contact.

Torque oscillations generated by inverter harmonics had a low amplitude in comparison with torque oscillations of mechanical origin. However, there may be transient higher amplitudes in the case of resonances or change of inverter voltage pulse pattern. Converter-excited oscillations are propagated throughout the entire drive, while measured mechanical oscillations were limited to the mechanical drive.

The highest oscillation amplitudes and peaks are caused by the rails. They may be propagated through the entire drive.

Tests on a vehicle test bench with fixed rollers eliminate rail influences, which increases the repeatability of tests but which excludes a significant source of oscillations and shock loads.

A tool for modelling and simulation has been developed which enables the simulation and analysis of oscillations in traction drives. Due to the flexibility of the tool, a variety of drive types can be investigated in a short time.

The interaction between the traction motor and the mechanical drive has been analyzed by two examples of mechanical drives, the hollow shaft drive and the quill shaft drive. Multi-body system modelling has been applied; this enables flexibility in modelling a variety of mechanical drive structures. Equations of motion are derived by an algorithm out of the mechanical structure.

Free oscillations are first damped by the damping of drive components. The motor itself has a damping influence on the mechanical drive.
Faults such as stator short-circuit of the motor cause torque peaks and subsequently free oscillations, which are not controlled but are attenuated by the wheel slip.

The wheel-rail contact may also generate oscillations of the wheel shaft. These oscillations are difficult to damp, there have been recent research efforts in this field [BUS95, ENG96]. A fast motor torque control provides fast torque responses which damp motor oscillations and provides the possibility of damping slip-stick oscillations.

Forced torque oscillations caused by inverter voltage harmonics have been considered. Torque harmonics may cause resonances in poorly damped shafts, and resonances in elastic couplings. In order to limit the amplitudes of torque oscilla-

tions, shaft resonance frequencies have to be obviated and damping of couplings has to be sufficiently high.

Analysis of oscillations has to include the electrical drive, the mechanical drive and the wheel-rail contact. In order to investigate sufficiently oscillations in traction drives, traction cycles have to be simulated, including control dynamics, inverter harmonics, slip-stick phenomena and fault situations of the drive. By using the developed tools, oscillations can be minimized to increase the lifetime of drive components.

The conclusions drawn from the measurements and simulations reported here have to be seen within the main limitations of the investigations. First, tests were performed on specific vehicles under specific circumstances. Then, simulations were carried out with models. These simulations were limited to the interaction of motor and mechanics, using specific parameter sets. Therefore the presented results remain samples from a variety of possible configurations of vehicle and operation parameters. The purpose of the conclusions is to focus the attention of the traction drive designer on oscillation phenomena, these demand consideration of the drive as an electromechanical system which is more than the sum of its components.

6.2 Recommendations for further research

In this thesis a basis has been created on which to further investigate oscillation phenomena in traction drives. The first step in future research is to include the control system and to analyze the interaction between the electrical and the mechanical parts of the drive. The model of the system as depicted in Figure 2.2.2, section 2.2, has to be extended step by step, adding possible oscillation sources and analysing the oscillation phenomena. The extension of models will include the implementation of control algorithms, power converter dynamics, catenary dynamics, vehicle dynamics and dynamics of the wheel-rail contact in two dimensions, to include track curves and irregularities.

Systematic research on model order, especially of the mechanical part of the drive including the bogie and car-body, will have to be carried out to derive the appropriate models for oscillation phenomena.

Analysis of experiments must include the statistical evaluation of tests. Further new methods of signal processing will have to be examined.

To date, the simulation results have been considered to be qualitative. To obtain a reliable prediction of oscillation amplitudes by simulation, parameters have to be known with a certain degree of precision. In particular, the damping of the mechanical part of the drive is not always known. The validation of models will have to be extended to system identification in practice, and to the estimation of model parameters such as described in section 5.2.2. Experiments are in preparation [BEC97].

Application of the proposed procedures will have to be done in future design and in the testing of light-rail vehicles to yield improved specification of drive components. In particular, the design of low-floor trams will have to be preceded by oscillation analysis because these trams include drive structures which differ significantly from classical bogie design.
The variation of drive parameters must be investigated intensively in order to optimize drive design. In particular, the influence of variations in wheel-rail contact will have to be evaluated.

If the minimization of oscillations is to be obtained by optimizing the control system, or by optimizing the drive structure, components will have to be evaluated. This evaluation requires collaboration between control and construction engineers when designing rail vehicle drives.

References

ALT78 Althammer K., The Rolling Test Plant at Munich-Freimann, Elektrische Bahnen, Nr. 10, 1978, pp 257 - 262.

AND82 Andresen, E. CH., K. Bienik und R. Pfeiffer, Pendelmomente und Wellenbeanspruchungen von Drehstrom-Käfigläufermotoren bei Frequenzumrichterspeisung, etz Archiv Bd. 4, 1982, pp 25 - 33.

ASA92 Asano, K., O. Shigenobu and I. Norio, Vibration suppression of induction-motor-driven hybrid vehicle using wheel torque observer, IEEE transactions on Industry Applications Vol. 28, No.2, March/ April 1992, pp 441 - 446.

AUS96 Auslander D.M. and C.J. Kempf, Mechatronics: Mechanical System Interfacing, Prentice Hall 1996.

BAA94 Baars, G.E. van and P.M.M. Bongers, Validation of Dynamic Wind Turbine Models using System Identification: Application to an Industrial 300 kW Wind Turbine, Proceedings of Windpower '94 Conference, May 1994, Minneapolis, pp 803-812.

BAU86 Bauer, H.P., Untersuchungen an einem Lokomotivantrieb mit Asynchronmotoren und stromeinprägendem Wechselrichter, Dissertation TH Darmstadt, 1986.

BEC97 Beck, H.P., C. Söffker, W. Deleroi, and M.W. Winterling, Identification of low frequency oscillations in a high power drive for implementation of modern mechatronic traction control systems and stress analysis of drive components, 2nd Technical Scientific Report of the project "Hosting and Training of Researchers on the Study and Testing of Components and Systems for Urban and Rail Electrical Transport", Naples, Italy, 1997, pp 29-43.

BEE94 Beer, F.G. de, Electromagnetic Soft Transition, Ph.D. Thesis, TU Delft, 1994.

BEI94 Beitzen W, and K.H. Küttner (ed.), Dubbel Handbook of Mechanical Engineering, Springer 1994.

BEL94 Belmans, R., Recent Major Developments in CAE and Vibrations and Audible Noise Analysis of Rotating Electrical Machines, Garant Apeldoorn, 1994.

BES88 Best, R. Digital Signal processing, Technisches Messen, Nr. 5 1988 - Nr. 12 1992. (in German)

BLA73 Blaschke, F., Das Verfahren der Feldorientierung zur Regelung der Drehfeldmaschine, Dissertation, Technische Universität Braunschweig, 1973.

BLA93 Blaabjerg, F., et al., Determination of mechanical resonances in induction motors by random modulation and acoustic measurement, proceedings EPE'93 Brighton, UK, 1993.

BON94 Bongers, P.M.M., Modeling and Identification of Flexible Wind Turbines and a Factorizational Approach to Robust Control, Ph.D. Thesis, TU Delft 1994.

BOS94 Bosch, P.P.J. van den and A.C. van der Klauw, Modeling, Identification and Simulation of Dynamical Systems, TU Delft, 1994.

BRA91 Bradley, D.A., D.Danson, N.C. Burd and A.J. Loaden, Mechatronics: Electronics in Products and Processes, Chapman and Hill 1991.

BUS95 Buscher, M., Radschlupfregelung für Drehstromlokomotiven, Dissertation TH Darmstadt, 1995.

BUT92 Butler, D.H.E., M.A. Churches, Y. Anbe, and H. Naitoh, Compensation of a Digitally Controlled Static Power Converter for the Damping of Rolling Mill Torsional Vibrations, IEEE Transactions on Industry Applications, Vol. 28, No. 2, March/April 1992.

CHE93 Chen, D. and C. Moler, Symbolic Math Toolbox, The MathWorks 1993.

DEL82 Deleroi, W., Ausgleichsvorgänge der symmetrischen Drehfeldmaschine, der Asynchronmaschine, beschrieben durch freie Ausgleichswellen, Archiv für Elektrotechnik 65, 1982, pp 1-10.

DEP85 Depenbrock, M., Direkte Selbstregelung (DSR) für hochdynamische Drehfeldantriebe mit Stromrichterspeisung, etz Archiv Band 7, Heft 7, 1985, pp. 211-218.

DEP88 Depenbrock, M. und N. Klaes, Zusammenhänge zwischen Schaltfrequenz, Taktverfahren, Momentpulsation und Stromverzerrung bei Induktionsmaschinen am Pulswechselrichter, etz Archiv, Band 10, 4/1988, pp 131-134.

DIM92 Dimarogonas, A.D. and S. Haddad, Vibration for Engineers, Prentice-Hall 1992.

DOP74 Doppler, S., Drehschwingungen von Triebachsen elektrischer Triebfahrzeuge, Elektrotechnik und Maschinenbau 91. Jahrgang Heft 7, Juli 1974, pp 373-379.

DRE94 Dreimann, K. und D. Hallmann, Asynchron-Fahrmotoren in Antriebssystemen für leichte Nahverkehrsfahrzeuge, ETG Fachberichte 50, 1994, pp 29-40.

DUS92 Duscheck, J. und J. Schaarschmidt, Simulation moderner elektrischer Triebfahrzeuge in Drehstromantriebstechnik, Elektrische Bahnen 90(1992) 8, pp 255-263.

ENG96 Engel, B., Verschleißmindernde Kraftschlußregelung mit Zustandsregler für elektrische Traktionsantriebe, Dissertation TU Clausthal, 1996.

FIE79 Fiehn, H., Weinhardt, M. und N. Zeevenhooven, Drehstromversuchsfahrzeug der Niederländischen Eisenbahnen - Adhäsionsmessungen, Elektrische Bahnen 77, 12/1979, pp 329-338.

FRE83 Frederich, F., Möglichkeiten zur Hochausnutzung des Rad/Schiene - Kraftschlusses - Zusammenhänge, Einflüsse, Maßnahmen, Archiv für Eisenbahntechnik 38 (1983), H.1, pp 45-56.

GHI92 Ghiara, T., P. Pozzobon, G. Sciutto, and R. Zecchi, Simulation to investigate on torque ripple in locomotive chopper and rheostatic drives, Computer in Railways III, Vol. 2: Technology, 1992, pp 63-78.

GRI89 Grieve D.W. and I.E. McShane, Torque pulsations on inverter fed induction motors, IEE 4th International Conference on Electrical Machines and Drives, London, 1989, pp 328-333.

HEN94 Henneberger, G., and J.R. Hadji-Minaglou, Entwurf und Vergleich von verschiedenen Motortypen für den Einsatz in Elektrofahrzeugen, ETG Fachberichte 50, 1994, pp 7-28.

HIG90 Higgins, R., Digital Signal Processing in VLSI, Prentice Hall, Englewood Cliffs, 1990.

HOL93 Holtz, J. On the Performance of optimal Pulsewidth Modulation Techniques, EPE Journal, Volume 3, No. 1, March 1993, pp 17-26.

HON95 Hondius, H., 1984-1994, zehn Jahre Entwicklung der elektrisch angetriebenen Nieder- und Mittelflurfahrzeuge für Straßen- und Stadtbahnen. Markt, Technik, Erfahrungen, Kosten und Ausblick, ZEV + DET Glasers Annalen 119 (1995) Nr. 9/10, pp 351-371.

JAC92 Jacobs, T., Short circuit calculation of asynchronous machines, HOLEC Ridderkerk, 1992 (in Dutch).

JAE88 Jänecke, M., R. Kremer, and G. Steuerwald, Direct Self Control (DSC), a novel method of controlling asynchronous machines in traction applications, Elektrische Bahnen 88/3 1990, pp 81-87.

JOE95 Jöckel, A. und R. Pfeiffer, Regelungstechnische Bedämpfung der Reibschwingungen im Antriebsstrang von Drehstromtriebfahrzeugen, Elektrische Bahnen 5/95, pp 151-157.

JON90 Jonker, J.B. and J. Meijaard, SPACAR, a program system for dynamic analysis of spatial mechanisms and manipulators, in "Multibody Systems Handbook", W. Schiehlen (ed.) pp. 123-143, 1990.

JOR69 H. Jordan, M. Weis, Asynchronmaschinen, Braunschweig 1969.

KAL67 Kalker, J.J., On the Rolling Contact of Two Elastic Bodies in the Presence of Dry Friction, Ph.D. Thesis, TU Delft, 1967.

KAL90 Kalker, J.J., Three-Dimensional Elastic Bodies in Rolling Contact, Kluwer, Dordrecht 1990.

KAN85 Kane, T.R. and D.A. Levinson, Dynamics, theory and applications, McGraw - Hill series in mechanical engineering, 1985.

KEM94 Kempkes, J., Vergleich verschiedener Konzepte für Radnabenantriebe in Schienenfahrzeugen, ETG Fachbericht 50, 1994, pp 41-52.

KEV91 Keve, Th., Wirkung der Pendelmomente auf Antriebe mit Asynchronmotoren, etz, Band 112, Heft 6/7, 1991, pp 284-290.

KLE80 H. Kleinrath, Stromrichtergespeiste Drehfeldmaschinen, Wien 1980.

KOR93 Kortüm, W. and R.S. Sharp, Multibody Computer Codes in Vehicle System Dynamics, Sweth & Zeitlinger B.V., Amsterdam 1993.

KRA93 Kratz, G., B. Sauer und Ch. Segieth, GEALAIF, ein neues Antriebskonzept für Höchstleistungen im Traktionsbereich, ZEV + DET Glas. Ann. 117 (1993), Nr.6 Juni, pp 194-201.

KRA94 Krauss, Th.P., L. Shure, and J.N. Little, Signal Processing Toolbox, The MathWorks Inc. 1994.

LJU87 Ljung, L., System identification: theory for the user, Prentice Hall, Englewood Cliffs NJ, 1987.

MAT93 MATLAB® Reference Guide, The MathWorks 1993.

MEI92 Meister, W., Berechnung der Torsions-Beanspruchung in drehelastischen Antrieben mit stromrichtergespeister Asynchronmaschine, Archiv für Elektrotechnik, Band 75 1992. pp 121-130.

MUE96 Müller, G.H. and C.F. Landy, Vibration monitoring for broken rotor bars in squirrel cage induction motors with interbar currents, Proceedings SPEEDAM 1996, Capri, Italy., pp A2-1 - A2-6.

NAI94 Naitoh, H. and R. Kurosawa, Technological Stream for torsional vibration damping for rolling mill drives, Proceedings Speedam, Taormina 1994, pp 284-292.

NES58 Nestorides, E.J., A handbook on torsional vibration, Cambridge University Press 1958.

NOV76 Novotny, D. and J. Wouterse, Induction machine transfer functions and dynamic response by means of complex time variables, IEEE Transactions on Power Apparatus and Systems, Vol. PAS-95, no. 4, July/August 1976, pp 1325-1335.

NÜR63 Nürnberg, W., Die Asynchronmaschine, Springer Berlin 1963.

OVE94 Overloop, P.J. v., Modelling of the drive of traction vehicles, Master's Thesis, TU Delft, Faculty of Mechanical Engineering, Measurement and Control Group, 1994 (in Dutch).

OVE94/2 Overloop, P.J. v., Autorail User's Guide, HOLEC Ridderkerk, 1994 (in Dutch).

OVE94/3 Overloop, P.J. v., Autorail Programmer's Guide, HOLEC Ridderkerk, 1994 (in Dutch).

OVE95 Overloop, P.J. van, Measurements on the traction drive of the test locomotive E402, CRIS, Naples 1995.

PEE86 Peeken, H. und C. Troeder, Elastische Kupplungen, Springer Berlin 1986.

PES89 Pestle, J.P. and R.J. Varley, Design factors involved in mechanically coupling electrical machines to driving or driven equipment, IEE 4th International Conference on Electrical Machines and Drives, London, 1989, pp 389-393.

PIT89 Pittius, E. und H.O. Seinsch, Die Stoßdrehmomente bei symmetrischen und unsymmetrischen Kurzschlüssen in Asynchronmaschinen., Archiv für Elektrotechnik 72, 1989, pp 42-50.

POE92 Poeze, E., Pendelkoppels - de interactie tussen een mechanisch en een elektrisch systeem, report ltm 964, Laboratory of Engineering Mechanics, TU Delft, 1992. (in Dutch)

POL92 Polinder, H., The operation of the asynchronous machine fed by an arbitrary voltage, Master's Thesis, TU Delft 1992 (in Dutch).

PRO94 Profos, P. und T. Pfeifer, Handbuch der industriellen Meßtechnik, Oldenbourg 1994.

RIC54 R. Richter, Elektrische Maschinen, Band 4 Die Induktionsmaschinen, Basel 1954.

RON92 Rondel, M., W. Deleroi en H.P. Pruisken, Machine transients in inverter output currents, ICEM Manchester UK, 1992, pp 1187-1190.

SCH60 W. Schuisky, Berechnung elektrischer Maschinen, Wien 1960.

SCH90 Schiehlen, W., (Ed.), Multibody Systems Handbook, Berlin 1990.

SCH91 Schaechter, D.B., D.A. Levinson and T.R. Kane, AUTOLEV, User's Manual, Online Dynamics Inc., Sunnyvale CA, USA, 1991.

SCH92 Schwartz, H.-J., Regelung der Radsatzdrehzahl zur maximalen Kraftschlußausnutzung bei elektrischen Triebfahrzeugen, Dissertation, TH Darmstadt, 1992.

SCH94 Schrüfer, E., Interpolation bei der Diskreten Fourier-Transformation durch Einfügen von Nullen, Technisches Messen Nr.2 1994 pp 89-93.

SCH95 Schreiber, R., Kögel, R. und P. Häse, Regelung zur optimalen Kraftschlussausnutzung bei Drehstromlokomotiven auf der Basis der Steigung der Kraftschlusskennlinien, Elektrische Bahnen 5/95, pp 157-163.

SIM93 SIMULINK® User's Guide, The MathWorks 1993.

TAE71 F. Taegen, Einführung in die Theorie der elektrischen Maschinen II, Delft 1971.

TUI96 Tuinman, E., Traction motors show the way in motor technology, Polytechnisch Tijdschrift, Feb. 1996, pp 42-45, (in Dutch).

UED92 Ueda, R., T. Sonoda, K. Koga, and M. Ichikawa, Stability analysis in induction motor driven by V/f controlled general-purpose inverter, IEEE transactions on Industry Applications Vol. 28, No.2, March/April 1992, pp 472-481.

VEL94 Veltman, A., The Fish Method, Ph.D. Thesis, TU Delft 1994.

VIN93 Vinyolas, J., J.M. Abete and J.G. Gimenez, Design methodology and experimental results of a test facility for active and conventional railway suspensions, Vehicle System Dynamics, Vol. 22, 1993, pp 21-41.

VIT93 Vitrano, F., L. Pastena, and U. Flego, Roller Bench Testing of Railway Vehicles, Ingegneria Ferroviaria, July 1993, pp 480-490 (in Italian).

WAL91 Wallrapp, O., C. Führer, and I. Faye, Medyna 7.0 - Infoheft 7.1, Berlin 1991.

WAT82 Watanabe, K. and D.M. Himmelblau, Analysis of Trajectory Errors in Integrating Ordinary Differential Equations, Journal of the Franklin Institute, Vol 314, No. 5, November 1982, pp 283-321.

WEE95 Weerdt, R. de, Finite Element Modelling of Squirrel Cage Induction Motors, Ph.D. Thesis, KU Leuven 1995, (in Dutch).

WEL95 Welsch, H.M., Dauerstoß- und Tieftemperatur-Rollprüfstandsversuche am Niederflur-Triebfahrwerk der neuen Straßenbahnwagen der Stadt Frankfurt (Main), ZEV + DET Glasers Annalen 119, Nr. 7, 1995, pp 217-221.

WIN94 Winterling, M.W., Torque measurements metro vehicle, HOLEC Ridderkerk 1994 (in Dutch).

WIN94/2 Winterling, M.W., Low-floor tram motor on test bench, HOLEC Ridderkerk 1994. (in Dutch).

WIN94/3 Winterling, M.W., Electrical multiple-unit, tests on track, HOLEC Ridderkerk 1994 (in Dutch).

WIN95 Winterling, M.W., URBOS 1, Analysis of mechanical stress, HOLEC RIDDERKERK 1995.

WIN95/2 Winterling, M.W., URBOS 1, Analysis of system dynamics, HOLEC RIDDERKERK 1995.

WIN95/3 Winterling, M.W., Measurements of drive dynamics of the locomotive E402 on the test bench, CRIS, Naples 1995.

ZEE89 Zeevenhooven, N.H.C.E., Rail vehicle technology, lecture notes TU Delft, 1989 (in Dutch).

ZIJ94 Zijdemans, P.C.K. und C.P. Keizer, Entwicklung einer Drehgestellfamilie "The Flexy Bogie" für die neuen elektrischen Nahverkehrs-Triebzüge SM90 der Niederländischen Eisenbahnen, ZEV + DET Glasers Annalen, Heft 2/3, 1994, pp 83-88.

ZIJ94/2 Zijlstra, M., The influence of the stator winding harmonics on the torque of the induction motor at variable supply frequency, Master's Thesis, TU Delft 1994 (in Dutch).

List of Symbols

Underlined letters have been used for matrices and vectors.

Latin letters:

Symbol	Description
$\underline{A}$	system matrix
a	acceleration
$\underline{B}$	input matrix
$\underline{C}$	output matrix, damping matrix
$\underline{D}$	matrix of transition
$\underline{F}$	force vector
f	frequency, coefficient of friction
g	acceleration of gravity
i	current
J	moment of inertia
$\underline{K}$	vector of internal forces
k	spring constant
L	inductance
$\underline{M}$	mass matrix
m	mass
$\underline{q}$	vector of degrees of freedom
R	resistance
r	radius
s	slip
T	torque
t	time
u	motor voltage
$\underline{u}$	vector of generalized velocities

Symbol	Description
v	speed
x	longitudinal axis, longitudinal displacement
$\underline{x}$	vector of variables
y	lateral axis, lateral displacement
z	vertical axis, vertical displacement

Greek letters

Symbol	Description
α	axis of Cartesian coordinates of motor model, angular acceleration
β	axis of Cartesian coordinates of motor model
ν	order of harmonics
σ	leakage factor of induction motor
τ	time constant
ϕ	rotation angle of x-axis
χ	rotation angle of y-axis
ψ	rotation angle of z-axis
Ψ	magnetic flux, relative damping
ω	angular frequency, speed

Indices, latin letters

Symbol	Description
a	stator phase
b	stator phase
c	stator phase

cinv	inverter DC-link capacitor
cpm	coupling motor side
csh	cardan shaft
d	axis of rotating reference frame of motor model
fbk	feedback
gm	gearbox housing motor side
gw	gearbox housing wheel side
hsh	hollow shaft
inv	inverter
igw	intermediate gear wheel
lin	line, linear
m	motor
pc	wheel axle bearing housing, coupling side
pg	wheel axle bearing housing, gearbox side
q	axis of rotating reference frame of motor model
r	rotor
ref	reference
s	stator, suspension
u	inverter phase
v	inverter phase, vehicle
w	inverter phase, wheel
x	longitudinal direction
y	longitudinal direction
z	longitudinal direction

Indices, greek letters

Symbol	Description
ν	order of harmonics
σ	leakage

Appendix A

Transformation of Motor Equations

The traction motor and inverter are both three-phase and assumed to be symmetric. Voltages, currents and fluxes of the three phases can be expressed by space phasors as described in section 4.2.
The space phasor is placed in a coordinate frame. A rotating cartesian frame has been chosen to solve the differential equations of the motor. To calculate the phase quantities of the motor, the space phasors were transformed to the three-phase coordinate frame fixed to the stator. The transformation has to be power invariant. The coordinate frames of the motor are depicted in figure A1.

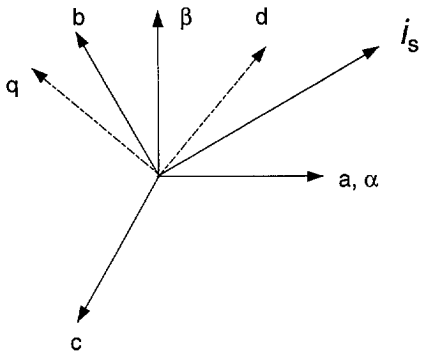

Figure A1 Coordinate frames of the motor model.

The rotor axis lies in the origin of the coordinate frame, vertically on its plane. The rotation of the rotor and the sign of the torque are given by the rotation and position of the motor's flux phasors. Torque and speed are positive in motor operation and during acceleration of the rotor.

The phase currents were calculated by first transforming the current phasor to a Cartesian frame fixed to the stator by

$$i_{s\alpha} = i_{sd}\cos(\omega_s t) - i_{sq}\sin(\omega_s t)$$

$$i_{s\beta} = i_{sd}\sin(\omega_s t) - i_{sq}\cos(\omega_s t) \quad .$$

The transformation from two-phase currents to three-phase currents is:

$$i_{sa} = \sqrt{\frac{2}{3}}\ i_{s\alpha}$$

$$i_{sb} = \sqrt{\frac{2}{3}}\ \left(-\frac{1}{2}\ i_{s\alpha} + \frac{\sqrt{3}}{2}\ i_{s\beta}\right)$$

$$i_{sc} = \sqrt{\frac{2}{3}}\ \left(-\frac{1}{2}\ i_{s\alpha} - \frac{\sqrt{3}}{2}\ i_{s\beta}\right) \quad .$$

Appendix B

Model Equations of a Suspended Drive

The model of the drive, including drive line and suspensions, was derived under the following assumptions:

- no lateral (y) and longitudinal degrees of freedom
- no rotation around the vertical axis (z).

Following these assumptions, a model with six bodies and eight degrees of freedom can be derived. The model with the reference frame of the housing is depicted in Figure B1.

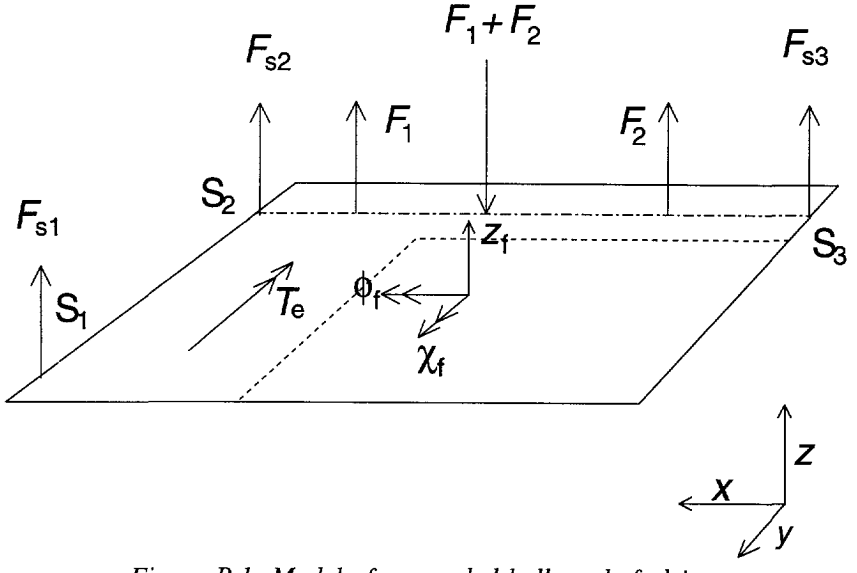

Figure B.1 Model of suspended hollow shaft drive.

The model's equations of motion are given by equation 4.15 with the mass matrix

$$\begin{pmatrix}
J_{a\chi} & 0 & 0 & 0 & 0 & 0 & 0 & 0 \\
0 & J_{b\chi} & 0 & 0 & 0 & 0 & 0 & 0 \\
0 & 0 & J_{c\chi} & 0 & 0 & 0 & 0 & 0 \\
0 & 0 & 0 & J_{d\chi} & 0 & 0 & 0 & 0 \\
0 & 0 & 0 & 0 & J_{e\chi} & 0 & 0 & 0 \\
0 & 0 & 0 & 0 & 0 & J'_{f\chi} & -\sum_{i=a}^{d} m_i x_i y_i & -\sum_{i=a}^{d} m_i x_i \\
0 & 0 & 0 & 0 & 0 & -\sum_{i=a}^{d} m_i x_i y_i & J'_{f\phi} & \sum_{i=a}^{d} m_i y_i \\
0 & 0 & 0 & 0 & 0 & -\sum_{i=a}^{d} m_i x_i & \sum_{i=a}^{d} m_i y_i & m'_f
\end{pmatrix}$$

with:

$$J'_{f\chi} = J_{f\chi} + \sum_{i=a}^{d} (m_i \; x_i^2)$$

$$J'_{f\phi} = J_{f\phi} + \sum_{i=a}^{d} (m_i \; y_i^2)$$

$$m'_f = m_f + \sum_{i=a}^{d} m_i \quad .$$

the stiffness matrix

$$\begin{pmatrix}
k_1 & -k_1 & 0 & 0 & 0 & 0 & 0 & 0 \\
-k_1 & k_1 + r_b^2 k_2 & r_b r_c k_2 & 0 & 0 & 0 & 0 & 0 \\
0 & r_b r_c k_2 & r_c^2 (k_2 + k_3) & r_c r_d k_3 & 0 & 0 & 0 & 0 \\
0 & 0 & r_c r_d k_3 & r_d^2 k_3 + k_4 & -k_4 & 0 & 0 & 0 \\
0 & 0 & 0 & -k_4 & k_4 & 0 & 0 & 0 \\
0 & r_b k_2 (x_b - x_c) & r_c k_2 (x_b - x_c) - r_c k_3 (x_c - x_d) & -r_d k_3 (x_c - x_d) & 0 & k_6 \sum_{i=1}^{3} x_{si}^2 & -k_6 \sum_{i=1}^{3} x_{si} y_{si} & -k_6 \sum_{i=1}^{3} x_{si} \\
0 & 0 & 0 & 0 & 0 & -k_6 \sum_{i=1}^{3} x_{si} y_{si} & k_6 \sum_{i=1}^{3} y_{si}^2 & k_6 \sum_{i=1}^{3} y_{si} \\
0 & 0 & 0 & 0 & 0 & -k_6 \sum_{i=1}^{3} x_{si} & k_6 \sum_{i=1}^{3} y_{si} & 3k_6
\end{pmatrix}$$

with

$\chi_{a,b,c,d,e,f}$	rotational degrees of freedom of bodies	[rad]
z_f	translational degree of freedom of housing	[m]
$J_{a,b,c,d,e,f}$	inertia of bodies	[kg m^2]
m_f	mass of motor and gearbox housing	[kg]
$k_{1,4}$	spring constants of couplings	[Nm/rad]
$k_{2,3}$	spring constants of gear teeth	[Nm/rad]
k_6	spring constant of motor and gearbox suspension	[N/m]
$x_{b,c,d}$	distance between centres of gravities of gear wheels and motor and gearbox housing	[m]
$x_{s1,s2,s3}$	distance between suspensions and motor and gearbox housing	[m]
$y_{s1,s2,s3}$	distance between suspensions and motor and gearbox housing	[m]

The vector of degrees of freedom is

$$(\chi_a \;\; \chi_b \;\; \chi_c \;\; \chi_d \;\; \chi_e \;\; \chi_f \;\; \phi_f \;\; z_f)^T \quad .$$

The vertical forces expressed in degrees of freedom are

$$F_{s1} = k\,(z_f - x_{s1}\,\sin(\chi_f) + y_{s1}\,\sin(\phi_f))$$

$$F_{s2} = k\,(z_f - x_{s2}\,\sin(\chi_f) + y_{s2}\,\sin(\phi_f))$$

$$F_{s3} = k\,(z_f - x_{s3}\,\sin(\chi_f) + y_{s3}\,\sin(\phi_f)) \quad .$$

For small rotation angles it can be stated

$$\sin(\chi) = \chi\,, \qquad \cos(\chi) = 1$$

so that the forces become

$$F_{s1} = k\,(z_f - x_{s1}\,\chi_f + y_{s1}\,\phi_f)$$

$$F_{s2} = k\,(z_f - x_{s2}\,\chi_f + y_{s2}\,\phi_f)$$

$$F_{s3} = k\,(z_f - x_{s3}\,\chi_f + y_{s3}\,\phi_f) \quad .$$

Parameters are listed in appendix F.

Appendix C

Wheel-rail contact parameters

As stated in section 4.4 to develop a practical friction curve, choices have to be made by taking into consideration:

- definition of the curve up to the maximum by
  - the maximum value of transmitted force
  - the difference of speed or creepage at maximum transmitted force
  - the gradient at the origin of the curve
- definition of the curve beyond the maximum.

The applied curve from zero speed difference up to the maximum of the friction coefficient f has been approximated by a function which is composed of a friction-characteristic defined by Vermeulen and Johnson which has been cited by Kalker [KAL90]:

$$f = f_{max} \left(1 - \left(1 - \frac{\Delta v}{\Delta v_{max}}\right)^3\right)$$

Beyond the maximum friction coefficient, the curve has been defined by the following formulae:

For $0 \leq \Delta v \leq 1.2\ \Delta v_{max}$:

$$f = f_{max} \left(1 - \left|1 - \frac{\Delta v}{\Delta v_{max}}\right|^3\right)$$

with

Δv the difference of speed between wheel and rail

Δv_{max} the difference of speed between wheel and rail at the maximum of adhesion

f the coefficient of friction

f_{max} the maximum coefficient of friction

and

$$f(\Delta v) = -f(-\Delta v) \quad .$$

For $1.2\ \Delta v_{max} < \Delta v < 2\ \Delta v_{max}$ the friction coefficient is falling as a linear function of the speed difference and for $2\ \Delta v_{max} < \Delta v$ the friction coefficient os constant.

Parameter values applied in the simulations, valid for dry rails and low vehicle speed, were

f_{max} = 0.3

Δv_{max} = 0.03 m/s.

Figure C.1 shows the friction coefficient with f_{max} = 0.35 and Δv_{max} = 0.03 m/s.

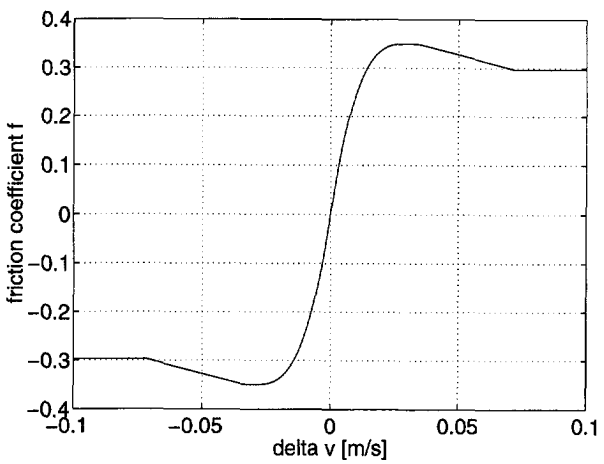

Figure C.1 Friction coefficient as function of speed difference.

Appendix D

Equations of motion of rolling wheels

In the case of rolling wheels as depicted in Figure D1, rotation and translation of the wheels are coupled by the following constraint

$$x_w = \chi_W \, r_w \quad .$$

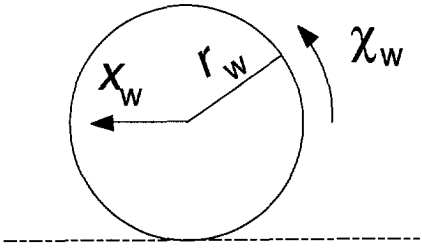

Figure D.1 Degrees of freedom of a rolling wheel.

The inertial torque of the wheel is

$$(J_w + m_w \, r_w^2) \, \ddot{\chi}_w$$

with

J_w inertia of the wheel
m_w mass of the wheel
r_w radius of the wheel
χ_w rotational degree of freedom of the wheel
x_w translational degree of freedom of the wheel

In the case of an active force on the wheel by a spring with stiffness k coupled with a second mass m, e.g., the bogie frame, the equation of motion of the wheel and coupled mass with degree of freedom χ is given by equation (4.13)

with the mass matrix $\underline{M}$

$$\begin{pmatrix} J_w + m_w r_w^2 & 0 \\ 0 & m\, r_w^2 \end{pmatrix}$$

with the stiffness matrix $\underline{K}$

$$\begin{pmatrix} k\, r_w^2 & -k\, r_w^2 \\ -k\, r_w^2 & k\, r_w^2 \end{pmatrix}$$

and the vector of degrees of freedom

$$\begin{pmatrix} \chi_w \\ \chi \end{pmatrix} .$$

Appendix E

System equations of a traction drive

In section 4.5 the system equation of a drive have been given by equation 4.18. An example of the equation of the quill shaft drive depicted in Figure 5.3.10, section 5.3.2, is given below by the system vectors and matrices.

$$A = \begin{pmatrix}
-\frac{1}{\sigma\tau_s} & \omega_s & \frac{1-\sigma}{\sigma\tau_m} & 0 & 0 & 0 & 0 & 0 & 0 & 0 & 0 & 0 \\
-\omega_s & -\frac{1}{\sigma\tau_s} & 0 & \frac{1-\sigma}{\sigma\tau_m} & 0 & 0 & 0 & 0 & 0 & 0 & 0 & 0 \\
\frac{1-\sigma}{\sigma\tau_k} & 0 & -\frac{1}{\sigma\tau_r} & \omega_r & 0 & 0 & 0 & 0 & 0 & 0 & 0 & 0 \\
0 & \frac{1-\sigma}{\sigma\tau_r} & -\omega_r & -\frac{1}{\sigma\tau_r} & 0 & 0 & 0 & 0 & 0 & 0 & 0 & 0 \\
0 & 0 & p\frac{1-\sigma}{\sigma L_h}\psi_{sq} & -p\frac{1-\sigma}{\sigma L_h}\psi_{sd} & -\frac{1}{J_a}c_1 & -\frac{1}{J_a}k_1 & \frac{1}{J_a}c_1 & \frac{1}{J_a}k_1 & 0 & 0 & 0 & 0 \\
0 & 0 & 0 & 0 & 0 & 1 & 0 & 0 & 0 & 0 & 0 & 0 \\
0 & 0 & 0 & 0 & \frac{1}{J_b}c_1 & \frac{1}{J_b}k_1 & -\frac{1}{J_b}(c_1+c_2) & -\frac{1}{J_b}(k_1+k_2) & \frac{1}{J_b}c_2 & \frac{1}{J_b}k_2 & 0 & 0 \\
0 & 0 & 0 & 0 & 0 & 0 & 0 & 1 & 0 & 0 & 0 & 0 \\
0 & 0 & 0 & 0 & 0 & 0 & \frac{1}{J_c}c_2 & \frac{1}{J_c}k_2 & -\frac{1}{J_c}(c_2+c_3) & -\frac{1}{J_c}(k_2+k_3) & \frac{1}{J_c}c_3 & \frac{1}{J_c}k_3 \\
0 & 0 & 0 & 0 & 0 & 0 & 0 & 0 & 0 & 1 & 0 & 0 \\
0 & 0 & 0 & 0 & 0 & 0 & 0 & 0 & \frac{1}{J_d}c_3 & \frac{1}{J_d}k_3 & -\frac{1}{J_d}c_3 & -\frac{1}{J_d}k_3 \\
0 & 0 & 0 & 0 & 0 & 0 & 0 & 0 & 0 & 0 & 0 & 1
\end{pmatrix}$$

$$\underline{x} = \left(\psi_{sd}\ \psi_{sq}\ \psi_{rd}\ \psi_{rq}\ \omega_a\ \chi_a\ \omega_b\ \chi_b\ \omega_c\ \chi_c\ \omega_d\ \chi_d\right)^T$$

$$\underline{u} = \left(u_{sd}\ 0\ 0\ 0\ 0\ 0\ 0\ 0\ 0\ 0\ 0\ 0\right)^T$$

$$\underline{B} = \underline{E}$$

Appendix F

Parameters of drive models

Two vehicle drives were modelled as described in section 5.3.2. Parameter sets of these models and parameters of excitation for simulation are described in this appendix.

Electrical multiple-unit hollow shaft drive

Motor parameters

stator resistance	R_s	=	0.127 Ω
rotor resistance referred to the stator	R_r	=	0.088 Ω
mutual inductance	L_h	=	72.8 mH
stator leakage inductance	$L_{s\sigma}$	=	1.81 mH
rotor leakage inductance referred to the stator	$L_{r\sigma}$	=	2.62 mH
pair of poles	p	=	2.

Parameters of the drive line

rotor inertia (rotor side)	3.9 kgm^2
inertia of motor side coupling half (rotor side)	0.05 kgm^2
inertia of transmission (wheel side)	20.925 kgm^2
with: inertia of motor side coupling half	0.93 kgm^2
inertia of pinion wheel	1.02 kgm^2
inertia of intermediate gear wheel	3.11 kgm^2

inertia of gear wheel and hollow shaft	9.745 kgm^2
inertia of hollow shaft coupling half	1.0 kgm^2
inertia of brake disc	6.05 kgm^2
inertia of driven wheel set half including hollow shaft coupling half	49 kgm^2
inertia of non-driven wheel set half	48 kgm^2

Number of gear teeth	pinion wheel	16
	intermediate wheel	38
	gear wheel	69
Stiffness of the gear teeth		2.7 10^9 N/m

Rolling circle of gear wheels	pinion wheel	133.09 mm
	intermediate wheel	316.09 mm
	intermediate wheel	310.819 mm
	gear wheel	564.381 mm

Stiffness of motor side coupling

Average torque	$k_{T,dyn}$ [Nm/rad]
0.25 T_{KN}	1.27 10^6
0.5 T_{KN}	1.96 10^6
0.75 T_{KN}	2.64 10^6
1.00 T_{KN}	3.33 10^6

with T_{KN} = 8650 Nm
relative damping ψ = 0.4.

Stiffness/relative damping of wheel side coupling

Average torque	$k_{T,dyn}$ [Nm/rad]	ψ
0.34 T_{KN}	1.995 10^6	0.64
0.67 T_{KN}	2.468 10^6	0.5
2.84 T_{KN}	2.84 10^6	0.36

with

T_{KN} = 13.65 kNm.

Stiffness of the wheel shaft	4.4 10^6 Nm/rad
Damping of the wheel shaft ψ	0.02
Wheel diameter	0.92 m

Parameters of the gearbox

mass of gearbox housing		1531 kg
mass of rotor		297 kg
mass of pinion wheel		25 kg
mass of intermediate gear wheel		50 kg
mass of gear wheel		347 kg
mass of hollow shaft and coupling half		
inertia of motor/gearbox housing ,	x-axis, z-axis	174 kgm^2
	y-axis	150 kgm^2
inertia of pinion wheel, x-axis, z-axis		2 kgm^2
inertia of intermediate gear wheel, x-axis, z-axis		8 kgm^2
inertia of gear wheel and hollow shaft, x-axis, z-axis		20 kgm^2

distance between centres of gravity of gearbox housing and rotor	x_a	0.102 m
	y_a	0.102 m
pinion wheel	x_b	0.102 m
	y_b	-0.568 m
intermediate gear wheel	x_c	-0.123 m
	y_c	-0..568 m
gear wheel	x_d	-0.568 m
	y_d	-0.568 m
suspension motor	x_{s1}	0.479 m
	y_{s1}	0.322 m
suspension gearbox motor side	x_{s2}	0.284 m
	y_{s2}	-0.568 m
suspension gearbox wheel side	x_{s3}	-0.981 m
	y_{s3}	-0.568 m

stiffness of suspensions	$6.7\ 10^7$ N/m
damping of suspensions	0

Parameters of the vehicle

inertia of car body	3990 kg m^2
inertia of motor bogie	667 kg m^2
inertia of wheel set and swivelling arm	410 kg m^2
stiffness of the swivelling arm from wheel to bogie frame	$2.56\ 10^6$ Nm/rad
stiffness of the centre pivot from bogie frame to car body	$3.15\ 10^5$ Nm/rad

Simulation parameters

Stator fundamental voltages during acceleration:

Time(s)	0	0.7	1.2	2	2.5	3.2	7.3	21.5
Frequency (Hz)	0.7	0.7	0.7			4.8	13.5	45
Voltage u_{sd} (V)	18	18	26.7	100	128		516	1715

Ratio of amplitude of stator harmonic voltages to fundamental during acceleration:

Stator voltage harmonic	5	7
Fundamental frequency from 0 Hz to 18 Hz	0.02	0.03
Fundamental frequency from 18 Hz to 45 Hz	0.2	0.1

Quill shaft drive

Motor parameters

stator resistance	R_s	=	0.359 Ω
rotor resistance referred to the stator	R_r	=	0.199 Ω
mutual inductance	L_h	=	77.57 mH
stator leakage inductance	$L_{s\sigma}$	=	3.877 mH
rotor leakage inductance referred to the stator	$L_{r\sigma}$	=	3.168 mH
pair of poles	p	=	2

Parameters of the drive line

rotor inertia and coupling half	2.268 kgm^2
inertia of coupling half and quill shaft half	0.09 kgm^2
inertia of second coupling half and quill shaft half	0.094 kgm^2
inertia of transmission, wheel set and vehicle (motor side)	136.4 kgm^2
stiffness of couplings	1.15 10^5 Nm/rad
relative damping of rubber coupling	2.4
relative damping of steel coupling	0.12
stiffness of quill shaft	1.076 10^5 Nm/rad
damping of quill shaft	0.06

Simulation parameters

Stator fundamental voltages during acceleration

Time(s)	0	0.7	1.5	2	5.9	17.9
Frequency (Hz)	0.7	0.7	3.3	4.9	17.6	56.6
Voltage (V)	30	30	158	195	539	1660

Ratio of amplitude of stator harmonic voltages to fundamental during acceleration

Stator voltage harmonic	11	13
Fundamental frequency from 0 Hz to 18 Hz	0.02	0.03
Fundamental frequency from 18 Hz to 45 Hz	0.2	0.1

Samenvatting

Vervoer maakt een steeds belangrijker deel uit van het dagelijks leven. Door het woon-werkverkeer en buitenlandse reizen is de dichtheid in auto-, vliegtuig- en treinverkeer toegenomen. Hoge snelheidstreinen zijn een alternatief voor het vliegtuig, terwijl treinstellen, metro's en trams een alternatief voor de auto zijn. Door de toenemende files op de snelwegen is het openbaar vervoer via rails een serieus alternatief, maar het moet aantrekkelijk zijn. Dat betekent comfortabele treinen, metro's en trams, die de passagiers snel en met een hoge frequentie kunnen vervoeren. Deze eisen vragen om nieuwe ontwikkelingen. Een voorbeeld is de lage vloertram met een instaphoogte van 30 centimeter.

De ontwikkeling van railvoertuigen zoals treinstellen, metro's and trams, uitgerust met asynchrone tractiemotoren en nieuwe draaistel- en rijtuigbakconstructie, heeft geleid tot zowel vermindering van gewicht als tot hogere prestaties. Daardoor kan het energieverbruik verlaagd en de capaciteit voor het personenvervoer verhoogd worden.
Tegenwoordig behoort de levensduur bij de specificaties van nieuw te ontwikkelen railvoertuigen. Specificaties van componenten van tractieaandrijvingen zoals tandwielkasten, koppelingen en verende ophangingen moeten een levensduur van minstens 30 jaar garanderen. De levensduur van de componenten wordt beïnvloed door de dynamische belasting. Voor de ontwikkeling van tractieaandrijvingen moeten derhalve de pieken en oscillaties van de optredende koppels en krachten bepaald worden. Hiervoor moet de gehele aandrijving bestaande uit elektrische aandrijving, mechanische aandrijflijn en wiel-rail-contact beschouwd worden. Gezien het grote aantal van concepten voor de elektrische en mechanische aandrijving moet een flexibele procedure voor het bepalen van het trillingsgedrag ontwikkeld worden.
Er kunnen gedempte vrije trillingen of gedwongen trillingen optreden in de mechanische aandrijving. De elektrische aandrijving is een bron van oscillaties door de pendelkoppels die de motor genereert als gevolg van de invertervoeding, door de dynamica van de regeling en door foutsituaties in de aandrijving zoals statorkort-

sluiting van de motor. Oscillaties opgewekt door het wiel-rail-contact komen tot stand door stoten en door slip-stick-verschijnselen, die de hele aandrijving exciteren.

In dit proefschrift wordt een procedure voorgesteld waarmee mechanische trillingen in tractieaandrijvingen op experimentele en rekenkundige manier bepaald kunnen worden om in korte tijd een overzicht van het trillingsgedrag van een aandrijving te verkrijgen.

Metingen aan tractieaandrijvingen moeten worden uitgevoerd door sensoren zowel in de elektrische als in de mechanische aandrijving te plaatsen en simultaan te bemonsteren. Een standaard tractiecyclus van aanzetten en remmen verschaft een overzicht van de optredende trillingen, door analyse in het tijddomein en het frequentiedomein in cascadeplots uit te voeren. Toerentalafhankelijke trillingen en resonanties kunnen eenvoudig worden gedetecteerd. Er zijn metingen uitgevoerd aan drie verschillende voertuigtypen op de baan en aan een locomotief op een rollenbank.
De meest belangrijke bronnen van trillingen bleken de invertergevoede motor, de mechanische aandrijflijn en het wiel-rail-contact te zijn. De hoogste amplitudes traden op bij het aanstoten van zwak gedempte eigenfrequenties zoals slip-stick-oscillaties van de wielas en resonantie door pendelkoppels van een cardanas.

Flexibele modelvorming is mogelijk door de mechanische structuur als multibody systeem te modelleren, waardoor de bewegingsvergelijkingen afgeleid worden vanuit een beschrijving van een mechanische structuur van starre lichamen in drie dimensies. Door het model van de mechanische structuur te koppelen met de elektrische aandrijving en het wiel-rail-contact kunnen trillingen van de aandrijflijn, het draaistel en het hele voertuig worden onderzocht. Voor de flexibele modelvorming en simulatie is software ontwikkeld.

Aan de hand van twee voorbeelden van tractieaandrijvingen is de dynamica tijdens het aanzetten van een voertuig gesimuleerd. Daarbij is rekening gehouden met pendelkoppels, wielslip en eventuele kortsluiting van de tractiemotor. De demping van de aandrijfcomponenten speelt een belangrijke rol voor de amplitude en propagatie van de trillingen. Een toereikend gedempte aandrijflijn is altijd aan te bevelen om de amplitude van trillingen te beperken. Het optimaliseren van pulsmodulatie van de inverter heeft rekening te houden met mogelijke resonanties en transiënten als gevolg van pulsovergangen.

De optredende wielslip beperkt de koppelpiek bij statorkortsluiting van de motor. Bij aanzetten of remmen dicht bij het maximum van de over te brengen kracht van wiel naar rail kunnen slip-stick-oscillaties optreden die deels door de aandrijflijn gedempt worden. Om de optredende hoge amplitudes te beperken is actieve demping door de tractieregeling gewenst.

De resultaten van het onderzoek laten zien dat voor de analyse van trillingen in tractieaandrijvingen het gehele systeem onderzocht moet worden. Voor optimalisatie van een tractieaandrijving moet niet alleen de regeling maar moeten ook de componenten van de aandrijving geoptimaliseerd worden. Specificaties van de componenten moeten rekening houden met de dynamische belasting die berekend en gemeten kan worden met de in dit proefschrift beschreven middelen. De interactie van de variabelen die nodig zijn voor optimalisatie maakt deze tot een moeilijke opgave.

Zusammenfassung

Verkehr ist ein wichtiger Teil unseres täglichen Lebens. Durch den Berufsverkehr und Auslandsreisen ist das Verkehrsaufkommen gestiegen. Hochgeschwindigkeitszüge sind eine Alternative für den Luftverkehr geworden, während Nahverkehrsfahrzeuge eine Alternative für das Auto sind. Durch zunehmende Staus auf den Autobahnen ist der schienengebundene Verkehr eine ernsthafte Alternative, aber nur dann, wenn er attraktiv genug ist. Dazu gehören komfortabele Züge, U-Bahnen und Straßenbahnen, die den Fahrgast zügig und im raschen Wechsel befördern. Diese Anforderungen erfordern Neuentwicklungen, wie zum Beispiel die Niederflurstraßenbahn mit einer Einstiegshöhe von 30 Zentimetern.

Die Entwicklung von Nahverkehrsschienenfahrzeugen wie Triebwagen, U-Bahnen und Straßenbahnen mit Asynchronmotoren und Neuentwicklungen von Drehgestellen und Wagenkasten hat zu einer Verminderung des Fahrzeuggewichts und einer Erhöhung der Leistung geführt. Damit kann Energie gespart und die Beförderungskapazität erhöht werden.
Anforderungen an die Lebensdauer von Bahnantrieben sind heutzutage Bestandteil eines Pflichtenhefts für den Neubau von Fahrzeugen. Spezifikationen von Antriebskomponenten wie Getriebe, Kupplungen und Federungen müssen eine Lebensdauer von mindestens 30 Jahren gewährleisten. Die Lebensdauer wird durch die dynamische Belastung beeinflußt. Schwingungen und Spitzen von Drehmoment und Kräften müssen bekannt sein, um Antriebe für Schienenfahrzeuge spezifizieren und entwickeln zu können. Daher muß der gesamte Fahzeugantrieb mit elektrischem Antrieb, mechanischem Antriebsstrang und Rad Schiene Kontakt untersucht werden. Angesichts der Vielzahl von Antriebssystemen der Fahrzeuge ist eine universelle Methode notwendig, um die Antriebsdynamik bestimmen zu können.
Mechanische Schwingungen können freie, gedämpfte oder erzwungene Schwingungen sein. Schwingungsquellen sind der elektrische Antrieb durch die Momentenpulsationen, die der umrichtergespeiste Motor erzeugt, durch die Regelung und durch Fehler im Antrieb wie der Ständerkurzschluß des Motors. Der Rad Schiene Kontakt ruft Schwingungen sowohl durch Schienenstöße hervor als durch Slip-Stick

Vorgänge, die den gesamten Antrieb beeinflussen.

Diese Arbeit leistet einen Beitrag zur Erfassung des Schwingungsverhaltens von Bahnantrieben durch meßtechnische und rechnerische Methoden. Ziel der entwickelten Methodik ist die Optimierung des Antriebssystems, um in kurzer Zeit eine Übersicht über das Schwingungsverhalten zu erhalten.

Messungen sollten mit Meßaufnehmern sowohl im mechanischen als im elektrischen Antrieb während eines Standardfahrzyklus ausgeführt werden. Simultanes Erfassen der Signale im gewünschten Frequenzbereich verschafft eine Übersicht über das Schwingungsverhalten des Antriebs. Analyse im Zeit- und Frequenzbereich durch Wasserfalldiagramme verdeutlichen geschwindigkeitsabhängige Schwingungen und Resonanzen. Messungen wurden durchgeführt an drei verschiedenen Fahrzeugtypen bei Streckenfahrten und mit einer Lokomotive auf einem Rollprüfstand.
Die Messungen ergaben, daß Schwingungen hauptsächlich durch den Traktionswechselrichter, durch den mechanischen Antriebsstrang und durch den Rad Schiene Kontakt entstehen. Die höchsten Amplituden wurden bei der Anregung schwach gedämpfter Eigenfrequenzen gemessen wie Reibschwingungen des Radsatzes und Resonanz einer Kardanwelle.

Flexible Modellbildung der Antriebe wurde durch die Anwendung eines Mehrkörpersystemalgorithmus erreicht, wodurch die Bewegungsgleichungen aus der Struktur des Antriebs als System starrer Körper in drei Dimensionen abgeleitet werden. Modelle des elektrischen Antriebs und des Rad Schiene Kontakts integriert in Modelle des mechanischen Antriebs ermöglichen die Berechnung der Schwingungen von Antriebssträngen, Drehgestellen und Fahrzeugen. Zur flexiblen Modellbildung und Simulation der Antriebsdynamik ist Software entwickelt worden.

Anhand zweier Beispiele von Antrieben von Nahverkehrsfahrzeugen ist die Dynamik während eines Anfahrvorgangs simuliert worden, wobei Drehmomentpulsationen des Motors, Radschlupf und Kurzschluß des Fahrmotors berücksichtigt wurden. Die Dämpfung der mechanischen Antriebskomponenten bestimmt die Amplitude und Verbreitung mechanischer Schwingungen. Ein ausreichend gedämpfter Antrieb ist Voraussetzung um Amplituden von Schwingungen einschließlich Resonanzen zu begrenzen. Optimale Pulsmuster des Wechselrichters müssen sowohl Resonanzen als auch Momententransienten ausschließen. Möglich auftretender Radschlupf begrenzt Momentenspitzen bei

Kurzschluß des Fahrmotors. Bei Anfahren und Bremsen in der Nähe des Kraftschlußmaximums können Reibschwingungen auftreten, die teilweise durch den Antrieb gedämpft werden. Um jedoch die Schwingungen entscheidend zu begrenzen ist eine aktive Schwingungsdämpfung durch die Antriebsregelung notwendig.

Die Resultate der Forschung haben gezeigt, daß Schwingungsanalyse in Bahnantrieben die Analyse des Gesamtsystems voraussetzt. Um Schwingungen zu begrenzen muß nicht nur die Antriebsregelung sondern müssen auch die Antriebskomponenten optimiert werden. Spezifikationen von Komponenten müssen die dynamische Belastung des Antriebs berücksichtigen, die mit der in dieser Arbeit dargestellten Methodik berechnet und gemessen werden können. Die Wechselwirkung zwischen den Variabelen, die zur Optimierung beitragen, gestaltet die Schwingungsoptimierung des Antriebs zu einer schwierigen Aufgabe.

Curriculum Vitae

Max Wolfgang Winterling was born 1959 in Wiesbaden, Germany. After having finished secondary school in Wiesbaden in 1978 he studied electrical engineering at the Technological Universities of Munich, Germany, and Delft, The Netherlands. He graduated "cum laude" from the Electrical Machines Group in Delft with Professor Deleroi in 1987. His thesis, titled "Steady-state operation of a rectifier loaded synchronous machine with cylindrical rotor without damper winding", won the "HOLEC Prize" award in 1988. From 1984 to 1987 he was student assistant at the Electrical Machines Laboratory, involved with experimental work and teaching. After graduation he joined the scientific staff of the Power Electronics and Electrical Machines Group. From 1989 to 1992 he was employed in the electrotechnical industry in Milan, Italy, in the field of research and development of electronics for industrial and servo drives. Meanwhile, he attended postgraduate courses on control theory at the Technological University of Milan. From 1993 he has been with HOLEC Ridderkerk, The Netherlands, Department of Machines, working as a development engineer in the field of system design and the analysis of traction drives in collaboration with Delft University. This thesis has been written as a result of his research activities.